RSC Advances

Cite this: *RSC Advances*, 2012, **2**, 64–98

www.rsc.org/advances

REVIEW

Graphene–inorganic nanocomposites

Song Bai and Xiaoping Shen*

Received 1st June 2011, Accepted 2nd October 2011
DOI: 10.1039/c1ra00260k

Graphene (GN) has received intense interest in fields such as physics, chemistry, biology and materials science due to its exceptional electrical, mechanical, thermal and optical properties as well as its unique two-dimensional (2D) structure and large surface area. Recently, GN–inorganic nanocomposites have been opened up an exciting new field in the science and technology of GN. From the viewpoint of chemistry and materials, this account presents an overview of the synthesis and application of GN–inorganic nanocomposites. The challenges and perspective of these emerging nanocomposites are also discussed.

1. Introduction

Graphene (GN), a two-dimensional material (2D), composed of layers of carbon atoms packed into a honeycomb network, has become a sparkling rising star on the horizon of material science in the last several years.[1,2] Even though GN is the mother of all graphitic forms, including 0D fullerene, 1D carbon nanotubes (CNT) and 3D graphite, which have been intensively studied for decades, not too much attention was paid to GN before.[3] Until in 2004, Geim and Novoselov at Manchester University first isolated single-layer sheets of GN from bulk graphite, which were awarded the 2010 Nobel Prize in Physics for their groundbreaking experiments regarding GN.[4–6]

Long-range π-conjugation in GN yields remarkable and unique properties, such as high values of its Young's modulus (~1.0 TPa),[7] large theoretical specific surface area (2630 $m^2 g^{-1}$),[8] excellent thermal conductivity (~5000 W m^{-1} K^{-1}),[9] high mobility of charge carriers (200 000 cm^2 V^{-1} s^{-1}),[10] and optical transmittance (~97.7%).[11] These excellent properties support GN as an ideal building blocks in nanocomposites. Nanocomposites are multiphase materials, in which one phase (dispersed phase) in the nanosize regime is dispersed in a second phase (matrix/continuous phase), resulting in a combination of the individual properties of the component materials. It is well known that a new type of nanocomposite—CNT–inorganic nanocomposites—have attracted significant research attention in the last decade, due to the combination of the intrinsic properties of CNTs and inorganic materials, thus their exceptional performance in various applications.[12,13] In comparison with CNTs, GN exhibits some similar behaviors, but some vastly distinct properties, such as quantum Hall effect,[6,14,15] and ambipolar electric field effect.[4,16] More important is the tubular geometry of CNTs while GN has a planar structure. All of these make the emergence of novel nanocomposites—GN–inorganic nanocomposites—*viz.* the hybrids of GN with inorganic nanomaterials. Over the past few years, GN–inorganic nanocomposites have been intensively

School of Chemistry and Chemical Engineering, Jiangsu University, Zhenjiang, China, 212013. E-mail: xiaopingshen@163.com

Song Bai

Song Bai is a Master degree candidate under the supervision of Prof. Xiaoping Shen at School of Chemistry and Chemical Engineering, Jiangsu University, China. His current research concentrates on the preparation and application of graphene-based materials.

Xiaoping Shen

Xiaoping Shen is a Professor at Jiangsu University, China and a Director of the Department of Chemistry. His current research interests focus on synthesis and property of nanostructural materials including metal oxides, metal sulfides, graphene-based composites and coordination polymers. He received his PhD degree in inorganic chemistry from Nanjing University, China (2005). From 2008 to 2009 he worked as a visiting scholar at University of Wollongong, Australia. He is author or co-author of more than 80 original papers in peer-reviewed international journals and 10 patents.

developed, and found to exhibit a range of unique and useful properties, which are attracting more and more attention from researchers.

In this review, we focus on synthesis and potential applications of GN–inorganic nanocomposites. Starting with an attempt to introduce GN as building blocks for nanocomposites (section 2), we discuss the preparation of GN for nanocomposite synthesis. This will be followed by the classification of GN-based nanocomposites. In the second part, we provide a comprehensive summary of various techniques in synthesizing GN–inorganic nanocomposites, which are grouped into two main categories: *in situ* synthesis (section 3.1) and *ex situ* approaches (section 3.2). Finally, we demonstrate the superb advantages of GN–inorganic nanocomposites for a wide range of applications (section 4) and discuss the remaining challenges and future prospects (section 5).

2. Graphene in nanocomposite materials

2.1. Why choose graphene?

Not surprisingly, the main motivating factor for probing the research of the GN-based nanocomposites is the desire to combine the favorable properties of GN with other constituent nanomaterials (the second components).[17,18] The benefits of GN in constructing inorganic nanocomposites include the following:

(1) Planar structure. It is usually difficult to achieve a good decoration of nanomaterials on the CNTs, when the size of them is in the same range as or larger than the diameters of the CNT. Whereas, GN have a unique basal plane structure, which make it possible for GN to load microspheres with diameter size even bigger than several hundred nanometres.[19] Furthermore, the 2D structure makes it possible for GN-based nanocomposites to be synthesized by new synthesis methods which could not be used in CNT-based nanocomposites synthesis, such as the thermal decomposition of GN precursor-intercalated inorganic materials.[20,21]

(2) High surface area. Compared with CNTs, GN, with higher surface area, improves interfacial contact with the other components. The large surface of GN could prevent the aggregation of secondary components, so that some unique properties in the nanoscale could be preserved.[22] On the other hand, most of the extraordinary properties of GN nanosheets are only associated with individual sheets. However, the high surface area make GN tend to form irreversible agglomerates.[23] While the second components could act as spacers between GN nanosheets to minimize the agglomeration.[24]

(3) Electrical and optical properties. Most of the research on GN focuses on the electrical properties. As a zero band gap semiconductor, GN displays a remarkably high electron mobility under ambient conditions, with reported values up to 15 000 $cm^2\ V^{-1}\ s^{-1}$.[5] Moreover, the observed mobilities are nearly independent of temperature, suggesting that an ultrahigh mobility could be realized in GN at room temperature.[25] By minimizing impurity scattering, mobilities of GN in excess of 200 000 $cm^2\ V^{-1}\ s^{-1}$ were achieved.[10] This is of importance as nanocomposites with GN as the electron carrier may perform better in applications that involve charge transfer processes, such as sensors, supercapacitors, and electrocatalysis. Moreover, considering the high optical transparency of GN, GN-based nanocomposites could be fabricated into transparent conductive films,[26,27] which show promise for application in solar cells, advanced electronics, *etc.*

(4) Mechanical properties. It was reported that defect-free monolayer GN has a Young's modulus of 1.0 TPa and a fracture strength of 130 GPa.[7] Despite some structural distortion, the measured elastic modulus of freely suspended GN monolayers is still as high as 0.25 TPa.[28] The advantages of GN in mechanical properties make it facile to fabricate and process GN-based nanocomposites into devices with various application. Furthermore, it was also reported that the mechanical stability of GN nanosheets could be improved by dispersing inorganic nanomaterials on them.[29]

(5) Thermal properties. In a noncontact measurement using the confocal micro-Raman spectroscopy, a thermal conductivity value of about 5000 $W\ m^{-1}\ K^{-1}$ was obtained for a suspended single-layer GN.[9] The high thermal conductivity make GN-based nanocomposites with excellent thermal stability, which could be important in some electronic devices or catalytic reactions with heat release, such as fuel cells and lithium-ion batteries (LIBs).

(6) Low cost and simple procedure of production. GN can readily form stable colloids dispersion in various solvents,[30] which make it possible to process GN-based nanocomposites directly using solution processing techniques, while the chemical functionlization in advance is necessary for CNT, due to their poor dispersion.[31] In addition, the solution processing methods start with graphite as the raw material, resulting in the production cost of GN-based materials in large quantities much lower than that of CNT.[32]

2.2. Preparation of graphene for use in nanocomposite materials

2.2.1. Preparation of graphene oxide. Up-to-date, six widely used methods have been reported to prepare GN: (1) micromechanical exfoliation method,[4,33] (2) chemical vapor deposition (CVD) techniques,[34,35] (3) epitaxial growth,[36–38] (4) longitudinal "unzipping" of CNTs,[39–41] (5) organic synthesis routes,[42,43] and (6) colloidal suspension from graphite or graphite derivatives.[44–46] The advantages and disadvantages of these methods were discussed in detail in several reviews,[47,48] which are summarized in Table 1.

Among the six methods, the colloidal suspension method from graphite or graphite derivatives (method 6) stands out as the primary strategy that can not only yield large amounts of chemically modified graphene (CMG), but also be suited to chemical functionalization and used for a wide range of applications.[49] Among the synthesized CMG, reduced graphene oxide (RGO) is the most common product, which is often obtained through graphite oxide exfoliation-chemical reduction route.[50] Graphite oxide, formerly called graphitic oxide or graphitic acid, is obtained by treating graphite with strong oxidizers. Nowadays, most GN-based nanocomposites are fabricated with graphite oxide as the starting material. This is much similar to the acid-treated CNT, which is often used in CNT-based nanocomposites synthesis. In fact, most of "GN" in GN-based nanomaterials is CMG, or to be exact RGO.

Methods for the oxidation of graphite to graphite oxide include: Brodie,[51] Staudenmaier,[52] Hummers method,[53] and

Table 1 Advantages and disadvantages of various GN synthesis techniques

Synthesis technique	Description	Product	Advantages	Disadvantages
micromechanical exfoliation	exfoliation from bulk graphite using Scotch tape	GN particles	simple process, few defects	small area, low yield,
CVD	surface segregation of carbon or decomposition of hydrocarbons.	GN films	large area	low yield, poor scalability
epitaxial growth	high temperature evaporation of Si on SiC wafer surfaces	GN films	few defects	costly method, small area, low yield
longitudinal "unzipping" of CNTs	Ar plasma etching or edge oxidation	GN nanoribbons	high yield, controllable widths, smooth edges	poor scalability
organic synthsis	stepwise organic reactions to extend polycyclic aromatic hydrocarbons	GN quantum dots (QDs)	few defects, easy scalability	small area, costly method
colloidal suspension	exfoliation suspension of graphite or graphite derivatives	CMG/GO/RGO nanosheets	high yield, large area, easy scalability	significant numbers of defects

some of these methods with minor modifications.[54,55] A comparison of these methods can be seen in a related review.[56] The oxidation of graphite can destroy the sp^2 hybridized structure with a increase of layer distance.[57] The precise structure of graphite oxide is still under debate today, but it is sure that graphite oxide is strongly hydrophilic,[58] which can be exfoliated to colloidal suspensions of graphene oxide (GO) sheets in water and organic solvents by simple sonication due to the oxygen-containing functional groups on both basal planes and the edges of GO.[59,60] A thorough discussion on graphite oxide and GO can be found in a recent review.[61]

2.2.2. Reduction of graphene oxide. GO can be chemically reduced to RGO with various reducing agents, such as hydrazine monohydrate,[62–64] sodium borohydride,[65,66] hydroquinone,[67,68] strongly alkaline,[69] sulfur-containing compounds,[70,71] amines,[72,73] *etc.* Among the reducing agents described above, hydrazine monohydrate is most widely used, mainly due to its strong reduction activity to eliminate most oxygen-containing functional groups of GO and its ability to get a stable RGO aqueous dispersion.[64] However, with hydrazine as the reducing agent, its trace residual may strongly decrease the performance of RGO in devices. In addition, hydrazine is a highly toxic and potentially explosive chemical. To avoid using hydrazine, many environmentally friendly and high-efficiency reductants have been developed to be substitutes, such as vitamin C,[74,75] amino acid,[75] reducing sugar,[76] alcohols,[77] hydrohalic acids,[78] reducing metal powder,[79,80] sodium citrate,[81] tea,[82] lysozyme,[83] *etc.*

Besides reducing agents, some other methods have also been used to reduce GO. Thermally-mediated reduction including oil-bath,[84,85] hydrothermal,[86] solvothermal,[87] and microwave-assisted heating approaches,[88] have been implemented to reduce GO at high temperatures. With no hazardous reductants used and only simple equipment, the thermally-mediated methods are believed to be perfect for mass production of RGO. Another clean method showing promise for the reduction of GO relies on the electrochemical removal of the oxygen functional groups.[89,90] This reduction process can be monitored and controlled by its reduction peaks and the redox current peaks.[91] However, this method mostly yields solid RGO films on the surface of electrode, which is less suitable for processing of GN colloid dispersions. Furthermore, other methods, such as photo-irradiation,[92] bacterial respiration,[93] laser,[94] and plasmas[95] were also used to reduce GO. Liu and Sun *et al.*[96] also propose an evaluation criterion for the reduction method of GO with several factors, including dispersibility, reduction degree, defect repair degree, and electrical conductivity. The production of RGO from graphite oxide is a hotspot in the field of GN-based materials, and a recent review was dedicated to this topic.[97]

2.2.3. Functionalization. The reduction is a route to remove oxygen functional groups from GN, while functionalization is a way to add groups to GN. The functionalization of GN is important in making GN nanosheets achieve desired properties and materialize their prospect applications, such as enhancing the solubility of GN in various solvents,[98,99] increasing the ability of GN to load nanomaterials or disperse in matrices,[100,101] improving the manipulation and processing capability of GN to fabricate various devices,[102,103] *etc.* In general, GN can be functionlized by either covalent attachment or noncovalent adsorption of various functional molecules.

Covalent functionalization is achieved through the chemical bonding of the functional molecules with the basal planes and edges of GN nanosheets. However, the functionalization of defect-free GN is not so easily accomplished, and most reported covalent chemical modifications of GN occurred with GO or RGO (GO/RGO) at reactive sites of oxygen-containing functional groups. Actually, GO itself can be also regarded as covalent functionalized GN with oxygen functional groups. At present, introduction of amines to conjugate with oxygen functional groups is a common approach to covalent functionalizaion of GN,[104,105] which have been investigated for various applications.[106,107] In contrast, GN can also be non-covalently functionalized *via* hydrogen bonding,[108,109] π–π stacking,[110,111] electrostatic interactions,[108,112] and van der Waals interactions.[108,113] The main advantage of the noncovalent functionalization of GN is that functional groups could be introduced into GN without affecting its structure and electronic network, so that the novel properties of GN are retained.

2.3. Classification of graphene-based nanocomposites

In 2006, Ruoff's group reported the first GN-based nanocomposite, a GN–polystyrene nanocomposite,[114] which has attracted tremendous attention and was followed by further development a broad of new class of GN-based nanocomposites. So far, there has not been an authoritative classification of GN-based nanocomposites. Herein, we classified the GN-based nanocomposites according to two criteria: the second component of the nanocomposites and the architecture of the nanocomposites.

Table 2 Classification of GN-based nanocomposites by the second components

GN-based nanocomposites		Second component	Ref.
GN–polymer nanocomposites		Polymer	114–120
GN–inorganic nanocomposites	GN–metal nanocomposites	Metal	121–138
	GN–carbon nanocomposites	Carbon building blocks	139–145
	GN–metal compound nanocomposites	Metal compound	146–160
	GN–nonmetal nanocomposites	Nonmetal	162–172

2.3.1. Classification with the second component of the nanocomposites. With different second components involved, GN-based nanocomposites are classified into two main categories: GN–polymer nanocomposites and GN–inorganic nanocomposites. GN–polymer nanocomposites are hybrid materials of GN nanosheets with polymers. In GN–polymer nanocomposites, GN can dramatically improve properties such as electrical conductivity, thermal conductivity, and mechanical strength. Moreover, these improvements are often observed experimentally at low loadings of GN, owing to their large interfacial area and high aspect ratio.[115,116] There are several excellent reviews on GN–polymer nanocomposites.[117–120]

Based on the different kinds of inorganic components, GN–inorganic nanocomposites could be further classified into: GN–metal nanocomposites, GN–carbon nanocomposites, GN–metal compound nanocomposites, and GN–nonmetal nanocomposites. In GN–metal nanocomposites reported in literature, the majority of the second components are noble metals, such as Au,[121–124] Ag,[125–127] Pt,[126,128–130] and Pd[131,132]. GN can not only reduce the consumption of noble metal, but also establish significant electronic interaction with them.[133] In addition, other metal nanomaterials such as Cu,[126,134,135] Sn,[126,136] Co,[137] bimetals,[138] and alloys[126] were also used for fabricating inorganic composites of GN.

The combination of GN with other carbon building blocks (CNT,[139–141] fullerene,[142] carbon black (CB),[143] carbon sphere,[144] and carbon nanofibers[145]) offers fascinating prospects for the design of new carbon materials, especially the composites of GN with CNT. Both GN and CNT show remarkable electrical, thermal, mechanical and structural properties. The assembly of them into nanocomposites produces carbon materials with large specific surfaces, high electrical conductivities, and unique mechanical properties.

The integration of metal compound nanomaterials with GN forms GN–metal compound nanocomposites. The reported metal compounds include: oxides,[146–151] hydroxides,[152,153] sulfides,[154,155] selenides,[156,157] nitride,[158] inorganic salt,[159] clay,[160] *etc.* Among these metal compounds, semiconductor and magnetic nanomaterials were intensively studied. It has been demonstrated that there exists charge-transfer as well as electronic and magnetic interactions between GN and the attached semiconducting oxide or magnetic nanomaterials.[161] GN as an electron transport channel could bring enhanced properties and improved performance of metal compound nanomaterials in various applications.

Non-metallic materials such as S,[162,163] Si,[164,165] SiO_2,[166] Si_3N_4,[167] SiOC,[168] CN,[169,170] and C_3N_4[171,172] have also been reported for preparing their corresponding nanocomposites with GN. Some of the GN–nonmetal nanocomposites were synthesized to develop metal-free catalysts to substitute metal catalysts. For example, a GN–C_3N_4 nanocomposite was reported to be a high-performance catalyst to activate molecular oxygen for selective oxidation of secondary C–H bonds of saturated alkanes with good conversion and high selectivity to the corresponding ketones.[171] The classification of GN-based nanocomposites by the second component was listed in Table 2.

2.3.2. Classification with the architectures of the nanocomposites. The classification with the second component has its limits if more than two components were blended in a nanocomposite. Therefore according to the different architectures of the nanocomposites, we also classify the GN-based nanocomposites into four types as illustrated in Fig. 1: GN-supported nanocomposites, GN-encapsulated nanocomposites, GN-incorporated nanocomposites and GN-based multilayered nanocomposites. In GN-supported nanocomposites, GN nanosheets form a continuous phase and act as a substrate for supporting the second component. The majority of GN–inorganic nanocomposites were fabricated in this form. Inorganic nanoparticles (NPs),[173,174] nanorods,[175,176] nanosheets,[153,177,178] nanoplates,[179,180] nanowires,[181,182] nanowalls,[182–184] nanotubes,[185,186] nanoneedles[148] have been attached on GN nanosheets to form GN–inorganic nanocomposites. It is worth mentioning that the nanotubes (nanorods, nanofibers) could be either grown vertically on GN nanosheets,[187] or parallelly deposited on them.[188] Occasionally, polymer nanostructures could also attach on the surface of GN nanosheets to form GN-supported polymer nanocomposites.[189,190] The large surface area of GN as well as uniformly distributed active sites of NPs make this structure appropriate for applications

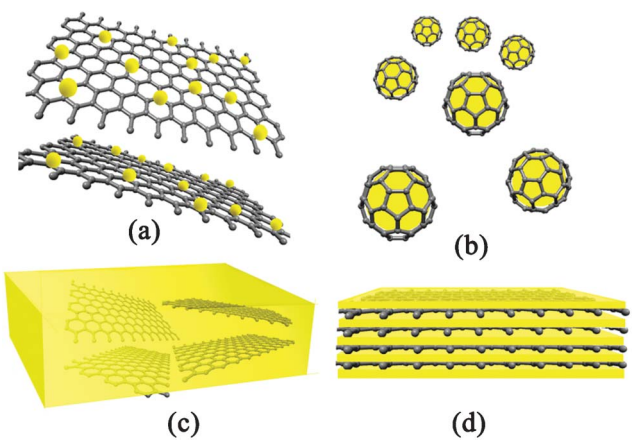

Fig. 1 Schematic illustration of architectures of GN-based nanocomposites: (a) GN-supported nanocomposites; (b) GN-encapsulated nanocomposites; (c) GN-incorporated nanocomposites and (d) GN-based multilayered nanocomposites.

such as catalysis and sensing. The planar GN-supported nanocomposites could also further roll up into nanoscrolls and nanostructured textiles, which is much similar to CNT-supported nanocomposites.

GN-encapsulated nanocomposites are fabricated through enwrapping the second components with GN nanosheets. The nanostructures of the second component could be NPs,[191] hollow particles,[192] nanotubes,[193] *etc.* In this structure, GN nanosheets functioned as protection layers, which could more effectively prevent the aggregation of the second components in comparison with GN-supported nanocomposites. Meanwhile, the contact surface between GN and the second components is much larger, and thus this structure could be more stable to avoid the exfoliation of the second components from the GN. This structure has been fabricated for high-performance lithium storage electrode materials with the reason that GN could compensate for the volume change of the inner active material during the Li^+ insertion and extraction as well as improve the electrical conductivity.

In GN-incorporated nanocomposites, GN nanosheets play the role of nanofillers and distribute in the matrix of second components. The second matrix could be bulk materials,[194] or made-up of nanomaterials.[195] In this structure, usually, the second components were polymers. However, some inorganic compounds, particularly, the ceramic materials were also embedded with GN nanosheets to form GN-incorporated inorganic nanocomposites. The large surface area and high electrical conductivity of GN functionalize the inorganic materials with interesting properties and valuable applications. For example, by incorporation of individual GN sheets into a silica matrix, GN–ceramic composite thin films were fabricated as transparent conductors.[196] GN-incorporated alumina ceramic composites were prepared by spark plasma sintering, which show far higher electrical conductivities than CNT–alumina ceramic composites with the same conductive phase content.[197,198] Corral *et al.*[167] also reported that incorporating a small amount of GN nanosheets could greatly increase the toughness of silicon nitride ceramics.

GN-based multilayered nanocomposites are formed by stacking GN nanosheets with the second components alternately. This structure could maximize the interfacial area, and is propitious to charge generation, transfer, and separation, thus has potential applications in energy storage. The second components could be NPs. As an example, Yang *et al.*[199] reported a multilayered structure of a GN–NiO composite. The tightly fixed NiO NPs and planar GN form the skeleton of such structures, which acts as an ideal buffer to accommodate volume changes of the NiO, and thus has a better resilience and structural stability in the electrochemical charge–discharge process. However, in most cases, the second components were in the form of nanosheets. Jin *et al.*[200] reported the multilayered composite of GO sheets with Co-Al layered double hydroxide (LDH) nanosheets for application as a pseudocapacitor. Their results demonstrated that the composite exhibited a high specific capacitance. This is due to the single atomic layered structure, in which all Co atoms occupy the surface of sheets and thus have an opportunity to contribute to redox reaction. In addition, the face-to-face assembly of GO and Co-Al LDH nanosheets optimizes their contact area, which is advantageous to efficient electron transport. Table 3 summarizes the classification of GN-based nanocomposites by the architectures of the composites.

3. Synthesis of graphene–inorganic nanocomposites

Nowadays, a number of strategies have been put forward for the fabrication of GN–inorganic nanocomposites. Nonetheless, they fall into two basic classes. One main approach involves the formation of nanocrystallites in the present of pristine or functionalized GN nanosheets, and then the nanocrystallites directly grow into nanomaterials such as NPs, nanowires, nanorods and nanofilms on the surface of the GN nanosheets, which belong to *in situ* techniques; while the second key approach involves the prior synthesis of nanomaterials in the desired dimensions and morphology, then modified and subsequently connected to the surface of functionalized GN nanosheets, which is named as *ex situ* techniques here.

3.1. *In situ* growth on a graphene surface

Among the two approaches, *in situ* growth is more widely used in the synthesis of GN–inorganic nanocomposites. The main advantage of this route is that the protecting surfactant or extra linker molecules could be avoided, which may imply a tedious experimental procedure, and also influence the functions of the nanocomposites. Another advantage of the *in situ* approach is that a variety of chemical and physical synthesis techniques could be used, including solution deposition methods, direct decomposition of precursors, hydrothermal/solvothermal techniques, gas-phase deposition, sol–gel processing, template method, and so on.

3.1.1. Solution deposition methods. The *in situ* deposition of inorganic NPs on GN is generally obtained in a mixed solution system with GO/RGO as precursors of GN. The groups and defects on the surface of GO/RGO could not only improve the solubility of the nanosheets, but also offer the nucleation sites of nanocrystallites.[122,201] In this sense, the GO/RGO nanosheets can also act as stabilizers of NPs.

Table 3 Classification of GN-based nanocomposites by the architectures

GN-based nanocomposites	Dispersed phase	Matrix/continuous phase	Ref.
GN-supported nanocomposites	NPs, Nanorods, Nanosheets, Nanoplates, Nanowires, Nanotubes, *etc.*	GN nanosheets	173–190
GN-encapsulated nanocomposites	NPs, Nanotubes, *etc.*	GN nanosheets	191–193
GN-incorporated nanocomposites	GN nanosheets	Bulk materials or Buildup of NPs	194–198
GN-based multilayered nanocomposites	Alternating layers of GN nanosheets with the second components (NPs or nanosheets)		199, 200

3.1.1.1. Synthesis of graphene–metal nanocomposites by reduction of mixed solution. The simultaneous reduction of metal precursors and GO in a mixed solution is a common way to prepare GN–metal nanocomposites. During the synthesis process, $NaBH_4$ is a frequently-used reducing agent. For example, RGO–Ag nanocomposites have been prepared by reducing $AgNO_3$ with $NaBH_4$ in a GO suspension[127,202,203]. Pt[204] and Sn[136] NPs were grown on RGO nanosheets through a similar procedure with H_2PtCl_4 and $SnCl_2$ as the metal precursors, respectively. Furthermore, this method was also used to synthesize RGO–alloy nanocomposites.[205–207] Ethylene glycol (EG) is another important reducing agent for producing RGO–metal nanocomposites. Xu and Wang *et al.*[208] developed a general approach for producing RGO–metal nanocomposites. They dispersed GO and a metal precursor (K_2PtCl_4, K_2PdCl_4, or $HAuCl_4{\cdot}3H_2O$) in a water–EG mixed solvent. Then, both GO and the metal precursor were reduced by EG, forming the corresponding nanocomposites. Through this EG co-reduction route, RGO nanosheets supported Pt and Pt-based alloy NPs were also fabricated.[209–211] Recently, Yu *et al.*[201] demonstrated an efficient one-step approach to prepare RGO–Ag nanocomposites with formaldehyde as the reducing agent under mild conditions. In this case, formaldehyde is highly effective in reducing both Ag^+ and GO within several minutes at 60 °C.

However, the co-reduction route also has challenges to obtain uniformly dispersed metal NPs on GN with high-dispersibility. On the one hand, before the reduction of GO, randomly distributed oxygen-containing groups on the its surface could result in non-homogenous distribution of metal NPs. On the other hand, reduction of GO could result in poor dispersibility due to π–π stacking interactions. An important and effective improvement is to attach capping agents on GO/RGO nanosheets, which could evenly bind *in situ* reduced metal NPs, control the size and shape of the NPs, and also make obtained composites well-dispersed after reduction of GO. For example, sodium citrate was introduced to *in situ* reduce Au NPs onto the surface of RGO nanosheets.[212] In this case, the hydrophilic property of sodium citrate binding on Au NPs make the composites well-dispersed in water. Chen *et al.*[213] adhered a perylene thiol derivative on the basal plane of GO and then reduced GO into well-dispersed RGO nanosheets, which serve as an excellent stabilizer in solution for *in situ* nucleation and orderly growth of Au nanodots (NDs) *via* thiol–Au bonding. Transmission electron microscopy (TEM) images indicate that the small Au NDs are uniformly decorated on RGO surface with a narrow size distribution (Fig. 2).

3.1.1.2. Precipitation of graphene–metal compound nanocomposites from a mixed solution. A variety of GO–metal oxide nanocomposites have been synthesized by precipitating the mixed solution of metal salts and GO, which would then be reduced to RGO–metal oxide nanocomposites. For example, *in situ* decomposition of cobalt nitrate and $Cu(OAc)_2$ in the dispersion of GO give GO–Co_3O_4 and GO–CuO nanocomposites, respectively.[214,215] Precipitation of Fe^{3+}/Fe^{2+} ions and GO in an alkali solution produce GO–Fe_3O_4 nanocomposites, which could be reduced to RGO–Fe_3O_4 nanocomposites by hydrazine.[216–218] RGO–TiO_2,[219] and RGO–SnO_2[220] nanocomposites were also prepared by mixing GO with corresponding metal salts in solutions, followed by the reduction of GO. The advantage of this method is that the abundant oxygen-containing groups distributed on the GO nanosheets ensure the high dispersion of NPs during the whole fabrication process. However, the two-step procedure could be avoided, with the growth of metal oxide NPs and reduction of GO synchronistically. For instance, a one-pot method has been reported to synthesize a RGO–TiO_2 composite using $TiCl_3$ as both a precursor of TiO_2 and a reducing agent of GO.[221,222] SnO_2 NPs could be *in situ* grown on RGO nanosheets based on a redox reaction between GO and Sn^{2+}, in which Sn^{2+} ions were oxidized and hydrolyzed to form SnO_2 NPs, while GO were synchronously reduced to RGO nanosheets.[222–224]

Also, surfactants have been used in directing the assembly of oxide nanomaterials on GN. Liu and coworkers developed a unique process for the construction of ordered CMG–metal oxide nanocomposites.[225] In their synthetic system, anionic surfactants were used to assist the dispersion of CMG nanosheets in the hydrophobic domains of the surfactant micelles and self-assembly of the oppositely charged metal cations on the CMG surface. After converting the metal cations to oxides, ordered nanostructures of CMG–NiO, CMG–SnO_2 and CMG–MnO_2 nanocomposites were formed. Müllen and coworkers chose cetyltrimethyl ammonium bromide (CTAB) as cationic surfactants to electrostatically adsorb onto the surface of highly negatively charged GO, which not only effectively solved the incompatibility and aggregation problems between GO and inorganic materials, but also directed the formation of mesoporous silica through the hydrolysis of TEOS around the surface of GO sheets.[226] The constructed GO-based mesoporous silica sheets would then be reduced to RGO–silica sheets *via* thermal treatment at high temperature.

Precipitation by a one-pot reaction could be also used to prepare GN–chalcogenide nanocomposites. Apart from metal salts and GO in the mixed solution, S/Se sources were also needed. For instance, RGO–sulfide nanocomposites were prepared from the mixed aqueous solution of metal ions (Cd^{2+}, Zn^{2+}) and GO with H_2S as both of sulfur source and

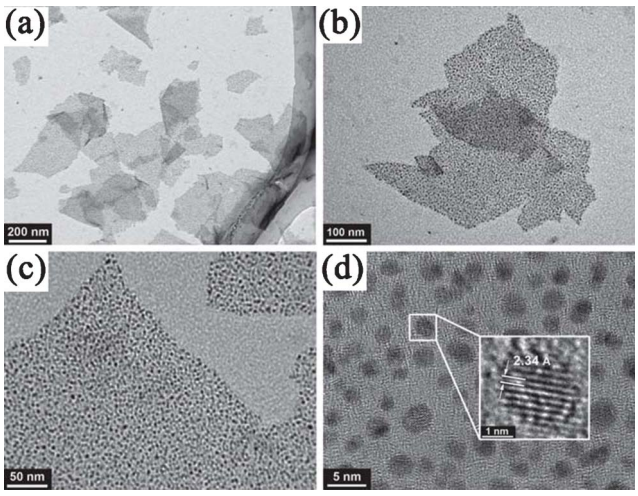

Fig. 2 TEM images of Au NDs uniformly decorated on RGO sheets. Reprinted with permission from ref. 213. Copyright 2011, Royal Society of Chemistry.

reducing agent.[227] Pan and coworkers reported the *in situ* synthesis of a RGO–CdSe nanocomposite by adding RGO directly into the reaction solution during the process of synthesizing CdSe NPs.[157] Li *et al.*[228] synthesized CdS QDs on an electrophoretically deposited GN layer using a sequential chemical bath deposition (S–CBD) from Cd^{2+} and S^{2-} aqueous solutions, and repeating the electrophoretic deposition and S–CBD gives a multilayered GN–CdS nanocomposite (Fig. 3).

3.1.1.3. Electrochemical deposition and electroless deposition. As mentioned above, the electrochemical approach is simple, fast and green, which does not result in contamination of the synthesized materials. Recently, electrochemical deposition methods have been developed to fabricate GN–inorganic nanocomposites, which are typically carried out *via* two steps, namely, GN nanosheets being first assembled on the electrodes, shortly thereafter, the GN-coated electrodes being immersed in electrolyte solution containing metallic precursor to perform the electrochemical synthesis. Nowadays, noble metals such as Au[229–232], Pt,[233,234] and bimetallic Pt–Au[235] with high purity have been formed quickly on GN nanosheets through an electrochemical reduction of the corresponding metal salts under an applied potential. For example, Xia *et al.*[234] proposed three strategies to electrochemically deposit Pt NPs on RGO nanosheets. The first route is the electrochemical reduction of GO at −1.5 V, and electrodeposition of Pt NPs at −0.25 V. In the second route, Pt NPs were deposited on GO first and then GO was reduced. While in the third approach, electrochemical reduction of Pt and GO was simultaneously performed. It is found that only with the third approach, highly dispersed Pt NPs with small sizes could be formed on RGO nanosheets.

Although research currently concentrates on the electrodeposition of metal NPs on GN nanosheets, there have also been several reports on the electrodeposition of metal oxides. For instance, Zhang's group[236] have successfully electrochemically deposited ZnO nanorods, as well as p-type and n-type Cu_2O films on RGO electrodes with polyethylene terephthalate (PET) as the substrate. In the deposition of ZnO, the electrochemical reactions occurred with the reduction of O_2 and precipitation of ZnO at a potential of −1.9 V in an oxygen-saturated Zn^{2+} aqueous solution electrolyte, while the electrochemical deposition of Cu_2O includes the reduction of Cu^{2+} ions and the formation of Cu_2O, in which the pH of the electrolyte affects the type of the obtained Cu_2O semiconductor. They also demonstrated the electrochemical deposition of Cl-doped n-type Cu_2O on RGO electrodes.[237] Tang *et al.*[238] fabricated RGO–MnO_2 composite by *in situ* anodic electrodeposition of γ-MnO_2 nanoflowers on the RGO electrode. The fabrication process includes making a RGO suspension into paper by vacuum filtering, after which the RGO paper is cut into pieces of designated dimensions for anodic MnO_2 electrodeposition as the electrode.

Similar to electrochemical deposition, electroless deposition is another clean method to deposit metal NPs, which take advantage of the redox potential differences between substrate and the metal ions without any reducing agent used. The

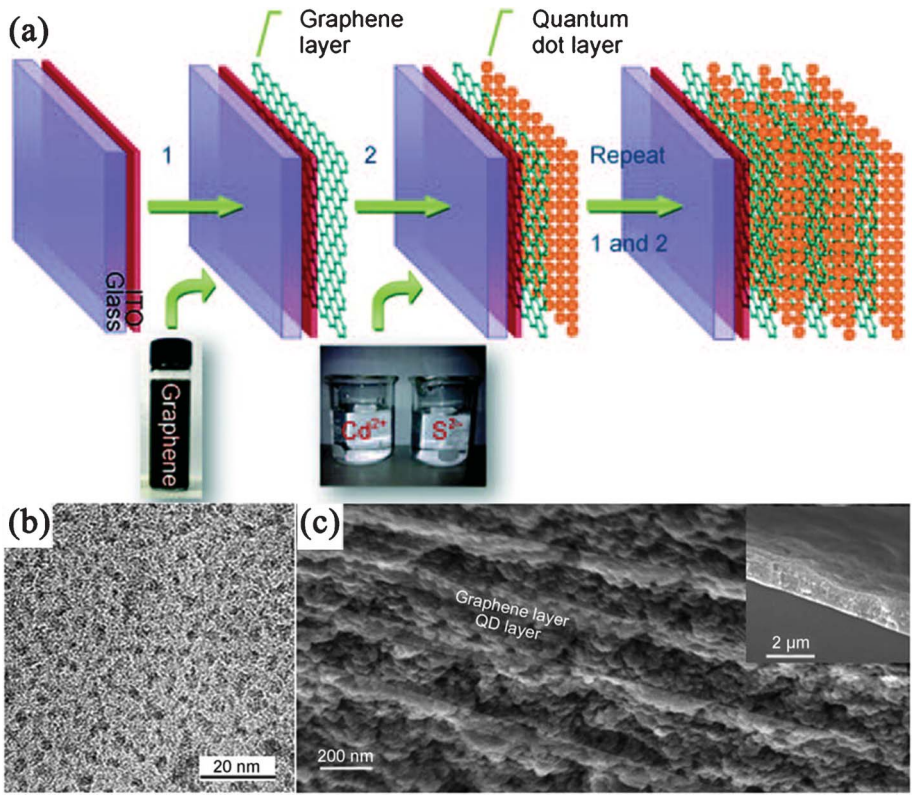

Fig. 3 (a) Fabrication of multilayered GN–CdS QDs nanocomposite. (b) TEM images of CdS QDs on GN nanosheets, (c) Cross-sectional scanning electron microscopy (SEM) image of a $(GN–CdS\ QDs)_{10}$ sample. The inset shows its thickness. Reprinted with permission from ref. 228. Copyright 2010, John Wiley & Sons, Inc.

galvanic displacement between metal cations and negatively charged GO/RGO could *in situ* reduce the metal ions into metal NPs on the GO/RGO nanosheets. For example, Zhang *et al.*[239] reported that Ag NPs formed spontaneously on RGO nanosheets when RGO substrate was immersed in an aqueous solution of $AgNO_3$ under N_2 protection at 75 °C. It was proposed that negatively charged RGO acted as the electron-donating source to reduce Ag^+ to Ag NPs, with the reason that the reduction potential of the RGO is +0.38 V *vs.* SHE (standard hydrogen electrode), much lower than that of Ag^+ (+0.73 V *vs.* SHE). With the galvanic displacement mechanism, noble metal nanoparticles such as Au[124,240] and Pd[241] NPs were also deposited on GO/RGO nanosheets driven by the difference between the reduction potential of $AuCl_4^{2-}$ (+1.002 V *vs.* SHE), $PdCl_4^{2-}$ (+0.83 V *vs.* SCE, saturated calomel electrode) and RGO (+0.38 V *vs.* SHE)/GO (+0.48 V *vs.* SCE). However, with this method, RGO can't reduce the metal ion with reduction potential lower than +0.38 V, such as Cu^{2+}. Wei *et al.*[242] fabricated various RGO–metal (Ag, Au, Pd, Pt and Cu) composites with an improved electroless deposition method. Instead of using negatively charged RGO, they made use of the redox potential differences between substrates (Cu or Zn foil) of RGO and the metal ions with RGO as an electron transport carrier. The reduction potentials of Cu or Zn were much lower than that of RGO, thus it could be performed to reduce metal ion which can't be reduced by RGO.

3.1.1.4. Photo-assisted reduction. Photochemical reduction is another "green" process, which can provide a uniform reducing environment in solution and no additional reagents are introduced. Semiconductors with large-band-gaps are photo-catalytically active under UV-visible light irradiation, which could be used to reduce GO through a photogenerated electron transfer process, thus RGO–semiconductor nanocomposites can be obtained.[243] Kamat *et al.*[244] reported the photo-assisted preparation of a RGO–TiO_2 composite with the UV irradiation of GO–TiO_2 dispersion in an inert atmosphere using ethanol as a hole scavenger for the TiO_2 photocatalyst. So far, several semiconductors have been reported to blend with RGO nanosheets through a photo-assisted reduction process, such as UV active TiO_2[245,246] and ZnO[247,248] as well as visible light driven WO_3 and $BiVO_4$.[249]

Besides the photocatalytic reduction of GO in the synthesis of GN–semiconductor nanocomposites, GN-supported metal NPs could also be produced *via* the photo-irradiation reduction of metal salts. One-pot synthesis of Au NDs on RGO nanosheets was performed by the photochemical reduction of $HAuCl_4$ in the presence of octadecanethiol (ODT) molecules (Fig. 4a).[250] Interestingly, the Au NDs assembled *in situ* into particle chains along the <100> directions of the RGO lattice, directed by the thiol groups of the self-assembled ODT molecules (Fig. 4b, c). Later, Kamat *et al.*[251] demonstrated that the RGO nanosheets could store photogenerated electrons from UV-irradiated TiO_2, and then shuttle the electrons to reduce Ag^+ into Ag NPs at a location distinct from the TiO_2 anchored site on RGO nanosheets. More recently, Choi *et al.*[252] deposited Au, Ag and Pd NPs on RGO nanosheets using a phosphotungstate as a homogeneous photocatalyst under UV irradiation. Photoreduced phosphotungstates as well as electrons stored in RGO directly reduced the metal ions.

3.1.1.5. Microwave-assisted deposition. The main advantage of microwave irradiation (MWI) over other conventional methods is heating the reaction mixture uniformly and rapidly. As a consequence, a variety of nanomaterials including metals, alloy, and semiconductors with very small particle size and narrow size distribution could be obtained. The MWI process allows the simultaneous reduction of GO and metal ions, resulting in the fast formation of GN–metal nanocomposites. El-Shall and co-workers[253] reported a microwave-assisted synthesis of various RGO–metal (Au, Ag, Cu, Pd, CuPd) nanocomposites in aqueous and organic media, respectively. In their experiments, GO and a variety of metal salts were reduced simultaneously with reductants such as hydrazine hydrate or reducing solvent such as oleylamine during the MWI process. Besides, RGO–Pt nanocomposites were synthesized by employing a microwave-assisted polyol process with EG as both dispersing and reductive agent for both metal ions and GO.[254,255] Berry *et al.*[256] also demonstrated that without any reducing agents, bare-surfaced Au NPs could also be produced *in situ* on GO sheets by a microwave reduction process.

Microwave-assisted methods have also been used in the synthesis of RGO–metal compound nanocomposites. A facile MWI method for the synthesis of RGO–CdSe nanocomposites were developed by EI-Shall and co-workers, which allows the simultaneous reduction of GO and the nucleation and growth of CdSe nanocrystallites.[257] In this system, dimethyl sulfoxide (DMSO) was used as both the reducing agent of GO and solvent for the reaction between the Cd and Se precursors, resulting in the formation of hexagonal and cubic CdSe NPs on RGO nanosheets. Furthermore, metal compounds, such as

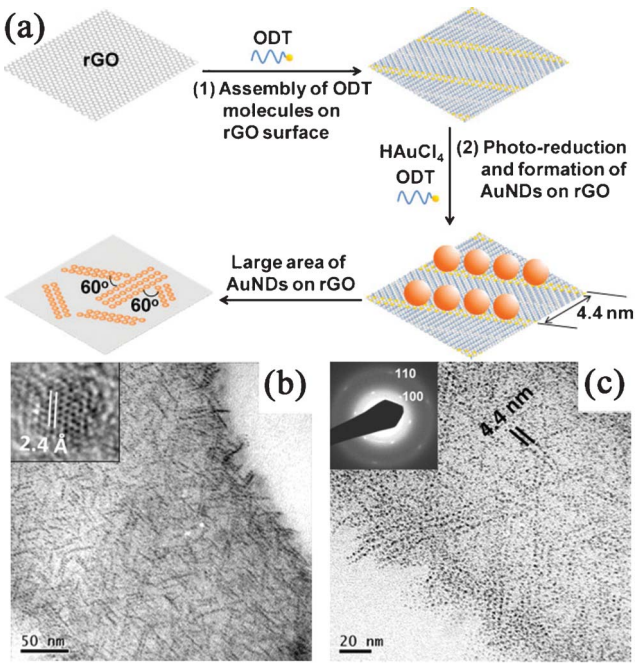

Fig. 4 (a) Schematic illustration of the *in situ* synthesis and assembly of Au NDs on RGO. (b) TEM and (c) magnified TEM images of ODT-capped Au NDs synthesized *in situ* on RGO surface. Reprinted with permission from ref. 250. Copyright 2010, John Wiley & Sons, Inc.

ZnS,[258] Fe_3O_4,[259] Co_3O_4,[260] SnO_2,[261] and ZnO[262] were reported to grow on RGO nanosheets with MWI methods. Lin and coworkers also reported a solvent-free method to prepare GN-supported metal (Ag, Au, Co, Ni, Pd, Pt) and metal oxide (Fe_3O_4, MnO, TiO_2) NPs in high yields through direct solid-state Joule heating of GN and various organic metal salts within short duration of MWI.[263]

3.1.1.6. Sonication-assisted deposition. Similar to microwave-induced heating, sonication of a liquid also results in rapid heating, although the mechanism is fundamentally different. The sonication of a liquid results in sonic cavitation (the growth and violent collapse of microbubbles) that creates localized "hot spots" with effective temperatures of 5000 K and lifetimes on the order of a few nanoseconds or less. As such, the chemical reactions largely take place inside the bubbles. Nowadays, sonication has been used in exfoliation of graphite into GN nanosheets and cut them into GN nanoribbons.[264] Also, sonochemical synthesis has become a new method to synthesize GN–inorganic nanocomposites. Vinodgopal *et al.*[265] reported the ultrasound-induced reduction of GO and $HAuCl_4$ in 2% aqueous solution of poly(ethylene glycol) at an ultrasonic frequency of 211 kHz to prepare RGO–Au nanocomposites. The proposed mechanism is as follows: highly reactive $H^{\bullet}$ and $OH^{\bullet}$ radicals are generated within the bubbles by the homolysis of water molecules due to the high-temperature conditions in aqueous solutions. The oxidizing radicals are scavenged by adding alcohols, thus providing a reducing condition. Finally, RGO–Au nanocomposites could be produced through simultaneous and sequential sonolytic reduction of GO and Au^{3+}, respectively. Besides, sonochemical strategy has been successfully implemented to prepare RGO–Rh and RGO–TiO_2 composites.[266,267] Shi and Zhu *et al.*[268,269] also used the sonoelectrochemical technique to fabricate RGO–Pd and RGO–PdPt alloy nanocomposites, in which an ultrasound emitter also acts as a cathode.

3.1.2. Direct decomposition of precursors. The methods of thermolysis precursors directly have advantages over other methods in the simplified fabrication procedure and the high purity of the products. Thermal decomposition of hydroxide on GN sheets is a powerful strategy for preparing GN–metal oxide nanocomposites. The superiority of this synthesis route is that the annealing process can simultaneously achieve GO reduction and metal oxide nanocrystallite growth. As a result, metal oxide NPs with small-size, uniform-crystallization, and often nanoporous structures were tightly adhered to RGO nanosheets. Through the heat-treatment of corresponding hydroxide composites, metal oxide, such as Co_3O_4,[270,271] RuO_2,[272] Fe_3O_4,[273] and NiO[274] have been uniformly formed on RGO nanosheets. Rajamathi *et al.*[20] fabricated RGO–metal oxide (CoO, NiO and Co_3O_4) nanocomposites through the thermal decomposition of GO-intercalated hydroxides of Ni and Co. Hu *et al.*[275] presented a novel two-step strategy for preparing RGO–oxide nanocomposites: precipitating hydroxides onto GO followed by microwave-assisted hydrothermal/solvothermal annealing. With this method, several unitary and binary oxides (Mn_3O_4, TiO_2, SnO_2, $NiCo_2O_4$, Zn_2SnO_4) NPs were uniformly anchored on the RGO nanosheets. Compared with annealing in air at elevated temperatures, the solvent-enriched surroundings of hydrothermal/solvothermal annealing method was believed to limit the coalescence of nanocrystallites and guarantee the formation of nanometre-sized crystals. In addition, Co–Ni LDH (Co/Ni molar ratio of 2 : 1) were assembled on negatively charged GO nanosheets.[276] Subsequent thermal treatments resulted in the formation of the RGO–$NiCo_2O_4$ composites.

So far, decomposition of metal complexes has also been used to prepare GN–inorganic nanocomposites, such as the utilization of metal acetylacetonate in synthesis of GN–metal oxide composites,[277–279] and metal carbonyl complex in fabrication of GN–metal nanocomposites.[280,281] In this case, functional groups of the metal complex can connect to the surface of GN through covalent or noncovalent interaction, which could ensure a homogenous dispersion of the NPs on GN. For instance, Müllen and coworkers reported the dispersion of cobalt phthalocyanine onto GN through π–π stacking interactions, which could then turn into RGO–Co and RGO–Co_3O_4 nanocomposites after simple pyrolysis and oxidation processes, respectively.[282] Gotoh *et al.*[283,284] investigated the preparation of RGO–metal/metal oxide nanocomposites by heat treatment of ion-exchanged graphite oxide, which include cations of amine complexes ($[M(NH_3)_n]^{x+}$, M = Pt, Ru, Pd, Cu, Co, Ni), bipyridyl complex ($[Au(bipy)Cl_2]^+$), and imidazole complex ($[Ag(imH)_2]^+$). In obtained materials, it is found that all noble metals existed on RGO sheets were metal NPs, whereas Cu and Co existed as metal oxides, and Ni with a partly oxidized surface.

3.1.3. Hydrothermal/solvothermal techniques. Recently, hydrothermal and solvothermal syntheses have been frequently used in making GN–inorganic nanocomposites. These syntheses were usually performed in high-temperature solutions with high vapor pressure using a steel pressure vessel called autoclave. The advantage of hydrothermal/solvothermal techniques is the ability to form NPs or nanowires without the need for post-annealing and calcination. By far, GN-supported metal oxide, hydroxide, and chalcogenide NPs have been synthesized by hydrothermal/solvothermal techniques with GO as the precursor of GN. Occasionally, the hydrothermal/solvothermal synthesis of RGO–noble metal composites were also reported.[285] Due to the high-temperature and long-time reaction process, GO can be partly or completely reduced.[86] But in most cases, reducing agents were also used to make sure the complete reduction.

GN-supported metal oxide and hydroxide NPs synthesized through hydrothermal/solvothermal process mainly include ZnO,[286,287] TiO_2,[288–291] Fe_3O_4,[19,292–295] SnO_2,[296,297] Co_3O_4,[298] Bi_2O_3,[299] Fe_2O_3,[300] CoO,[300] MnOOH,[301] and $Co(OH)_2$.[302] Also, hydrothermal synthesis can also be employed to grow vertically aligned metal oxide nanowires on GN films. Kim *et al.*[303] reported a nanocomposite consisting of ZnO nanowires hydrothermally grown on RGO substrates. Firstly, a ZnO seed layer was obtained by spin casting of ethanol solution of zinc acetate on RGO surface for several times, and then dried at 90 °C. In the second step, ZnO nanowires were grown by suspending the seeded RGO substrates in an aqueous solution of zinc nitrate hexahydrate and hexamethylenetetramine at 90 °C for 3 h. The two-step method for the synthesis of GN-supported ZnO nanowires could also be found in other literature.[304,305]

Wang and Dai *et al.*[179,306] also developed a two-step method for growing Ni, Fe, and Co hydroxide and oxide nanocrystals with well-defined morphologies on GN surfaces. In the first step, they uniformly nucleated dense $Ni(OH)_2$ NPs onto GN by hydrolysis of $Ni(CH_3COO)_2$ in a *N*,*N*-dimethylformamide (DMF)/water mixture at 80 °C. In the second step, they hydrothermally treated the product of the first step at 180 °C and the dense $Ni(OH)_2$ NPs coated on GN nanosheets diffused and recrystallized into single-crystalline hexagonal $Ni(OH)_2$ nanoplates. However, this phenomenon was not observed from the GO–$Ni(OH)_2$ nanocomposite with the reason that $Ni(OH)_2$ NPs precoated on GO were pinned by the high concentration functional groups and defects on GO without recrystallization into well-defined morphologies (Fig. 5). These results confirm that GN with various degrees of oxidation can be used as a novel substrate for the growth of nanocrystals into various sizes and morphologies. The two-step hydrothermal method has also been developed to grow Mn_3O_4,[307] TiO_2,[308] and CuO[309] nanocrystals on the surface of GN nanosheets.

Currently, various chalcogenide QDs, such as CdS,[310–312] ZnS,[311,313] Cu_2S,[297] MoS_2,[314] Sn_3S_4,[155] and CdTe[315] have been successfully immobilized on GN through hydrothermal/solvothermal processes. Besides GO and metal salts, sources of S or Te were also needed. In the fabrication of RGO–sulfide nanocomposites, sulfur sources often acted as reducing agents of GO.[310,313,314] For instance, Cao *et al.*[310] developed a solvothermal process to synthesize RGO–CdS composite directly from GO and $Cd(CH_3COO)_2$ in DMSO at 180 °C. In the one-pot reaction, DMSO not only serves as a solvent and a source of sulfur, but also produces H_2S to reduce GO simultaneously.

3.1.4. Gas-phase phase deposition. Gas-phase deposition techniques are common methods to deposit inorganic materials onto various surface. Here, we provide examples of synthesis of various GN–inorganic nanocomposites using gas-phase deposition techniques including physical vapor deposition (PVD), CVD, and atomic layer deposition (ALD).

3.1.4.1. Physical vapor deposition. PVD is a general term used to describe a variety of purely physical methods to deposit solid material by condensation of a vaporized form of the material onto various surfaces, which involves vacuum deposition and sputtering deposition. The advantage of PVD in GN-based inorganic nanocomposites synthesis is that it can directly deposit films on the basal planes of defect-free pristine GN without any functionlization, which can preserve the intrinsic properties of GN. Sun *et al.*[316] evaporated the Au film onto the surface of micromechanical exfoliated *n*-layer (*n*: 1∼4) GN in a vacuum thermal evaporator at a deposition rate of 1.0 Å s^{-1} under a vacuum of $\sim 10^{-4}$ Pa, followed by heat treatment at 1260 °C. It was found that the morphologies of Au film on *n*-layer GN are dependent on the layer number, the lower GN layer number, the smaller average size of Au NPs, and the higher density of NPs. They also thermally deposited Ag films onto *n*-layer GN and found that the morphologies of Ag NPs on *n*-layer GN are also dependent on the layer number.[317] This phenomenon was also observed and further researched by Johnson and co-workers.[318] They proposed a theoretical model predicting a particle size distribution characterized by a mean diameter *D* that follows a $D \propto n^{1/3}$ scaling law where *n* is the number (1∼9) of layers in the GN film. This method could be applied in checking the different layer numbers of GN and growing NPs with controlled dimensions. Besides, an ultra-high vacuum (UHV) system was often used for the deposition of metal nanoclusters on moiré-patterned GN supported on transition metals, such as Ir, Pt, W, Re on GN/Ir(111);[319,320] Pt, Pd, Rh, Co and Au on GN/Ru(0001).[321,322] Moreover, magnetron sputtering has been used to deposit Pt on the CVD-growth's GN nanoflakes.[323] The thickness of Pt nanoclusters, ranging from 2.1 to 85 nm, could be simply controlled by tuning the sputtering time. The deposition of high dielectric constant Al_2O_3 by radio frequency magnetron sputtering on multilayer epitaxial GN grown by graphitization of SiC was also reported.[324]

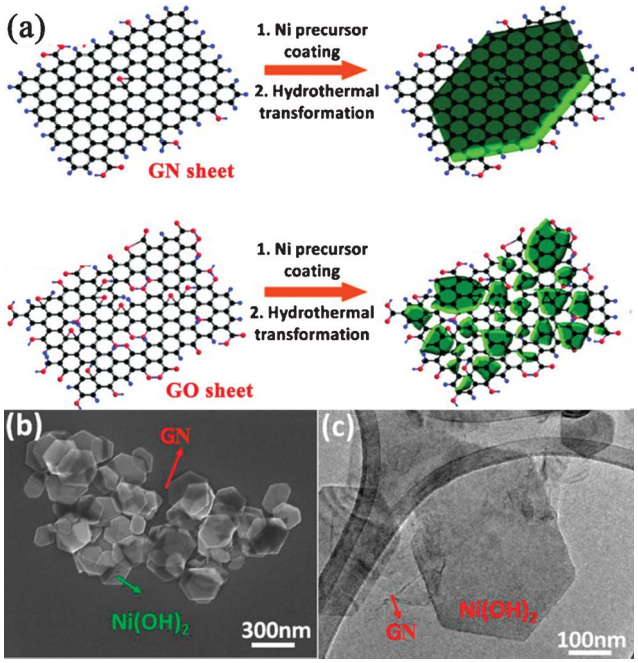

Fig. 5 (a) Schematic illustration of two-step $Ni(OH)_2$ nanocrystals hydrothermal growth on (top) GN and (bottom) GO sheets. (b) SEM and (c) TEM images of hexagonal $Ni(OH)_2$ nanoplates formed on top of GN sheets. Reprinted with permission from ref. 306. Copyright 2010, American Chemical Society.

3.1.4.2. Chemical vapor deposition. CVD is a chemical process used to produce high-purity, high-performance solid materials on a substrate surface. In a typical CVD process, one or more gaseous precursors flow over a substrate surface, which react or decompose to produce the desired material on it. In comparison with PVD, the advantages of CVD include high deposition rate, controllable composition and inexpensive equipment. CVD has been used to synthesize GN-supported semiconductors, such as CdSe NPs,[325] ZnO nanorods,[326] and ZnS nanowires.[181] It is interesting that through CVD, nanocrystals with various morphologies can grow on the surface of GN. A representative example is that ZnO nanostructures were successfully grown on GN with zinc powder as a precursor carried by Ar flow at different temperature, and followed by oxygen flow in a tube furnace.[326] It was observed that ordered crystalline ZnO with high density is preferably vertically grown along the <0001>

direction. Different nanorods and nanoneedles were obtained when the growth temperatures were 450 °C, 550 °C and 650 °C, respectively.

The more important aspect in CVD synthesis of GN–inorganic composites is the vertical growth of CNTs on GN nanosheets.[327–329] Different from the CVD synthesis of GN-semiconductor composites, catalysts were indispensable in the formation process of GN–CNT composites. Zhao *et al.*[328] prepared the GO/RGO sheets pillared with CNTs using CVD method with acetonitrile as the carbon source and Ni NPs as the catalyst. The Ni NPs were deposited on GO/RGO platelets, and CNTs were then grown on them through a tip growth model with Ni catalysts residing at the top of them. Both the amount and length of CNTs could be adjusted by the amount of Ni catalyst and CVD times, respectively (Fig. 6). With the same growth mechanism, Fan *et al.*[329] prepared a RGO–CNT composite with Co as a catalyst and CO as the carbon source. They also employed Co NPs as a catalyst to deposit carbon nanofibers on the RGO sheets stemming from the pyrolysis of GO during the CVD process.[145]

3.1.4.3. Atomic layer deposition. ALD is a thin-film growth technique with atomically precise control over thickness and uniformity. ALD is different from the CVD method with the distinctive feature of alternate and cyclic supply of each gaseous precursors with two sequential half-reactions, which makes film growth self-limiting based on surface reactions. The work of Dai *et al.* provides an excellent example of ALD in coating GN with metal oxide films.[330] Through alternating pulses of trimethylaluminum and water as precursors at ~100 °C, the authors deposited Al_2O_3 NPs on pristine and 3,4,9,10-perylene tetracarboxylic acid (PTCA)-coated GN respectively. They found Al_2O_3 cannot directly be deposited on pristine GN due to the lack of dangling bonds and functional groups, and only preferentially grow actively on edges and defect sites, which could be used as a simple and effective probe to defects in GN. Uniform ultrathin Al_2O_3 deposition was achieved on PTCA-coated GN because of their densely packed functional groups (Fig. 7). Besides Al_2O_3, other dielectrics such as HfO_2 films grown on GN by ALD were also reported,[331,332] revealing that the ALD method is promising to be used for depositing ultrathin high-κ dielectrics for future GN electronics.

The ALD strategy exhibits many unique advantages in fabricating GN–metal oxide nanocomposites, which can tune and control the deposited metal oxide on both morphologies and structural phases. Sun *et al.*[333] demonstrated the coating of SnO_2 on RGO sheets with $SnCl_4$ and H_2O as the ALD precursors. Both amorphous and crystalline SnO_2 NPs have been uniformly grown on RGO sheets by adjusting the growth temperature to 200 and 400 °C, respectively. The change of structural phases was attributed to the temperature dependent surface reactions. By adjusting their cycling numbers, the as-deposited SnO_2 could present NPs or nanofilms on RGO. They also deposited TiO_2 on RGO nanosheets by ALD with titanium isopropoxide and water as precursors.[334] It was found that a lower temperature (150 °C) contributed to amorphous TiO_2, while a higher temperature (250 °C) produced crystalline anatase TiO_2.

3.1.5. Sol–gel processing. The sol–gel process is a cheap and low-temperature technique that undergoes a series of hydrolysis and polycondensation reactions. One of the major drawbacks is that the product typically consists of an amorphous phase rather than defined crystals and, thus, requires crystallization and post-annealing steps. Nowadays, the sol–gel process in synthesis of GN–metal oxide nanocomposites has rarely been explored. For instance, Ruoff and co-workers[196] fabricated RGO–silica

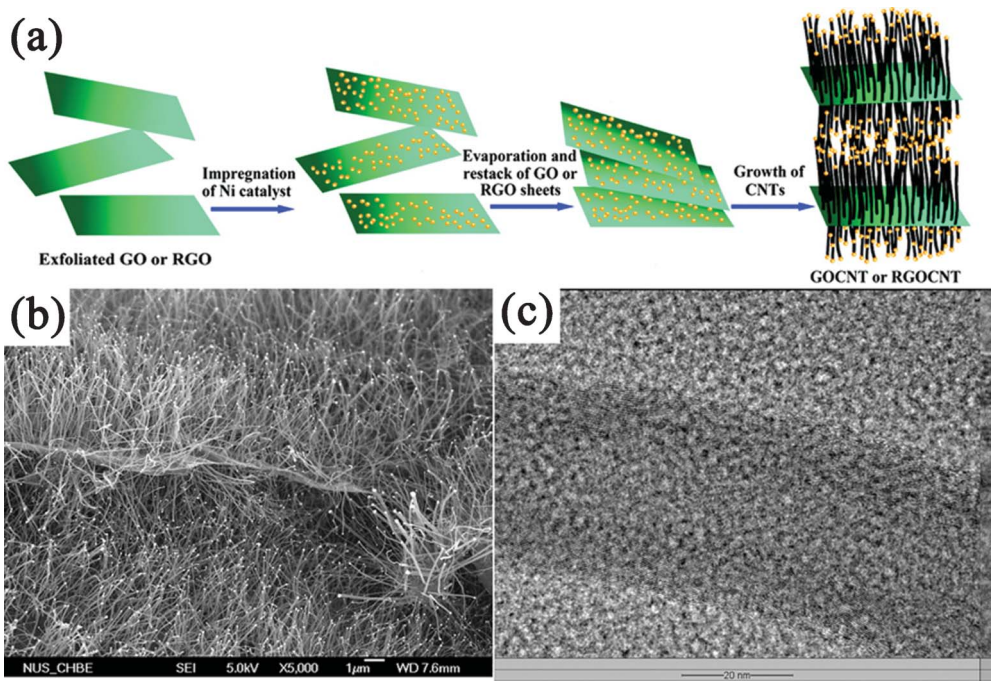

Fig. 6 (a) Scheme illustrating the experimental steps of pillaring GO/RGO platelets with CNTs. (b) Field emission SEM (FESEM) and (c) TEM images of the CNT-pillared GO nanosheets. Reprinted with permission from ref. 328, Copyright 2010, American Chemical Society.

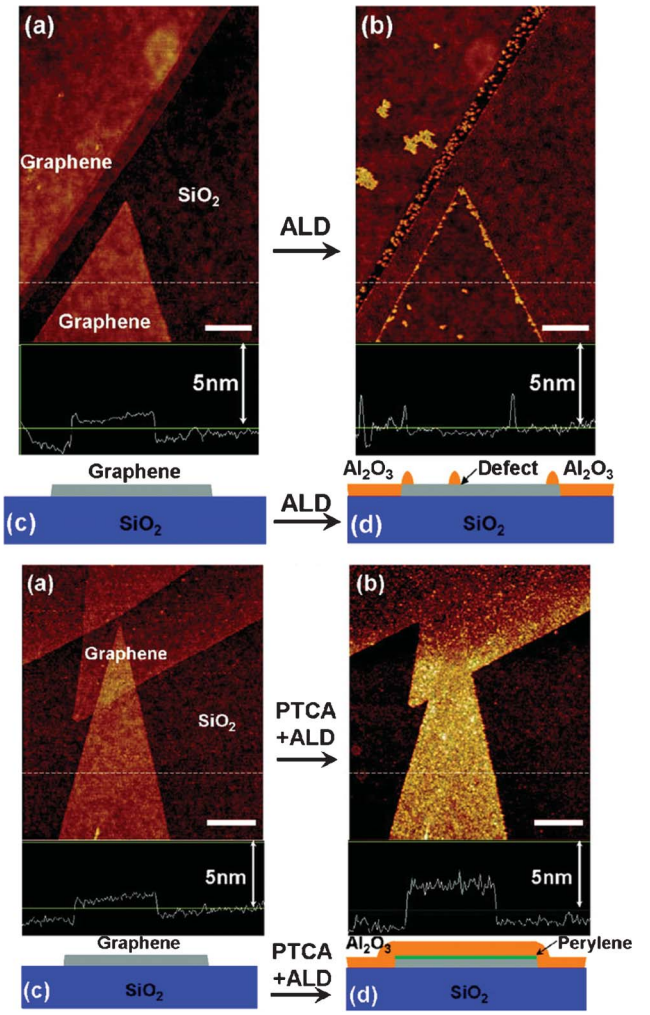

Fig. 7 ALD of Al_2O_3 on (Top) pristine GN and (Bottom) PCTA-coated GN. (a) Atomic force microscopy (AFM) image of GN on SiO_2 before ALD. (b) AFM image of the same area as (a) after Al_2O_3 ALD deposition. (c) and (d) Schematics of GN on SiO_2 before and after ALD. Reprinted with permission from ref. 330. Copyright 2008, American Chemical Society.

composite thin films by the hydrolysis of TMOS a the water–ethanol dispersion of GO, followed by spin-coating into composite films, chemical reduction with hydrazine monohydrate vapor, and thermal curing into consolidated films. Cui *et al.*[335] reported a sol–gel route in coating TiO_2 on RGO sheets, including: adding tetrabutyl titanate into the ethanol dispersion of RGO sheets. After magnetically stirring for 2 days, acetic acid and water were added, separately. The obtained sol was dried with water bath at 80 °C and annealed at 450 °C for 2 h in the end. Besides, the sol–gel processes in the fabrication of hydrous RuO_2,[272] $Li_3V_2(PO_4)_3$,[336] and $Li_4Ti_5O_{12}$[337] NPs on GN were also reported.

3.1.6. Template methods. Template methods encompass a broad array of synthetic strategies, and frequently involve methods which are hybrids of the above-mentioned techniques. In the synthesis procedure, templates can serve multiple roles, such as nucleation centers during synthesis, stabilizing agents for synthesized materials, and directing matrices assembly. Nowadays, sacrificial templates methods are usually used in fabricating GN–inorganic nanocomposites. For instance, Fu *et al.*[338] fabricated a RGO–Pd nanocomposite *via* the sacrifice of a Cu template: RGO–Cu nanocomposites with large size and poor distribution of Cu NPs were prepared first, and then Pd NPs with small size and uniform dispersion were formed on RGO nanosheets by a simple galvanic displacement process between Pd^{2+} and Cu. It is found that the galvanic displacement process not only occurred between the Pd^{2+} and Cu connected to each other, but also between unconnected Pd^{2+} and Cu through the electron transmission of RGO nanosheets. Zhao *et al.*[144] fabricated RGO–carbon sphere nanocomposites with mesoporous silica spheres as the template. Colloidally dispersed negatively charged GO sheets strongly interacted with positively charged mesoporous silica spheres to form a GO–mesoporous silica composite. The mesoporous silica was then used as a template for replicating mesoporous carbon spheres *via* a CVD process, during which the GO sheets were reduced to RGO nanosheets. Removal of the silica spheres with HF solution left behind a RGO–carbon sphere composite. Besides, GO–periodic mesoporous silica sandwich nanocomposites with vertically oriented channels were fabricated with surfactant admicelles as the sacrificial template.[339] RGO–silica sheets were also employed as a sacrificial template to fabricate GN-based mesoporous carbon and Co_3O_4 sheets by a simple nanocasting approach with sucrose as the carbon source and cobalt nitrate as the cobalt source, respectively.[226]

Through template approaches, regular distribution of arrays on GN sheets was also realized, which is difficult to achieve through other methods. Kim *et al.*[340] created a nanopatterned iron catalyst array on the GO film by means of self-assembled block-copolymer nanoporous templates and then highly aligned CNTs were grown from the catalyst by plasma-enhanced CVD (PE-CVD). In this growth method, GO films were reduced during the high-temperature PE-CVD process, and the nanoporous templates enabled the precise adjustments of the particle size of the catalyst, and thus tuning the CNT diameter. Hong *et al.*[341] synthesized a CdSe QDs array on the basal plane of GN using a mesoporous silica thin film as a template: (a) GN nanosheets were synthesized by CVD of methane on thin Ni layers formed on SiO_2/Si substrates; (b) a mesoporous silica film was formed on top of the GN by spin-coating, aging and calcination; (c) CdSe was electrochemically deposited onto a GN surface through the pores of the mesoporous silica film; (d) silica template and Ni layer underneath the GN was removed (Fig. 8). Other nanoarrays such as ZnO nanorods,[342] and NiO nanocapacitors[343] have also been fabricated on GN following the template procedures.

3.2. *Ex situ* approach: assembly on graphene surface

In the *ex situ* approach, inorganic components were synthesized in advance and then attached to the surface of GN *via* linking agents that utilize covalent or noncovalent interactions (van der Waals interactions, hydrogen bonding, π–π stacking, or electrostatic interactions). In this approach, either the inorganic components or GN (or both) require modification with functional groups. The type of functionalization and thus, the strength of interaction determine the loading of the inorganic

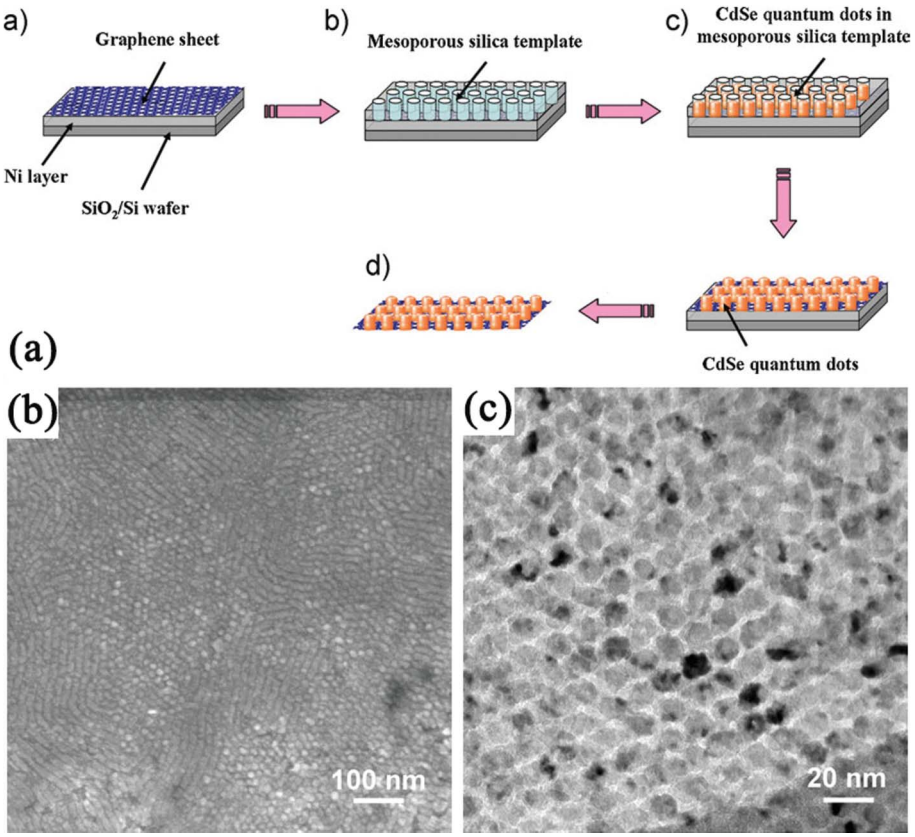

Fig. 8 (a) Procedure to synthesize a CdSe QDs array on the basal plane of a GN using a mesoporous silica thin film as a template. (b) TEM and (c) High-resolution TEM (HRTEM) images of a CdSe quantum-dot array grown on the GN. Reprinted with permission from ref. 341. Copyright 2010, John Wiley & Sons, Inc.

nanomaterials on the GN surface. This self-assembly based method is excellent at overcoming any incompatibilities between nanomaterials syntheses and the formation of nanocomposites. Compared to *in situ* growth, the better distribution, size, and feeding amount control of the second components on GN could be obtained by the self-assembled methods.[344] For example, Bovine serum albumin (BSA), a complex amphiphilic protein were reported to absorb on the basal plane of GN for the assembly of NPs.[345] In this system, BSA could not only attach to GO, but also reduce GO to RGO at a suitable pH value and reaction temperature. By simply mixing BSA–GO/RGO with pre-synthesized Au, Pt, Ag or Pd NPs, corresponding GO/RGO-metal nanocomposites were prepared (Fig. 9). The density of metal NPs on BSA–GO could be easily controlled by changing the concentrations of BSA during the assembly process. This well-controlled self-assembly method also produces coassembly of presynthesized NPs with distinctively different sizes, compositions, shapes, and properties on the same GO/RGO nanosheets.

3.2.1. Covalent interactions. In covalent interactions, GO rather than RGO is preferred to be used in immobilizing inorganic components, due to its large amount of oxygen-containing groups, to facilitate the linkage with other functional groups. Fan *et al.*[346] modified Fe_3O_4 with tetraethyl orthosilicate and (3-aminopropyl) triethoxysilane to introduce amino groups on its surface, and the amino groups of Fe_3O_4 were reacted with the carboxylic groups of GO with the aid of 1-ethyl-3-(3-dimethyaminopropyl)carbodiimide and *N*-hydroxysuccinnimide to form a GO–Fe_3O_4 nanocomposite. Zhang *et al.*[347] reported another route to covalent assemble of Fe_3O_4 NPs on GO nanosheets. Fe_3O_4 NPs were modified by hydrophilic 2,3-dimercaptosuccinnic acid (DMSA), followed by assembling the DMSA-modified Fe_3O_4 NPs onto polyetheylenimine (PEI)-grafted GO sheets *via* the formation of amide bonds between COOH groups of DMSA molecules and amine groups of PEI. Jeong *et al.*[348] used a multistep procedure to attach CdS on GO sheets with amide bonds: (1) 4-aminothiophenol-functionalized CdS NPs were prepared; (2) GO sheets were acylated with thionyl chloride to introduce acyl chloride groups on their surface; (3) CdS NPs were linked to the GO sheets through an amidation reaction between the amino groups located on the CdS surface and the acyl chloride groups bound to the GO surface. With the covalent approach, they also immobilized Au and Fe-core–Au-shell NPs on GO sheets.[349,350]

In addition, covalent interactions were also used in synthesis of GN–carbon nanocomposites. For example, the covalent linkage between the aminated CNTs and the acid chloride-activated GO formed GO–CNT composites.[351] Chen *et al.* reported two methods for the covalent linkage of C_{60} with GO sheets. One was to adopt a mild coupling reaction between hydroxyl groups of fullerenol and carboxylic groups of GO,[352] while another was to form amide carbonyl groups between pyrrolidine fullerene and carboxylic group of GO *via* a coupling

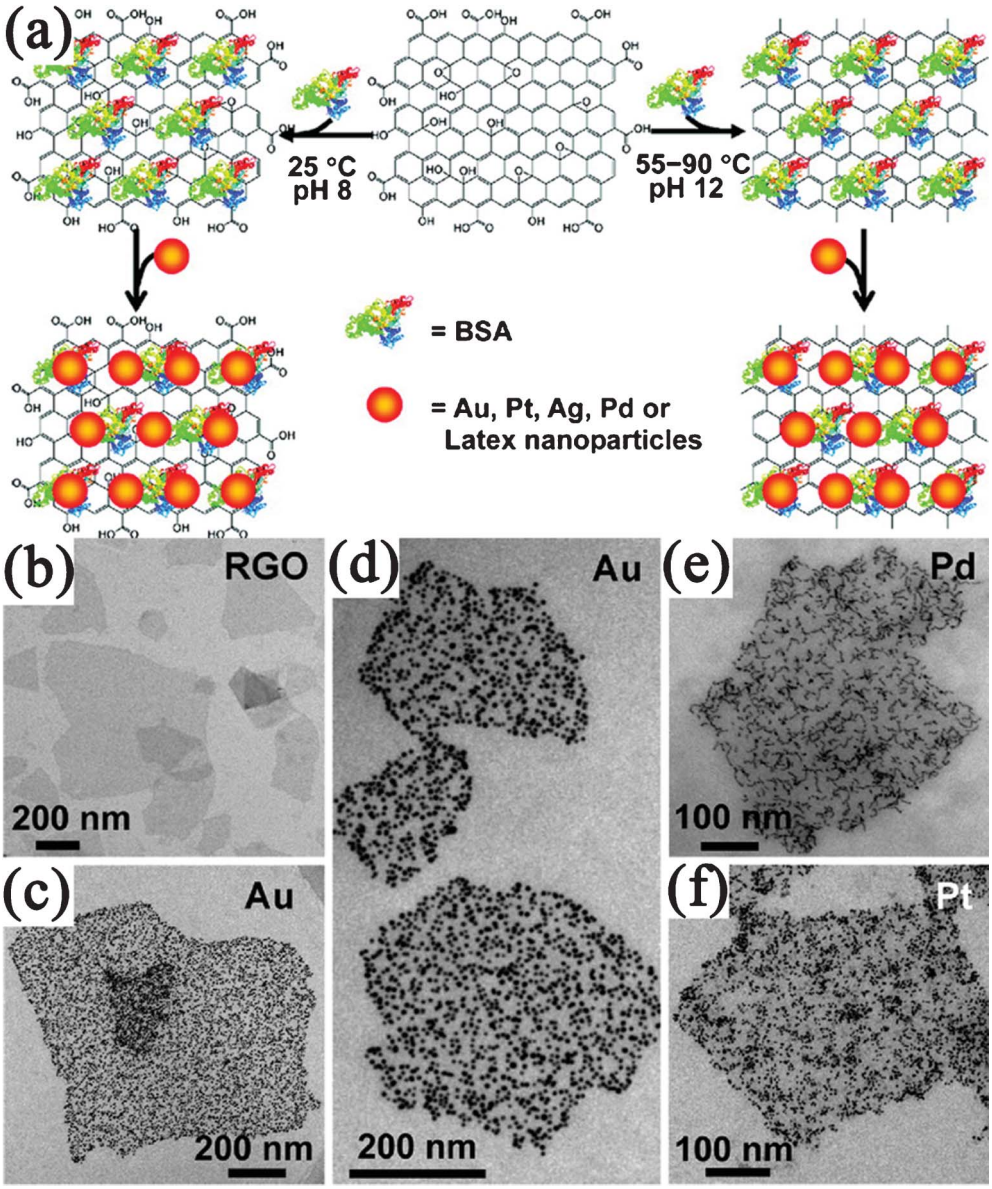

Fig. 9 (a) Illustration of assembly of noble metal NPs on GO/RGO nanosheets with the assistance of BSA. TEM images of (b) BSA–RGO nanosheets and BSA–RGO supported (c,d) Au, (e) Pd, and (f) Pt NPs. Reprinted with permission from ref. 345. Copyright 2010, American Chemical Society.

reaction.[353,354] Wang *et al.*[355] reported the covalent bonding of fullerenes onto GO by the chemical reaction through the Fisher esterification between the hydroxyl groups on GO and the carboxyl groups on (1,2-methanofullerene C_{60})-61-carboxylic acid.

3.2.2. Noncovalent interactions. Alternatively, inorganic components can be attached to GN *via* van der Waals interactions, hydrogen bonding, π–π stacking, or electrostatic interactions. Among the noncovalent techniques above, π–π stacking and electrostatic interactions have been widely used in the fabrication of GN–inorganic nanocomposites. Furthermore, the noncovalent approaches have also been extended to assemble GN nanosheets with the second components layer-by-layer (LBL).

3.2.2.1. π–π stacking. Noncovalent functionlization of GN with aromatic organic compounds through π–π stacking has been mentioned earlier (Section 2.1.3.). Herein, we discuss the attachment of inorganic nanomaterials on the surface of GN through this functionlization process. Generally, these aromatic compounds are terminated with thiol (mercaptan), amine, or acid groups, which can connect to the inorganic NPs and enable their attachment to GN *via* π–π stacking. For example, pyridine, with an aromatic structure, has provided π–π stacking interactions for anchoring Au[356] and CdSe[357] NPs on the basal planes of GO/RGO sheets. DNA molecules containing both purine and pyrimidine bases could be also used to mediate the fabrication of GN nanocomposites *via* π–π stacking interactions. Both thiolated DNAs and pyrene-labeled DNAs have been used to stablize Au NPs on GN.[358,359]

Following a similar strategy, Huang *et al.*[360] fabricated DNA-conjugated Au and Ag NPs on GO nanosheets, respectively. Zhan *et al.*[361] reported the decoration of RGO with CdS QDs by using benzyl mercaptan (BM) as the interlinker. During the synthesis process, the mercapto substituent of BM binds to the CdS QDs during their nucleation and growth process, and then the phenyl comes into contact with the RGO sheets *via* the π–π stacking interaction.

It is also worthy of note that GO behaves like an amphiphilic molecule containing hydrophobic aromatic regions on the basal plane and hydrophilic oxygen groups on the edges, which can adsorb the pristine CNT through the π–π interaction with the hydrophobic basal plane, and assist to stabilize the dispersion of CNT in aqueous media due to the hydrophilic edges. This means that the GO–CNT composite films could be readily formed by vacuum filtration of the aqueous dispersion without any additional organic solvents or pre-functionalisation involved.[362,363]

3.2.2.2. Electrostatic interactions. Electrostatic interactions have also been utilized to modify GN with various inorganic NPs. GO/RGO are negatively charged as a result of the ionization of the oxygen functional groups on them, which could be used to assemble with positively charged inorganic NPs through electrostatic interactions. For instance, RGO–Fe_3O_4 nanocomposites have been formed by mixing the positively charged Fe_3O_4 NPs and negatively charged RGO nanosheets.[364] Chen *et al.*[365] noncovalently decorated GO sheets with oppositely charged aerosol Ag nanocrystals synthesized from an arc plasma source using an electrostatic force directed assembly technique. A novel strategy for the fabrication of RGO-encapsulated oxide (silica, Co_3O_4) NPs was developed by coassembly between negatively charged GO and positively charged oxide NPs with three steps: oxides were firstly modified by surface grafting of aminopropyltrimethoxysilane (APS) to render the oxide surface positively charged; then the modified oxide NPs were assembled with negatively charged GO by electrostatic interactions; finally, the resulting composites were chemically reduced with hydrazine (Fig. 10).[191,366] However, the negative charge of RGO is often too weak to assemble some NPs directly. So the functionlization of GN is also needed, such as the use of 1-pyrene butyric acid functionalized GN to anchor positively charged Au NPs.[367]

On the contrary, when the NPs are negatively charged, it is necessary to alter the surface of GO/RGO to positively charged. The deposition of a cationic polyelectrolyte is a common route. For example, RGO nanosheets could accept negatively charged Ag NPs after noncovalent functionalized with polyelectrolyte PQ11.[368] Cationic polyelectrolyte poly(diallyldimethyl ammonium chloride) (PDDA) coated GN nanosheets were served as platforms for citrate-capped Au NPs and thioglycolic acid modified CdSe QDs, respectively.[369,370] Wang *et al.*[371] self-assembled negatively charged mixed Pt and Au NPs onto positively charged PDDA-functionalized RGO nanosheets as effective electrocatalysts, while dispersed MnO_2 nanosheets were dispersed on PDDA-functionalized RGO nanosheets as

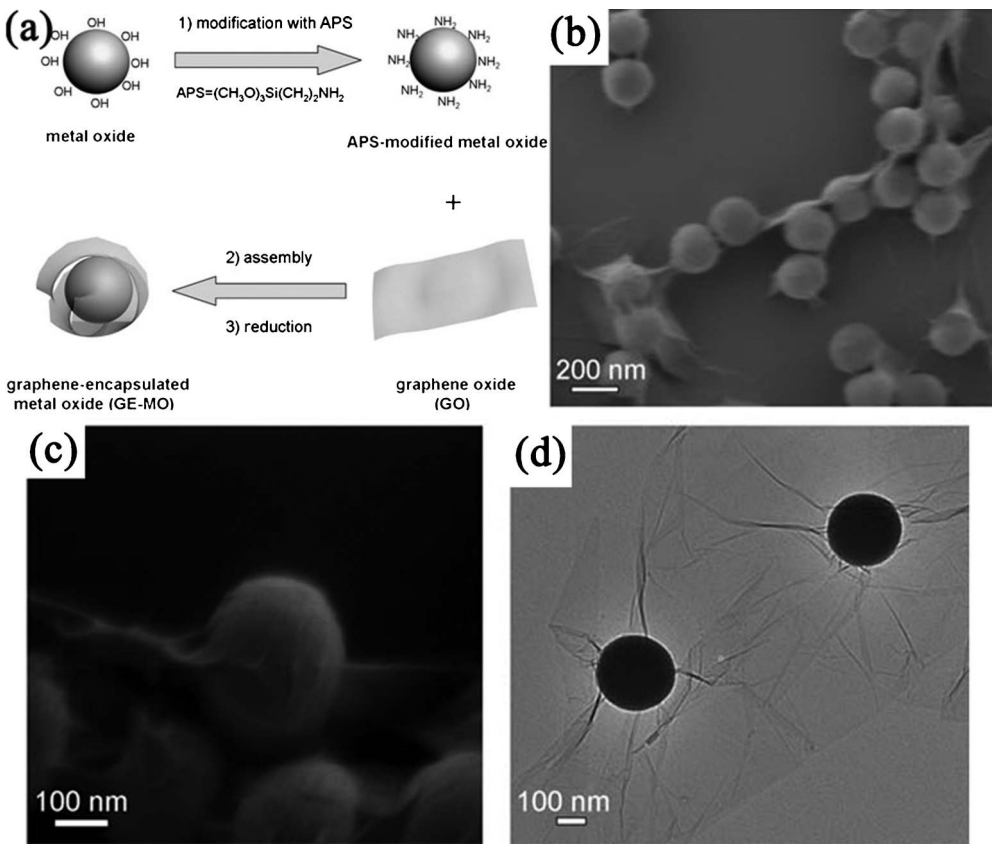

Fig. 10 (a) Schematic illustration of fabrication of RGO-encapsulated oxide NPs. (b,c) Typical SEM, and (d) TEM images of RGO-encapsulated silica spheres. Reprinted with permission from ref. 366. Copyright 2010, John Wiley & Sons, Inc.

electrode materials for pseudocapacitors.[372] Besides, the self-assembly of GN with CNT can also be accomplished with this approach. Cationic PEI modified RGO was used for assembly with negatively charged acid-oxidized CNT.[373] On the other hand, GN–CNT nanocomposites were prepared by a combination of positively charged aminated CNTs with negatively charged GO.[374]

3.2.2.3. Layer-by-layer self-assembly. LBL self-assembly is a widely used method for fabricating GN–inorganic nanocomposite films. The obtained films are typically formed by alternating layers of GN nanosheets with the second components. There are many advantages of the LBL assembly technique, such as simplicity and thickness controllability in the nanoscale. Moreover, the blending of two components into composites and the fabrication of composites into films were carried out simultaneously. Other film fabrication techniques, such as vacuum assisted self-assembly were also used in fabricating GN–inorganic nanocomposite multilayer films, but the composites usually need to be prepared in advance.[375]

The LBL self-assembly route to fabricate films of GN–inorganic composites were mainly performed through the electrostatic interaction of alternating layers with opposite charge. For example, positively charged imidazolium salt-based ionic liquid-functionalized GN were LBL self-assembled with negatively charged citrate-stabilized Pt NPs into 3D composite films.[376] Loh *et al.*[377] assembled negatively charged GO and negatively charged titania nanosheets into multilayer films with cationic PEI as linkers. Exposure of the films to UV irradiation allows both the reduction of GO and the photocatalytic removal of the PEI moiety, and multilayered composite films consisting of alternating RGO and titania nanosheets were obtained. RGO and CdSe NPs multilayers were fabricated by negatively charged pyrene-grafted poly(acrylic acid)-RGO nanosheets with positively charged CdSe NPs.[378] Also, with the electrostatic LBL self-assembly, thin films of $(RGO/CNT)_n$,[26] and $(GN/carbon\ nanospheres)_n$[379] composites were also fabricated.

Positively charged polyelectrolytes of PDDA were often used as building blocks to fabricate 3D multilayer architectures by the electrostatic LBL technique. Wang *et al.*[380] employed the negatively charged species of poly(sodium 4-styrenesulfonate) (PSS) modified RGO, negatively charged MnO_2 sheets, and positive charged PDDA as building blocks to fabricate 3D multilayer architectures $(PDDA/PSS\text{-}RGO/PDDA/MnO_2)_{10}$. Yu *et al.*[381] fabricated $(PDDA/GO/PDDA/TiO)_{20}$ composite films on the glass substrate through alternative LBL self-assembly with GO, titania nanosheets, and PDDA. Besides, hydrogen-bonding LBL assembly was also used to fabricate GN–inorganic composite films. By utilizing the hydrogen bonding interaction of poly(vinyl alcohol) (PVA) with both GO and LDH, followed with a reduction process, Liu *et al.* fabricated electrically conductive $(LDH/PVA/RGO/PVA)_{50}$ multilayer films.[382]

4. Applications of graphene–inorganic nanocomposites

As discussed above, GN can be combined with various inorganic nanomaterials through different architecture types and synthesis techniques. The GN–inorganic nanocomposites are expected to not only preserve the favorable properties of GN and the second components, but also greatly enhance the intrinsic properties due to the synergetic effect between them. In this section, we presents the improved performance of GN–inorganic nanocomposites in catalysis, energy storage and conversion, sensors, and other applications.

4.1. Catalysis

Carbon materials have been widely used as the support for immobilizing inorganic catalysts, mainly due to their large specific surface area, excellent electrical and thermal conductivity, low price, high chemical inertness, easy modification and loading. Like other carbon-based catalysts, GN–inorganic nanocomposites have been developed as active catalysts in chemical, electrochemical as well as photochemical reactions.

4.1.1. Catalysis of C–C coupling reactions. One of the catalytic applications in which GN support may provide some significant advantages is in the area of cross-coupling chemistry. C–C cross-coupling reactions have been extensively used in the synthesis of complex organic molecules for a wide variety of applications in chemical and pharmaceutical industries. With GN as the supporting materials, the noble metal heterogeneous catalysts exhibit high catalytic activity, selectivity and recyclability. The Suzuki reaction is one of the most important C–C coupling reactions, which is predominately catalyzed by Pd catalysts. Nowadays, GN–Pd nanocomposites have been employed as catalysts for Suzuki reactions.[131,132,383,384] Especially, Mulhaupt *et al.*[131] have demonstrated a RGO–Pd nanocomposite catalyst exhibiting extraordinary high activities with turnover frequencies up to 39 000 h^{-1} as well as very low Pd leaching (< 1 ppm (parts-per-million)) in the Suzuki–Miyaura coupling reaction. Moreover, these novel heterogeneous catalysts were readily available and easy to handle as they are stable in air. Also, another important coupling reaction, the Heck reaction, with GN–Pd composites as catalysts was also reported.[384,385] Wang *et al.*[385] immobilized Pd NPs on GO and assembled the composite into a 3D macroscopic porous structures. This catalyst exhibited excellent catalytic activity and selectivity for the Heck reaction. Both the selectivity and conversion were measured to be 100% when K_2CO_3 was used as the base in the reaction of iodobenzene and methyl acrylate. These values are much higher than the results obtained when the Pd catalyst is loaded onto other supports. The ideal supporting material also make GN–Au nanocomposites active catalysts for Suzuki reactions, though Au NPs alone were generally poor in catalyzing these reactions.[174,386]

4.1.2. Electrocatalysis. GN–inorganic nanocomposites for electrochemical catalysis have attracted great interest in the past few years. The introduction of GN nanosheets into the catalysis system was expected to present enhanced catalytic activities and improved stabilities towards some important electrochemical reactions such as the methanol oxidation reaction (MOR) and oxygen reduction reaction (ORR) for fuel cells. The role of GN is attributed to its large surface area in stabilization of high dispersed catalyst NPs, its high conductivity in acceleration of the charge transfer, its residual oxygen groups in attenuating CO poisoning, the electrocatalytic performance of GN itself,[387] and so on.

The most widely used electrocatalysts with GN as the supporting material were Pt-based NPs, such as Pt,[130,204,209,233,234,254,324,388–392] Pt-based alloy (PtRu,[210,393–396] PtCo,[205,397] PtCr,[397] PtNi,[207] PtAu,[398] and PtPd[269]), bimetal (Pt–Pd,[399] Pt–Au[235]), and mixed Pt and Au nanocatalysts.[371] For example, Honma *et al.*[130] reported the enhanced activity and improved tolerance of a GN–Pt electrocatalyst for MOR compared to the CB–Pt catalyst. Liu *et al.*[388] demonstrated GN–Pt nanocomposites exhibited a higher electrochemical surface area and oxygen reduction activity with improved stability as compared with the Pt catalysts supported with other carbon materials (CNT and Vulcan XC-72 carbon). They also synthesized indium tin oxide (ITO) NPs directly on functionalized GN sheets, and then deposited Pt NPs, forming a unique triple-junction structure.[400] The GN–ITO–Pt nanocomposite was investigated as an electrocatalyst for oxygen reduction for potential application in polymer electrolyte membrane fuel cell, which showed enhanced performance not only better than the widely used Pt electrocatalysts supported with other carbon materials, but also better than Pt supported on GN sheets.

Considering the high cost and CO poisoning of platinum, many other metals and metal oxides NPs have also been combined with GN nanosheets to construct highly active non-platinum electrocatalysts. RGO–Pd nanocomposites have been developed as alternatives in electrocatalytic oxidation of ethanol, methanol or reduction of oxygen.[241,401–403] Meanwhile, RGO–Pd nanocomposites also exhibit excellent electrocatalytic activity and stability towards formic acid oxidation.[241,338,404] Niu *et al.*[405] deposited Au–ionic liquid on PTCA functionalized GN. It is found that the composite showed good electrocatalytic behavior toward ORR. Dai *et al.*[406] reported a composite consisting of Co_3O_4 NPs grown on RGO nanosheets (Fig. 11a) as a high-performance catalyst for ORR. Although Co_3O_4 or RGO alone has little catalytic activity, their composite exhibits an unexpected, surprisingly high activity that is further enhanced by nitrogen doping of the GN nanosheets (Fig. 11b, c, d). The N-doped RGO–Co_3O_4 (*N*-RGO–Co_3O_4) composite exhibits similar catalytic activity but superior stability to a fresh commercial C–Pt catalyst in alkaline solutions (Fig. 11e, f). The unusual catalytic activity arises from synergetic chemical coupling effects between Co_3O_4 and GN. They also grew MoS_2 NPs on RGO nanosheets, which exhibited superior electrocatalytic activity in the hydrogen evolution reaction relative to other MoS_2 catalysts.[407] In other cases, nanocomposites such as RGO–MnO_2[408] and RGO–SnO_2[396] were also reported for electrocatalytic applications. Besides, possessing the advantages of low costs and environmental friendliness, GN-based metal-free electrocatalysts were also developed. A typical example of this is a RGO–CN nanocomposite, which exhibits an excellent electrocatalytic performance for ORR, including high electrocatalytic activity, long-term durability, and high selectivity, all of which are superior to those observed for CN sheets without GN as well as for commercially available C–Pt catalysts.[169,170]

4.1.3. Photocatalysis. Developing high-efficient photocatalytic materials for environmental purification and converting photon energy into chemical energy have attracted increasing attention during the past decades. In general, when the photocatalyst is illuminated with photons having energies greater than that of the material's band gap, electron–hole pairs are generated and separated, which could result in the production of hydrogen, decomposition of organic pollutants and reduction of heavy metal ions. However, the quick recombination of photo-generated electrons and holes diminishes the efficiency of the photocatalysis significantly. It is believed that GN with excellent electrical conductivity could be used as an electron transfer channel for reducing the recombination, and leading to improved photoconversion efficiency of the photocatalytic materials. Besides, GN is also expected to increase the adsorptivity to pollutants and extend the light absorption range of photocatalysts.

TiO_2 has been considered as one of the best photocatalytic materials, due to its efficient photoactivity, photo- and chemical stability, nontoxicity, and low production cost. To date, a large number of reports have focused on the photocatalytic application of GN–TiO_2 nanocomposites in removal of pollutants.[21,222,288,308,409–415] The GN–TiO_2 photocatalysts were reported to exhibit a significant enhancement in the photodegradation activity, compared with the bare TiO_2 and CNT–TiO_2.[409,410,414] However, the detailed research of Xu *et al.* towards the gas-phase degradation of benzene strongly manifested that RGO–TiO_2 nanocomposite was in essence the same as other carbon-based TiO_2 composites on enhancement of photocatalytic activity of TiO_2, although GN had unique structural and electrical properties.[411] Besides decomposition of organic compounds, RGO–TiO_2 composites have also been reported as photocatalysts for the evolution of hydrogen under UV-vis illumination.[335,416]

Despite of the advantages above, TiO_2 is mainly excited by high energy UV irradiation, which greatly limits its practical applications because of the low content of UV light in the solar spectrum. So efforts have been made to exploit visible-light responsive photocatalysts with GN as the support. For instance, RGO–Au,[417] RGO–Bi_2WO_6,[418] as well as 3D CNT-pillared RGO[328] nanocomposites have been found to display excellent performance in the photocatalytic degradation of dyes under visible light. Also, photocatalytic production of H_2 from water splitting under visible-light irradiation has been achieved by GN-supported photocatalysts. For instance, a remarkable 10-fold enhancement in photoelectrochemical water splitting reaction was observed on RGO-incorporated $BiVO_4$ nanocomposite compared with pure $BiVO_4$ under visible illumination.[419] This improvement was mainly attributed to the presence of GN, which serves as an electron collector and transporter to efficiently lengthen the lifetime of the photogenerated charge carriers. With the same charge recombination mechanism, a high efficiency of the photocatalytic H_2 production was achieved using RGO–CdS nanocomposite as visible-light-driven photocatalysts.[312] The composite reaches a high H_2-production rate of 1.12 mmol h^{-1} (about 4.87 times higher than that of pure CdS NPs) at RGO content of 1.0 wt % under visible-light irradiation. Xu *et al.*[420] also reported the N-doped RGO–CdS composite shows higher photocatalytic activity in the photocatalytic H_2 production, compared with RGO–CdS, and GO–CdS composites. This finding demonstrates that N-doped GN is a more promising candidate for the development of high-performance photocatalysts. As a metal-free photocatalyst in visible-light catalytic hydrogen production, RGO–C_3N_4 ($\sim$1.0 wt% RGO)

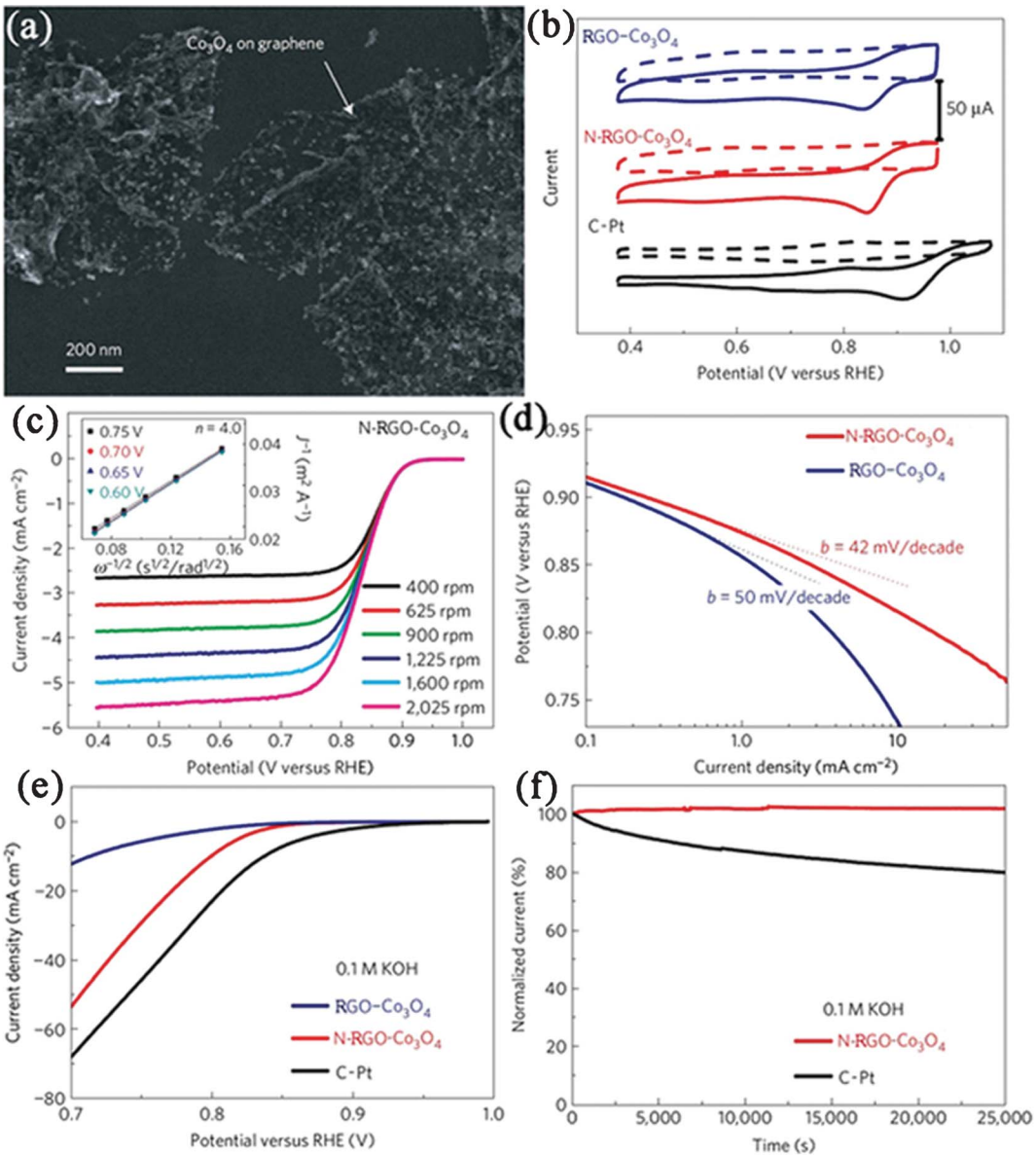

Fig. 11 (a) SEM image of *N*-RGO–Co_3O_4 composite deposited on a silicon substrate from a suspension in solution. (b) Cyclic voltammetry curves of RGO–Co_3O_4, N–RGO–Co_3O_4 and C–Pt on glassy carbon electrodes in O_2-saturated (solid line) or Ar-saturated 0.1 M KOH (dash line). (c) Rotating-disk voltammograms of *N*-RGO–Co_3O_4 composite in O_2-saturated 0.1 M KOH with a sweep rate of 5 mV s^{-1} at the different rotation rates indicated. (d) Tafel plots of RGO–Co_3O_4 and *N*-RGO–Co_3O_4 composites derived by the mass-transport correction of corresponding rotating-disk electrode data. (e) Oxygen reduction polarization curves of RGO–Co_3O_4, *N*-RGO–Co_3O_4 and C–Pt catalyst dispersed on carbon fibre paper in O_2-saturated 0.1 M KOH electrolytes. (f) Chronoamperometric responses of N–RGO–Co_3O_4 and C–Pt on carbon fibre paper electrodes kept at 0.70 V *versus* reversible hydrogen electrode in O_2-saturated 0.1 M KOH electrolytes. Reprinted with permission from ref. 406. Copyright 2011, Nature Publishing Group.

also shows a H_2-production rate of 451 μmol h^{-1} g^{-1}.[172] Besides, significantly promoted visible-light photocatalytic performance has also been observed in GN-supported ZnO,[421,422] SnO_2,[222] Bi_2MoO_6,[423] $InNbO_4$,[424] $ZnFe_2O_4$,[425] and GN-encapsulated Ag/AgX(X = Br, Cl)[426] composites, *etc.*

4.2. Energy storage and conversion

The increasing demand for energy and growing concerns about air pollution and global warming have stimulated considerable effort to the development of energy storage/conversion devices with high power and energy densities. GN-based materials have been considered as one of the promising alternatives as electrode materials in energy-related devices, because of their superior electrical and thermal conductivities, high surface area, good chemical stability, excellent mechanical strength and broad electrochemical window.[427,428] Recently, GN–inorganic nanocomposites have been demonstrated for applications in energy storage/conversion devices, such as supercapacitors, LIBs, solar cells, and fuel cells.

4.2.1. Supercapacitors. Supercapacitors are energy-storage devices that exhibit high power density and long cycle life. GN have been considered to be an excellent electrode material for supercapacitors.[429] Studies have shown that the specific

capacitances of GN can reach 135 F g^{-1} and 99 F g^{-1} in aqueous and organic electrolytes, respectively.[8] However, the experimentally observed capacitances are mainly limited by the agglomeration of GN and do not reflect the intrinsic capacitance of an individual GN nanosheet. A considerable enhancement can be expected from the introduction of metal oxide or hydroxide NPs to stabilize GN from aggregation, which not only increases the accessible surface area, but also effectively increases the supercapacitance due to their contribution to the additional pseudocapacitance. By far, a wide range of metal compounds have been investigated in GN–inorganic nanocomposites for supercapacitor electrode materials, containing MnO_2,[184,238,372,380,430–434] Mn_3O_4,[435] Co_3O_4,[436,437] SnO_2,[223,438] ZnO,[438–440] Bi_2O_3,[299] RuO_2,[272] Fe_3O_4,[295,441] NiO,[199,442] CeO_2,[443] Cu_2O,[444] $Ni(OH)_2$,[179,445] $Co(OH)_2$,[152] $NiCo_2O_4$,[276] and LDH.[153,200] In all of these cases, the nanocomposites exhibited enhanced capacitive behaviors with better reversible charging/discharging ability and higher capacitance values, when compared with pure GN and the bare compounds.

Among these compounds, MnO_2 is one of the most promising electrode materials for supercapacitor applications, due to its low-cost, being environment-friendly and high specific capacitance. Fan *et al.*[430] reported a rapid and facile method to prepare GN–MnO_2 composites as novel electrode materials by MWI (Fig. 12a). The obtained GN–MnO_2 (78 wt% MnO_2) nanocomposite shows a specific capacitance of 310 F g^{-1} at a scan rate of 2 mV s^{-1} (Fig. 12b), which is higher than other kinds of carbon-MnO_2 composites. After 15 000 cycles, the composite only shows 4.6% capacity loss, indicating a long cycle life (Fig. 12c). The excellent electrochemical performances are believed to be due to the unique microstructures of the composite, which not only improve the diffusion rate and reduce the diffusion length of the cations within the MnO_2 NPs, but also enhance the conductivity with GN as conductive channels (Fig. 12a). Besides metal oxides and hydroxides, other carbon materials (such as CNT,[329,373,446,447] CB,[143] and carbon spheres[144]) can also enhance the electrochemical performances of GN for supercapacitor applications. The incorporation of carbon materials into GN layers not only inhibits the agglomeration of GN nanosheets, but also provides highly conductive channels for electron transport and form well-defined nanopores for fast ion diffusion. The electrochemical performance of supercapacitors with various GN–inorganic composites as electrode materials is shown in Table 4.

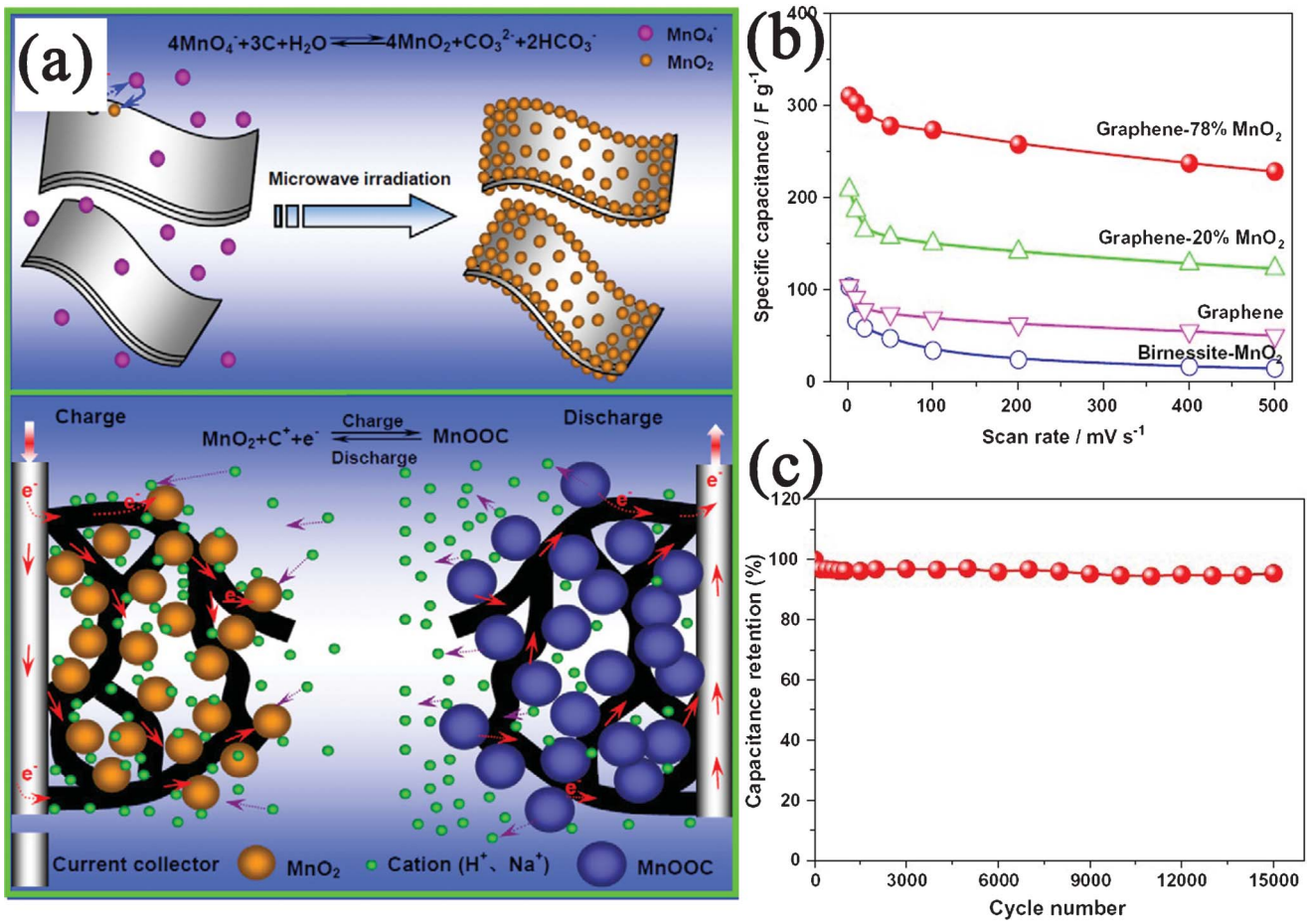

Fig. 12 (a) Schematic illustration for the synthesis and electrochemical performance of a GN–MnO_2 nanocomposite. (b) Specific capacitance of GN–MnO_2 as well as GN and pure MnO_2 at different scan rates in 1 M Na_2SO_4 solution. (c) Variation of the specific capacitance of GN-78% MnO_2 electrode as a function of cycle number measured at 500 mV s^{-1} in 1 M Na_2SO_4 aqueous solution. Reprinted with permission from ref. 430. Copyright 2010, Elsevier.

Table 4 The electrochemical performance of supercapacitors with various GN–inorganic nanocomposites as electrode materials

GN–inorganic nanocomposites	Specific capacitance (F g^{-1})	Current density (A g^{-1})	Electrolyte	Ref.
GN-supported MnO_2 nanowalls	122	—	1 M Na_2SO_4	184
GN-supported MnO_2 nanoflowers	328	—	1 M KCl	238
GN-supported MnO_2 nanosheets	188	4.0	1 M Na_2SO_4	372
GN–MnO_2 multilayer films	263	0.283	0.1 M Na_2SO_4	380
GN-supported MnO_2 NPs	310	—	1 M Na_2SO_4	430
GN-supported MnO_2 nanowires	24.5	0.5	1 M Na_2SO_4	432
GN-supported MnO_2 NPs	113.5	1.2	1 M Na_2SO_4	433
GN–MnO_2 textiles	315	2.2	0.5 M Na_2SO_4	434
GN-supported Mn_3O_4 NPs	175	—	1 M Na_2SO_4	435
	256	—	6 M KOH	
GN-supported Co_3O_4 NPs	243.2	10 (mA cm^{-2})	6 M KOH	436
GN–Co_3O_4 nanoscrolls	163.8	1	6 M KOH	437
GN-supported SnO_2 NPs	43.4	—	1 M· H_2SO_4	223
GN-supported ZnO NPs	61.7	—	1 M KCl	438
GN-incorporated ZnO composite	308	1	1 M· Na_2SO_4	440
GN-supported Bi_2O_3 NPs	255	1	6 M KOH	299
GN-supported RuO_2 NPs	~570	0.1	1M· H_2SO_4	272
GN-supported Fe_3O_4 NPs	480	5	1 M KOH	295
GN–NiO multilayer membranes	150~220	0.1	30% KOH	199
GN-supported porous NiO	400	2	1 M KOH	442
GN-supported CeO_2 NPs	208	1	3 M KOH	443
GN-supported Cu_2O NPs	24.0	0.2	Saturated KCl	444
GN-supported β-$Ni(OH)_2$ nanoplates	~1335	2.8	1 M KOH	179
GN-supported α-$Ni(OH)_2$ NPs	1215	—	6 M KOH	445
GN-supported $Co(OH)_2$ NPs	972.5	0.5	6 M KOH	152
GN-supported $NiCo_2O_4$ NPs	835	1	6 M KOH	276
GN-supported Ni–Al LDH nanosheets	781.5	10 (mA cm^{-2})	6 M KOH	153
GN–Co–Al LDH multilayered composite	1031	20	1 M KOH	200
GN-supported CNT	290.4	0.5	1 M KCl	447
GN-supported CB	175	5	6 M KOH	143
GN-supported carbon spheres	39.4	0.1	6 M KOH	144

4.2.2. Lithium-ion batteries. LIBs is a lithium ion-induced device for electricity supply, which is composed of an anode, electrolyte, and cathode. The energy density and performance of LIBs largely depend on the physical and chemical properties of the cathode and anode materials. Graphite with a theoretical lithium storage capacity of 372 mA h g^{-1} is currently used as the anode material in commercial LIBs. Owing to its large surface-to-volume ratio and highly conductive nature, GN has a higher lithium storage capacity (theoretical lithium storage capacity of 744 mA h g^{-1} for single layer GN).[448] However, GN nanosheets always naturally stack into multilayers and therefore lose their high surface area and intrinsic chemical and physical properties. A considerable enhancement can be expected from the incorporation of inorganic nanomaterials with high specific capacity into GN, which could not only limit the aggregation of GN, but also boost the lithium storage capacity.[449] For example, Honma *et al.*[450] demonstrated enhanced cyclic performance and lithium storage capacity of GN–SnO_2 nanoporous electrodes prepared with reassembly of GN in the presence of SnO_2 sol (Fig. 13a). It was demonstrated that the obtained GN–SnO_2 electrode exhibited an enhanced reversible capacity (810 mA h g^{-1}) as well as superior cycling performance (~70% retention after 30 cycles) in comparison with that of the bare SnO_2 electrode (Fig. 13b, c). It is believed that the dimensional confinement of SnO_2 NPs by the surrounding GN limits the volume expansion upon lithium insertion, and the developed nanopores between SnO_2 and GN could be used as buffered spaces during charge–discharge, resulting in the superior cyclic performances (Fig. 13a).

On the basis of this concept, a wide range of nanomaterials of oxides, hydroxides and chalcogenides, such as SnO_2,[220,224,296,451–455] Fe_3O_4,[259,273,293,441,456,457] Co_3O_4,[183,270,271,298,366,458] CuO,[309,459] TiO_2,[158,192,415,460,461] Mn_3O_4,[307] CoO,[183,300] Fe_2O_3,[300,462,463] NiO,[178] CeO_2,[464] $Li_4Ti_5O_{12}$,[337,465] $Co(OH)_2$,[302] $Ni(OH)_2$,[466] MoS_2,[314,467] and SnSe[180] have been anchored on GN nanosheets for application as anode materials for LIBs. Besides, GN-supported Si,[164,165,468] Sn-based[136,206] NPs, GN–Sn multilayered nanostructure,[469] and GN-incorporated ceramic composite[168] have also been developed as anode materials for LIBs. All these composites showed large reversible capacities, excellent cycling performances and high coulombic efficiencies. Furthermore, Honma and coworkers reported that the incorporation of CNT and C_{60} could further increase the specific capacity of GN as anode materials.[470] The enhanced performance of the composites were attributed to the improvement of lithium accommodation in the increased layered spaces between GN through intercalating CNT or C_{60}. Fan *et al.* also reported a RGO–carbon nanofiber composite for high-performance anode materials for LIBs.[145] The performance of LIBs with GN–inorganic composites as anode materials are summarized in Table 5.

In another case, GN nanosheets were also used as supporting materials to enhance the capacity delivery and cycle performances of cathode materials. $LiFePO_4$ has been a promising cathode-active material for LIBs because of its low-cost, low toxicity and high stability. However, its poor electronic conductivity and lithium-ion diffusivity limit its practical application. GN–$LiFePO_4$ composites have shown improved specific capacity and rate capability with the reason that GN can facilitate electron transport effectively and thus improve the kinetics and rate performance of $LiFePO_4$.[471–473] Besides, $LiMn_{1-x}Fe_xPO_4$ nanorods,[175] $Li_3V_2(PO_4)_3$ NPs,[336] $LiNi_{1/3}Co_{1/3}Mn_{1/3}O_2$ NPs,[474]

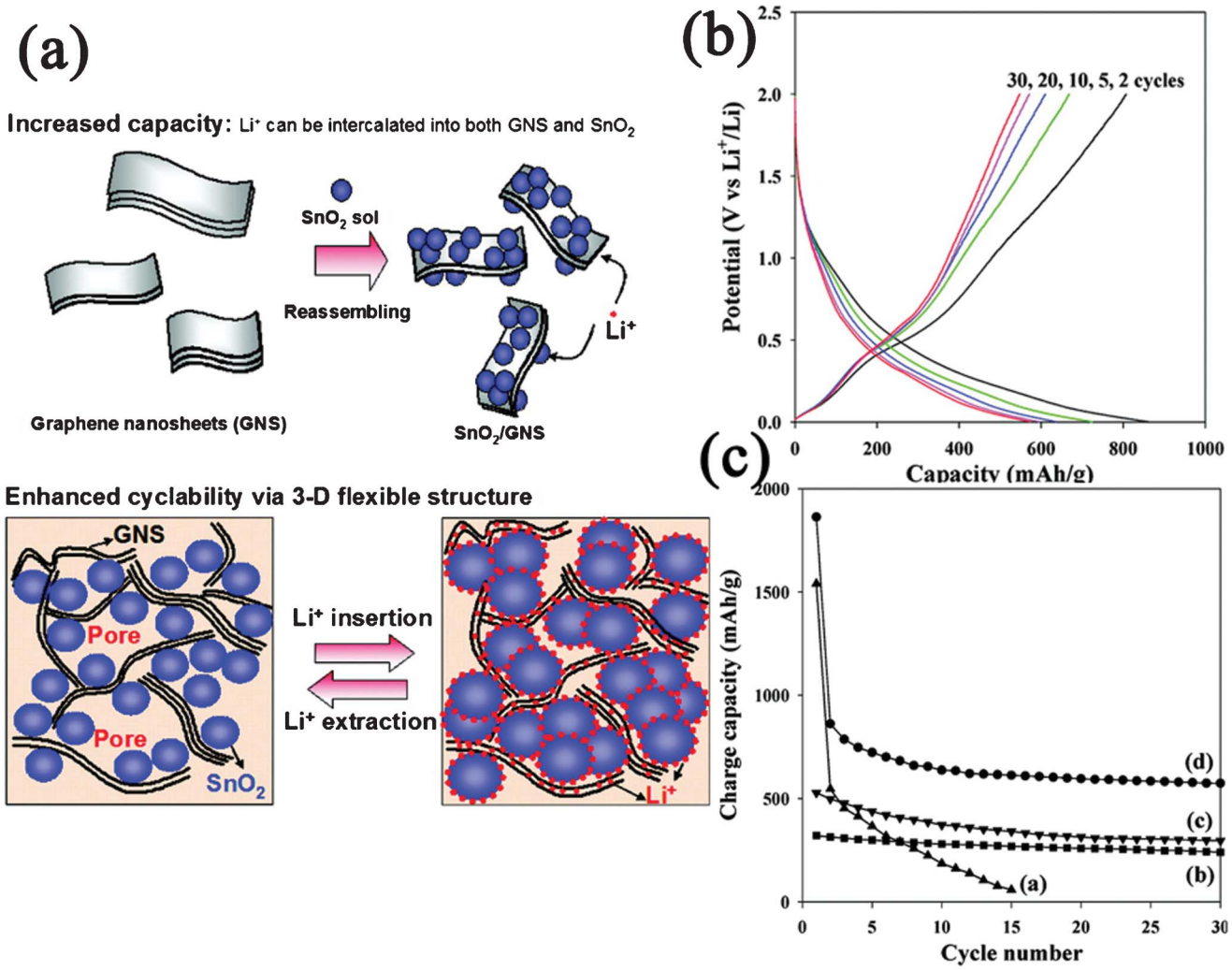

Fig. 13 (a) Schematic illustration for the synthesis and structure change of GN–SnO_2 nanocomposite during Li^+ insertion and extraction. (b) Charge–discharge profile for GN–SnO_2 nanocomposite. (c) Cyclic performances for (a) bare SnO_2 NPs, (b) graphite, (c) GN, and (d) GN–SnO_2 nanocomposite. Reprinted with permission from ref. 450. Copyright 2009, American Chemical Society.

and $V_2O_5{\cdot}nH_2O$ xerogel nanoribbons[475] were also grown on GN nanosheets as improved cathode materials for LIBs.

4.2.3. Solar cells. Solar cells are devices that convert the energy of sunlight into electricity by photovoltaic effect. Due to the high electron mobility and excellent optical transparency of GN nanosheets, GN–inorganic nanocomposites have emerged as one of the fascinating electrode materials for application in solar cells,[476] mainly in the dye-sensitized solar cells (DSSCs) and quantum dot-sensitized solar cells (QDSSCs). DSSCs have attracted much attention because of their moderate light-to-electricity conversion efficiency, easy fabrication, and low cost, which are mainly composed of a photoelectrode (photoanode and photocathode), a dye, an electrolyte, and a counter electrode. The photoanodes of DSSCs are typically constructed using thick films of TiO_2 NPs, which provide a large surface area for anchoring enough dye molecules. However, the random transport of photogenerated electrons in disordered TiO_2 NPs increases the chance of charge recombination and thus decreases the efficiency of DSSCs. The incorporation of GN into TiO_2 NPs as conduction pathways could resolve this bottleneck. GN-incorporated TiO_2 composites,[195,477,478] and also GN–CNT incorporated TiO_2 composites,[479] have been employed as the photoanode for DSSCs, which greatly increased the conversion efficiency, in comparison with the TiO_2 photoanode alone. The incorporation of GN could not only induce the faster electron transport and a lower recombination, thus significant longer electron lifetime, but also increase the dye adsorption, lead to the enhancement in the performance of DSSCs.[478] In addition, RGO–TiO_2 nanocomposites have also been reported as an interfacial layer between fluorine doped tin oxide layer and TiO_2 film to reduce the back-transport reaction of electrons in DSSCs.[480] Besides, GN–NiO composite films were used to fabricate photocathode for DSSCs.[481] GN-based CNT composites with vertically aligned CNT also served as one of the promising candidates for counter electrodes to achieve high performance in DSSCs.[482–484]

Another example of the successful application of GN–inorganic nanocomposites in solar cells is the development of QDSSCs.[485–487] QDs such as CdS and CdSe with large extinction

Table 5 The performance of LIBs with GN–inorganic nanocomposites as anode materials

GN–inorganic nanocomposites	Reversible capacity (mAh h^{-1})	Current density (mA g^{-1})	Cycles	Ref.
GN-supported SnO_2 NPs	840	67	~30	224
GN-supported SnO_2 nanorods	838	50	~20	296
GN-supported SnO_2 NPs	765	55	~100	451
GN-supported echinoid-like SnO_2 NPs	634	100	~50	454
GN-supported SnO_2 nanosheets	518	160	~50	455
GN-encapsulated Fe_3O_4NPs	1026	35	~30	273
	580	700	~100	
GN-encapsulated Fe_3O_4 NPs	650	100	~100	293
GN-supported Fe_3O_4 NPs	1048	100	~90	456
GN-supported Co_3O_4 nanowalls	673	180	~100	183
GN-supported Co_3O_4 nanosheets	931	4450	~30	270
GN-supported Co_3O_4 NPs	935	50	~30	271
GN-supported Co_3O_4 NPs	941	200	~60	298
GN-encapsulated Co_3O_4 composite	1000	74	~130	366
GN-supported CuO NPs	583.5	67	~50	309
GN-encapsulated CuO nanomicroflowers	600	65	~100	459
GN-encapsulated TiO_2 hollow NPs	~90	1700	~180	192
GN-supported mesoporous anatase TiO_2 nanospheres	97	8400	~100	415
GN-supported anatase TiO_2 nanosheets	161	170	~120	461
GN-supported Mn_3O_4 NPs	730	400	~40	307
GN-supported CoO nanowalls	732	150	~100	183
GN-supported CoO NPs	600	215	~90	300
GN-supported Fe_2O_3 NPs	881	302	~90	
GN-supported NiO nanosheets	1031	71.8	~40	178
GN-supported CeO_2 NPs	605	50	~100	464
GN-supported $Co(OH)_2$ NPs	910	200	~30	302
GN-incorporated β-$Ni(OH)_2$ composite	507	200	~30	466
GN-supported MoS_2 nanosheets	1290	100	~50	314
GN-supported MoS_2 nanosheets	~1100	100	~100	467
GN-supported SnSe nanoplates	470~640	40	~30	180
GN-supported Si NPs	1168	100	~30	164
GN-supported Si NPs	708	50	~100	165
GN-supported Sn NPs	508	55	~100	136
GN-Sn multilayered nanostructure	679	50	~30	469
GN-incorporated SiOC composite	357	40	~30	168
GN-supported C_{60}	600	50	~20	470
GN-supported CNT	480	50	~20	
GN-supported carbon nanofibers	667	0.12 (mA cm^{-2})	~20	145

coefficient and upon light absorption could harvest light energy and transfer excited electrons to the conduction band of TiO_2 or ZnO film. Similar to DSSCs, capturing photoinduced electrons as quickly as they are generated and efficiently transporting them in the metal oxide film is one of the most difficult challenges in QDSSCs system. The introduction of GN was reported to suppress electron recombination and back-transport reaction, enhance the electron transport as well as increase the QDs adsorption, thus improve the performance of QDSSCs. For example, Deng *et al.*[485] demonstrated the use of a GN–ZnO nanorod composite as a photoanode, leading to 54.7% improvement of power conversion efficiency in CdSe QDSSCs compared to a quantum dot sensitized ZnO nanorods without the RGO layer. Pan *et al.*[486] reported CdS QDSSCs, based on a GN-incorporated TiO_2 film photoanode, which demonstrated a maximum power conversion efficiency of 1.44%, 56% higher than that without RGO.

4.2.4. Fuel cells. Fuel cells are electrochemical devices involving electrocatalytic fuel oxidation at the anode and oxygen reduction at the cathode to produce electricity. As discussed in section 4.1.2., GN–inorganic nanocomposites exhibit excellent electrocatalytic performance, which show promising application in next-generation fuel cells, such as GN–Pt nanocomposite in direct methanol fuel cells,[234,324] and proton-exchange membrane fuel cells (PEMFCs),[129,388] as well as GN–Pd nanocomposites in direct formic acid fuel cells.[338,404] As an example, a PEMFC with RGO–Pt nanocomposites as the cathode and CB–Pt composites as the anode delivered a maximum power of 161 mW cm^{-2}, which is much higher than 96 mW cm^{-2} of the fuel cell with unsupported Pt as cathode.[129]

4.3. Sensing

The rapid development of GN provides new opportunities for the progress of analytical science. Nowadays, GN nanosheets with large active area and high conductivity have been introduced into analytical chemistry and implanted novel functions into analytical sensing systems.[427,488–490] In this section, we present the application of GN–inorganic nanocomposites in constructing high-performance gas sensors and biosensors.

4.3.1. Gas sensor. CNT-based gas sensors have attracted intensive research interest in the last several years because of their promising potential for the selective and rapid detection of various gas molecules. The better physical and chemical properties of GN over CNTs suggests that GN might have some advantages in this particular direction.[491] However, the challenge

is employing GN alone for high performance sensing applications due to the relatively weak and unstable sensing response. Nevertheless, some groups have demonstrated good sensitivity for the detection of H_2,[173,492–495] H_2S,[305], ethanol,[496] propanal,[497] and NO_2[498] molecules under ambient conditions by using GN–inorganic nanocomposites as gas sensing materials. GN-supported noble metal NPs, such as Pd,[492,493] Pt,[494,495] and PdPt alloy[173] have been used for H_2 sensing. The gas sensing mechanism in most of these cases is based on the resistance change of the composites due to dissolution and dissociation of H_2 molecules into atomic H at the catalytically active noble metal NPs. The large surface area and high conductivity of GN enhance the detection of the change in the resistance during H_2 sensing. For example, Ural *et al.*[492] demonstrated the application of multi-layer GN nanoribbon network-supported Pd NPs for H_2 sensing. These networks show excellent sensitivity to H_2 at ppm concentration levels at room temperature with fast response and recovery time and good repeatability. The sensing response shows a linear behavior as a function of H_2 concentration and the sensor resistance fully recovers upon exposure to air. The large surface area and high conductivity of GN enhance the detection of the change in the resistance during H_2 sensing. With the resistance change mechanism, GN–inorganic nanocomposites have also been fabricated to detect other gas molecules, such as vertically aligned ZnO nanorods on CMG films in detecting H_2S in oxygen,[305] vertical CNTs grown on RGO films as a NO_2 gas sensor.[498]

Besides, GN–inorganic nanocomposites were also developed to fabricate gas sensors based on cataluminescence (CTL), which refer to the kind of chemiluminescence (CL) that is emitted during the catalytic oxidization of organic vapors on the surface of sensing material in an atmosphere containing oxygen. GN–supported metal oxide NPs with good distribution can provide greater versatility in carrying out adsorption, selective catalytic and sensing processes. Their porosity and large specific surface area are attractive advantages for CTL sensing materials. For instance, RGO–Al_2O_3 composite was reported to display high CL sensitivity and high selectivity to ethanol gas.[496] The CTL sensor based on a RGO–SnO_2 composite demonstrated a linear range 1.34 ~ 266.67 μg mL^{-1} and detection limit of 0.3 μg mL^{-1} in propanal sensing.[497]

4.3.2. Biosensor. GN–noble metal (Au, Ag, Pt, and Pd) nanocomposite-modified electrodes have been applied for detecting various electroactive probe-labeled biomolecules or biology-related molecules, including H_2O_2,[368,369,499–501] glucose,[212,502–505] dopamine (DA),[506,507] ascorbic acid (AA),[506,507] uric acid (UA),[367,506] cholesterol,[508] protein,[509] DNA,[229,510] organophosphate pesticide,[511] histidine,[512] and nicotinamide adenine dinucleotide (NADH).[513] In another case, GN–metal compound nanocomposites also provide a promising platform for the development of biosensor. For instance, GN-supported Fe_3O_4,[292,514] MnO_2,[515] TiO_2,[289] ZrO_2,[516] CdS,[517,518] CdSe[378] NPs and GN-encapsulated SiO_2[191] NPs were used to construct biosensors for determination of H_2O_2, glucose, DA, thrombin, *etc.* In these biosensors, GN nanosheets not only act as an advanced support with large surface area for immobilizing different target biomolecules, but also effectively promote the electron transfer between electrode and analytes. It was found that these composite modified electrodes exhibited favorable electron transfer kinetics and high electrochemical reactivities, which indicates that these composites hold great promise for electrochemical sensing and biosensing.

Most of the reported biosensors were based on an eletrochemical strategy with techniques such as amperometric, voltammetric and electrochemiluminescence (ECL) methods. Occasionally, GN-based inorganic composites were also used to detect biomolecules based on field effect transistors (FETs) signal conversion strategies.[191,509,510] As an example, a specific protein detection FET biosensor was fabricated using thermally-reduced graphene oxide (TRGO) sheets decorated with Au NP–antibody conjugates.[509] In this sensing strategy, the Au NP–antibody conjugates were assembled onto the surface of TRGO sheets by electrostatic assembly. Then a blocking buffer was used to prevent possible nonspecific binding events. When the target proteins (IgGs) were introduced, the protein binding events induced significant changes in the electrical characteristics of the device, which could be studied by FET and direct current measurements. The schematic of the TRGO–Au NP FET device and the FET sensor fabrication process are shown in Fig. 14 a and b, respectively. The performance of the novel biosensor is among the best carbon nanomaterial-based protein sensors, which exhibited a low detection limit of ~13 pM.

Besides, GN–inorganic nanocomposites have initially been used as a advanced carrier to construct immunosensors,[370,519–521] which are important analytical tools based on the property of highly specific molecular recognition of antigen by antibodies. For instance, Zhu *et al.*[370] fabricated an advanced electrogenerated chemiluminescence immunosensor by using PDDA-protected GN–CdSe composites. After two successive steps of amplification *via* the conjugation of PDDA and Au NPs, the immunosensor has an extremely sensitive response to human IgG in the linear range 0.02 ~ 2000 pg mL^{-1} with a detection limit of 0.005 pg mL^{-1}. Table 6 summarizes the biosensors fabricated with GN–inorganic nanocomposites. It is also worthy of note that GN–inorganic nanocomposites have also been fabricated as sensing platforms for detection of pollutants and dangerous substances.[499,522]

4.4. Other applications

4.4.1. Surface-enhanced Raman scattering. Since the discovery of the enhanced Raman signals on a roughed metallic (normally Ag and Au) surface, surface-enhanced Raman scattering (SERS) has been proposed for a variety of ultrasensitive chemical and biological sensing applications. Raman spectroscopy has been utilized as a powerful tool to probe the structural characteristics of GN, as it can identify the number of layers, the electronic structure, the edge structure, the type of doping and any defects in the GN. However, Raman signals of GN were very weak, especially when observing single-layer GN sheets. SERS is able to overcome this limitation and provide a spectral intensity enhanced by many orders of magnitude for molecules touched with proper metal surface. Recently, the SERS of GN with GN–Ag[239,317,523] and GN–Au[240,256,265,356,524–526] nanocomposites were widely reported. It is found that the degree of the enhancement could be adjusted by the quantity,[523] size,[317] and nanostructure[526] of the noble metal NPs on the GN nanosheets.

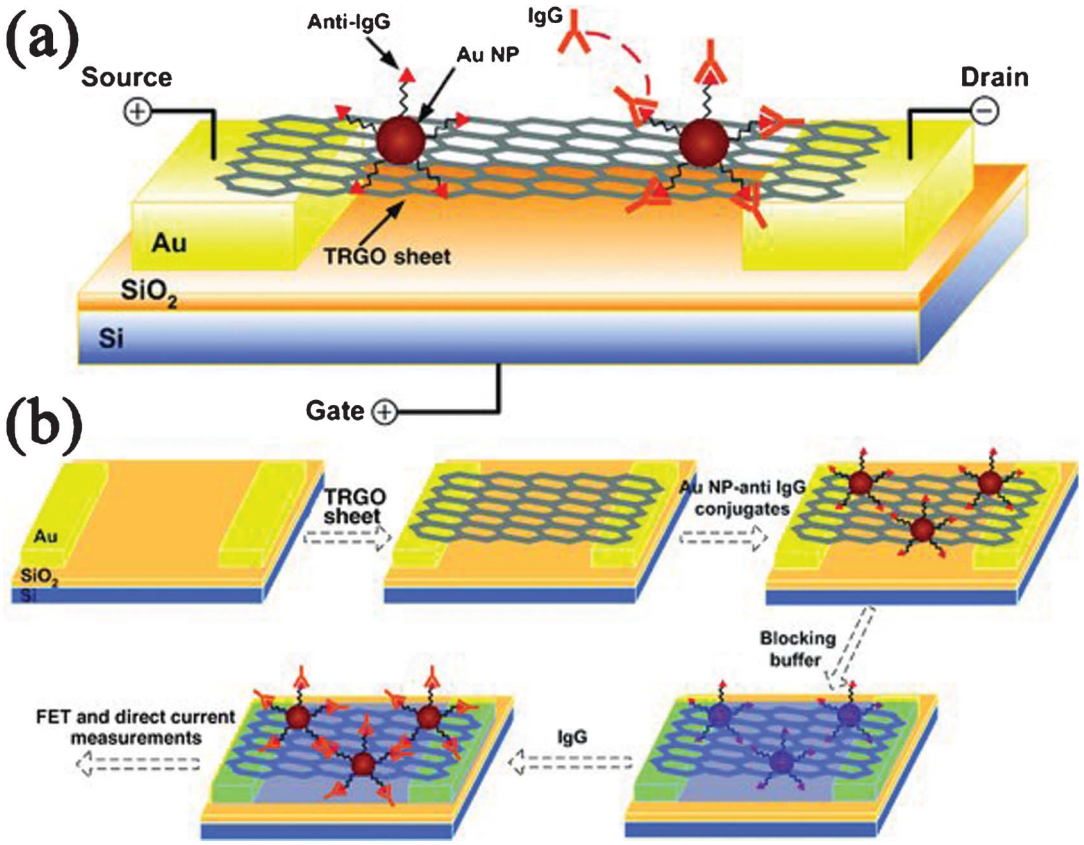

Fig. 14 (a) Schematic of the FET device. (b) Schematic illustration of the FET biosensor fabrication process. Reprinted with permission from ref. 509. Copyright 2010, John Wiley & Sons, Inc.

Table 6 Biosensors fabricated with GN–inorganic nanocomposites

Inorganic component	Analyte	Detection techniques	Detection limits	Ref.
Ag	H_2O_2	Amperometric	2.8 μμM	368
Au	H_2O_2	Amperometric	0.44 μμM	369
Pt	H_2O_2	Amperometric	80 nM	499
Au	glucose	Amperometric	35 μμM	212
Pd	glucose	Amperometric	1 μμM	502
Pt-Au	glucose	Amperometric	1 μμM	504
Pt	DA	Amperometric	0.03 μμM	506
	AA		0.15 μμM	
	UA		0.05 μμM	
Au	UA	Amperometric	0.2 μμM	367
Pt	cholesterol	Amperometric	0.2 μμM	508
Au	protein	FETs	~13 pM	509
Au	DNA	FETs	—	510
Au	organophosphate pesticide	Amperometric	0.1 pM	511
Au	L-histidine	Voltammetric	0.1 pM	512
Au	NADH	Amperometric	1.2 μμM	513
Fe_3O_4	H_2O_2	Amperometric	0.6 μμM	292
MnO_2	H_2O_2	Amperometric	0.8 μμM	515
TiO_2	DA	Voltammetric	2 μμM	289
ZrO_2	organophosphorus agents	Voltammetric	0.1 ng mL^{-1}	516
CdS	H_2O_2	ECL	1.7 μμM	517
CdSe	thrombin	Photocurrent	4.5 × ×10^{-13} M	378
SiO_2	cancer biomarker	FETs	1 pM	191
CdSe	human IgG	ECL	0.005 pg mL^{-1}	370
Au	human IgG	Voltammetric	70 ng mL^{-1}	519
Au–Ag	alpha-fetoprotein	Amperometric	0.5 pg mL^{-1}	521

It is also found that the corresponding enhancement factors are dependent on the layer number with single-layer GN having the largest SERS enhancement compared to few-layer GN.[317,524]

Also, works have been carried out to study the enhanced Raman signal of adsorbed molecules on GN–metal composites. For instance, Shen *et al.*[527] deposited Au films on single-layer GN as SERS substrates for the characterization of rhodamine molecules with low concentration. While Au films effectively enhance both the Raman and photoluminescence (PL) signals of the molecules, single-layer GN effectively quenches the PL signals from the Au film and molecules. Tang *et al.*[528] investigated the Raman signal of 4-aminothiophenol (4-ATP) with GN–Ag composite as SERS substrates. The Raman intensity of 4-ATP increased with increasing weight ratio of Ag in the composite. Based on the enhanced Raman mechanism, the GN–metal composites have been used as efficient SERS substrates to detect molecules.[529,530] The RGO–Ag and RGO–Au composites fabricated by Zhang *et al.* exhibited strong adsorption and dramatic Raman enhancement to aromatic molecules.[529] Subsequently, the SERS substrates were used to detect the adsorbed aromatic molecules with a low detection limit at nM level. Wang *et al.*[530] self-assembled Ag NPs with PDDA-functionalized GO as SERS substrates for the detection of folic acid. The modified GO with a positive potential exhibited strong enrichment of negatively charged folic acid due to the electrostatic interaction, and the self-assembled Ag NPs greatly enhanced the SERS spectra of folic acid with the strongest peak located at 1595 cm^{-1}. The intensity of the peak increased with the increase of the concentration of folic acid. The SERS spectra of the folic acid showed that the minimum detected concentration of folic acid in serum was as low as 9 nM with a linear response range from 9 to 180 nM (Fig. 15).

4.4.2. Biotechnology and pollutant removal. Nowadays, GN–magnetic nanocomposites have been used in various areas of biolotechnology/biomedicine and environmental remediation, such as targeted drug delivery,[216] magnetic resonance imaging,[151,279] as well as removal of organic pollutants,[531,532] and heavy metal ions.[148,218,533] GN with large surface could not only avoid the aggregation and growth of the magnetic NPs, often resulting in a special magnetic character, but also increase the adsorption capacity and enhance the dispersity of the composites. For instance, Chen *et al.*[216] developed GO–Fe_3O_4 composites to load doxorubicin hydrochloride (DXR) with the loading capacity as high as 1.08 mg mg^{-1}. Both of the composite before and after loading with DXR can congregate and move regularly under the force of an external magnetic field, and also redispersed reversibly under basic conditions, showing a promising candidate for controlled targeted drug delivery and release (Fig. 16). Also, the RGO–Fe_3O_4 nanocomposite showed a high binding capacity for As(III) and As(V), due to increased adsorption sites in the presence of RGO, which could remove

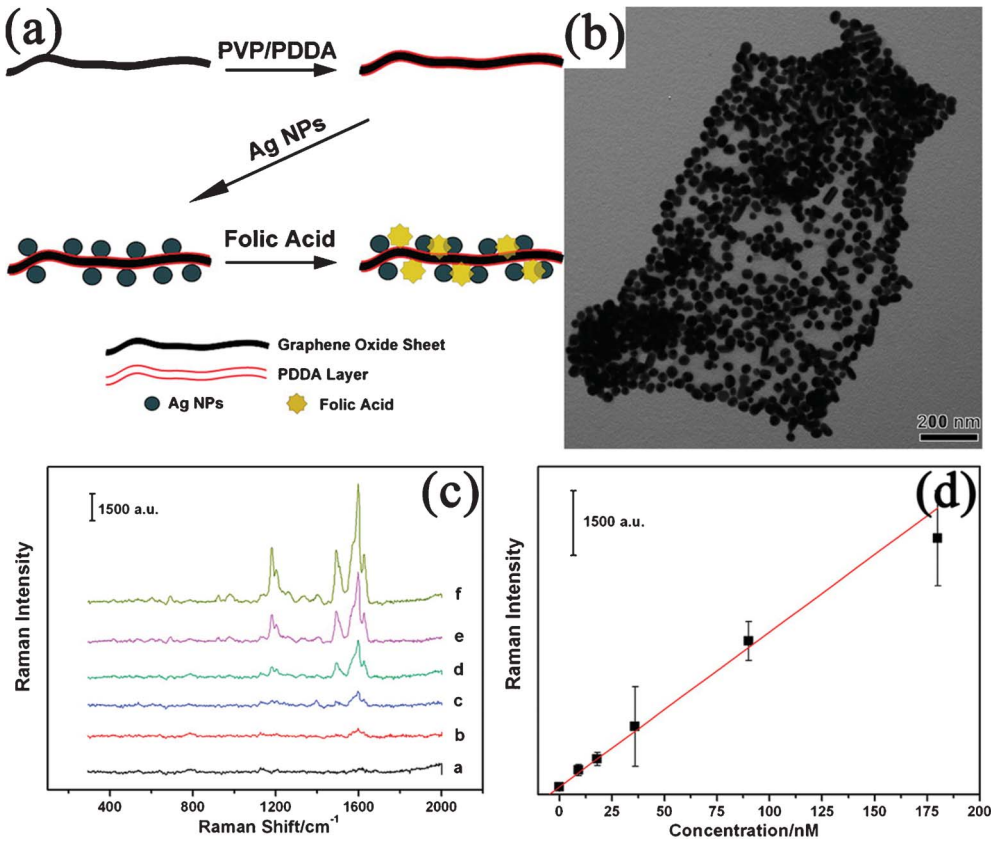

Fig. 15 (a) Scheme illustrated of the fabricated of PDDA–GO-supported Ag NPs and the procedure of SERS detection using PDDA–GO–Ag as substrates; (b) TEM image of PDDA–GO-supported Ag NPs; (c) SERS spectra of different concentrations of folic acid with PDDA–GO–Ag as SERS substrates in diluted serum: (*a*) blank, (*b*) 9 nM, (*c*) 18 nM, (*d*) 36 nM, (*e*) 90 nM, and (*f*) 180 nM; and (d) SERS dilution series of folic acid in diluted serum based on the peak located at 1595 cm^{-1}. Reprinted with permission from ref. 530. Copyright 2011, American Chemical Society.

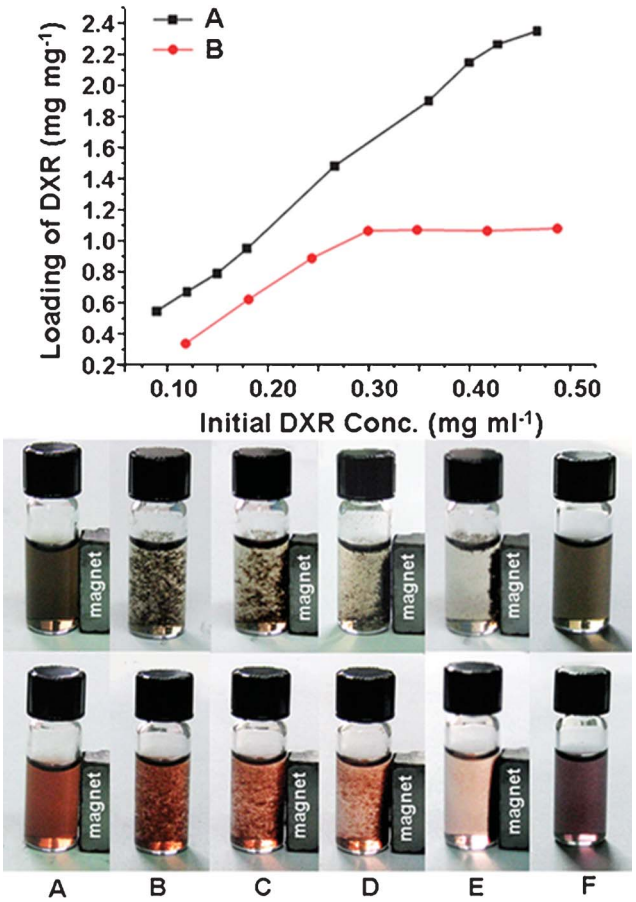

Fig. 16 (Top) Loading capacity of DXR on GO (A) and GO–Fe_3O_4 composite (B) in different initial DXR concentrations. (Bottom) Photographic images of the behaviors of GO–Fe_3O_4 composite (upper) and GO–Fe_3O_4 composite loaded with DXR (lower) in the magnetic field under different conditions: neutral conditions (A), acidic conditions (pH 2–3) (B–E) and basic conditions (pH 8–9) (F). Reprinted with permission from ref. 216. Copyright 2009, Royal Society of Chemistry.

more than 99.9% arsenic ions from their solutions with a concentration lower than 1 ppb (part per billion).[218] After absorbing the arsenic ions, the composite could be separated by an external magnetic field.

Besides GN-supported magnetic NPs as adsorbents as well as GN-supported photocatalyst NPs as reductants[262,414] (Section 4.1.3.), contaminants and heavy metal ion removal was also reported with other GN-supported NPs as adsorbents, such as ZnO,[421] Cu_2O,[444] ferric hydroxide,[534] MnO_2 and Ag.[535] Apart from anincrease of the adsorption capacity, the introduction of GN could also improve the chemical stability and mechanical strength of the adsorbents, which is important in separation technology. Also, GN–Ag composites were reported to exhibit excellent antibacterial activity towards bacteria such as *Escherichia coli*, *Pseudomonous aeruginosa*, *etc.*[202,536–539] Ag has been known as an antibacterial agent for centuries. Studies have shown that the toxicity of Ag NPs is size dependent and the smaller NPs exhibit higher antibacterial activity. GN can effectively stabilize highly monodispersed Ag NPs. Meanwhile, GN could adsorb the bacteria, and keep Ag NPs well-dispersed in solutions. Also GN (GO) nanosheets display antibacterial activity themselves. All of these contributed to the superior antibacterial activity of the nanocomposites.

5. Conclusion, challenges and perspective

In summary, GN nanosheets have been integrated with various inorganic components (including metal, nano-carbon, metal compounds, and nonmetal materials) to form nanocomposites. GN nanosheets could act as a substrate for supporting the inorganic nanomaterials, form shells to enwrap the inorganic nanostructures, play a role of fillers to disperse in inorganic matrices, and also stack with inorganic nanosheets alternately to form multilayer films. Diverse approaches and techniques, such as solution deposition methods, directly decomposition of precursors, hydrothermal/solvothermal techniques, gas-phase deposition, sol–gel processing, template method, covalent

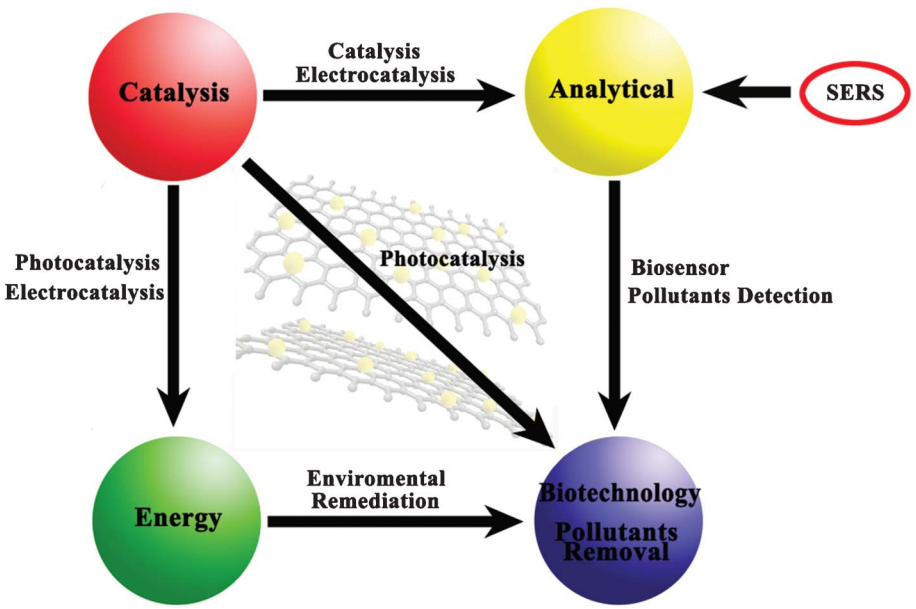

Fig. 17 Relationship between the various applications of GN–inorganic nanocomposites.

grafting and noncovalent interactions have been developed for fabricating GN–inorganic nanocomposites. GN–inorganic nanocomposites have become one of the most important GN-based materials.[540] The nanocomposites exhibit excellent properties and improved functionalities due to the synergetic effects between GN and the inorganic components, thus have been widely used in the fields of catalysis, energy, analytical, biotechnology and pollutants removal applications. Especially, the catalysis application is of significance in respect that it is the basement in developing many other applications of GN–inorganic nanocomposites, such as electrocatalysis in developing electrochemical sensors and fuel cells, as well as photocatalysis in hydrogen energy, solar cells, and pollutants removal applications (Fig. 17). It is expected that the development of clean and renewable energy resources to improve the quality of environment is one of the most promising directions in the progress of GN–inorganic nanocomposites.

With the rapid development of GN–inorganic nanocomposites, some new kinds of inorganic materials are being blended with GN, and many new applications are arising. For instance, GN-supported polyoxometalate,[541–544] and Prussian blue[545–547] NPs have been synthesized for application in hydrogen storage, electronics, electrochemical catalysis and sensing. However, further effort for GN–inorganic nanocomposites is still needed to realize their practical applications. First, as an essential component of the nanocomposites, high-quality GN was required, which greatly affect the reinforcement of GN in the novel properties and potential applications of the nanocomposites. So far, it is still difficult to synthesize GN with controllable sizes, shapes, layers, compositions and defects in a low-cost, high-yield, and environmentally friendly manner, although we have witnessed a promising step forward in this direction. The second challenge involves the control of the size, morphology, crystallinity, phase composition, and distribution of the inorganic components on GN nanosheets. The properties and functions of the nanocomposites depend strongly on micro structures of the second components. However, the exact mechanism of how the synthesis variable precisely correlates with inorganic nanostructures stabilized on GN is rarely known. Therefore, the assembly behaviors of GN sheets with inorganic building blocks are required to be investigated more clearly for synthesizing nanocomposites with uniform morphology and distribution in the nanoscale. The third one is the improvement of the adhesion between GN and inorganic components, which is especially important for applications that involve charge transfer processeses. A poor interfacial contact will destroy the synergetic effects, and thus diminish the performance of the nanocomposites. So various surface functionalization methods, synthesis techniques, and novel architectures should be developed to make sure a large interfacial area between GN and inorganic components. Fourthly, a successful design and application of GN–inorganic nanocomposites also requires improvements in methodology to ensure better understanding of the components interaction mechanism and structure–property relationship in the nanocomposites. This needs to be studied systematically from both theoretical and experimental aspects, which will be a key to guide the future work of researchers and promote the development of GN–inorganic nanocomposites. Finally, further development and successful implementation of GN–inorganic nanocomposites require the multidisciplinary efforts from physics, chemistry, biology and materials science.

Acknowledgements

The authors are grateful for financial support from the Natural Science Foundation of Jiangsu Province (No. BK2009196) and the National Natural Science Foundation of China (No. 51072071).

References

1 D. Li and R. B. Kaner, *Science*, 2008, **320**, 1170–1171.
2 V. Singh, D. Joung, L. Zhai, S. Das, S. I. Khondaker and S. Seal, *Prog. Mater. Sci.*, 2011, **56**, 1178–1271.
3 A. K. Geim and K. S. Novoselov, *Nat. Mater.*, 2007, **6**, 183–191.
4 K. S. Novoselov, A. K. Geim, S. V. Morozov, D. Jiang, Y. Zhang, S. V. Dubonos, I. V. Grigorieva and A. A. Firsov, *Science*, 2004, **306**, 666–669.
5 K. S. Novoselov, A. K. Geim, S. V. Morozov, D. Jiang, M. I. Katsnelson, I. V. Grigorieva, S. V. Dubonos and A. A. Firsov, *Nature*, 2005, **438**, 197–200.
6 A. K. Geim, *Science*, 2009, **324**, 1530–1534.
7 C. Lee, X. D. Wei, J. W. Kysar and J. Hone, *Science*, 2008, **321**, 385–388.
8 M. D. Stoller, S. J. Park, Y. W. Zhu, J. H. An and R. S. Ruoff, *Nano Lett.*, 2008, **8**, 3498–3502.
9 A. A. Balandin, S. Ghosh, W. Z. Bao, I. Calizo, D. Teweldebrhan, F. Miao and C. N. Lau, *Nano Lett.*, 2008, **8**, 902–907.
10 K. I. Bolotin, K. J. Sikes, Z. Jiang, M. Klima, G. Fudenberg, J. Hone, P. Kim and H. L. Stormer, *Solid State Commun.*, 2008, **146**, 351–355.
11 R. R. Nair, P. Blake, A. N. Grigorenko, K. S.Novoselov, T. J. Booth, T. Stauber, N. M. R. Peres and A. K. Geim, *Science*, 2008, **320**, 1308–1308.
12 D. Eder, *Chem. Rev.*, 2010, **110**, 1348–1385.
13 X. H. Peng, J. Y. Chen, J. A. Misewich and S. S. Wong, *Chem. Soc. Rev.*, 2009, **38**, 1076–1098.
14 Y. B. Zhang, Y. W. Tan, H. L. Stormer and P. Kim, *Nature*, 2005, **438**, 201–204.
15 K. S. Novoselov, E. McCann, S. V. Morozov, V. I. Fal''ko, M. I. Katsnelson, U. Zeitler, D. Jiang, F. Schedin and A. K. Geim, *Nat. Phys.*, 2006, **2**, 177–180.
16 S. Latil and L. Henrard, *Phys. Rev. Lett.*, 2006, **97**, 036803.
17 E. T. Thostenson, Z. F. Ren and T. W. Chou, *Compos. Sci. Technol.*, 2001, **61**, 1899–1912.
18 H. Qian, E. S. Greenhalgh, M. S. P. Shaffe and A. Bismarck, *J. Mater. Chem.*, 2010, **20**, 4751–4762.
19 K. F. Zhou, Y. H. Zhu, X. L. Yang and C. Z. Li, *New J. Chem.*, 2010, **34**, 2950–2955.
20 C. Nethravathi, M. Rajamathi, N. Ravishankar, L. Basit and C. Felser, *Carbon*, 2010, **48**, 4343–4350.
21 B. J. Jiang, C. G. Tian, W. Zhou, J. Q. Wang, Y. Xie, Q. J. Pan, Z. Y. Ren, Y. Z. Dong, D. Fu, J. L. Han and H. G. Fu, *Chem.–Eur. J.*, 2011, **17**, 8379–8387.
22 Z. Jin, D. Nackashi, W. Lu, C. Kittrell and J. M. Tour, *Chem. Mater.*, 2010, **22**, 5695–5699.
23 S. Stankovich, D. A. Dikin, R. D. Piner, K. A. Kohlhaas, A. Kleinhammes, Y. Jia, Y. Wu, S. T. Nguyen and R. S. Ruoff, *Carbon*, 2007, **45**, 1558–1565.
24 Y. C. Si and E. T. Samulski, *Chem. Mater.*, 2008, **20**, 6792–6797.
25 S. V. Morozov, K. S. Novoselov, M. I. Katsnelson, F. Schedin, D. C. Elias, J. A. Jaszczak and A. K. Geim, *Phys. Rev. Lett.*, 2008, **100**, 016602.
26 T. K. Hong, D. W. Lee, H. J. Choi, H. S. Shin and B. S. Kim, *ACS Nano*, 2010, **4**, 3861–3868.
27 V. C. Tung, L. M. Chen, M. J. Allen, J. K. Wassei, K. Nelson, R. B. Kaner and Y. Yang, *Nano Lett.*, 2009, **9**, 1949–1955.
28 C. Gomez-Navarro, M. Burghard and K. Kern, *Nano Lett.*, 2008, **8**, 2045–2049.
29 K. J. Jeon and Z. Lee, *Chem. Commun.*, 2011, **47**, 3610–3612.
30 S. Park, J. H. An, I. W. Jung, R. D. Piner, S. J. An, X. S. Li, A. Velamakanni and R. S. Ruoff, *Nano Lett.*, 2009, **9**, 1593–1597.

31 N. Karousis, N. Tagmatarchis and D. Tasis, *Chem. Rev.*, 2010, **110**, 5366–5397.
32 Y. Hernandez, V. Nicolosi, M. Lotya, F. M. Blighe, Z. Y. Sun, S. De, I. T. McGovern, B. Holland, M. Byrne, Y. K. Gun''ko, J. J. Boland, P. Niraj, G. Duesberg, S. Krishnamurthy, R. Goodhue, J. Hutchison, V. Scardaci, A. C. Ferrari and J. N. Coleman, *Nat. Nanotechnol.*, 2008, **3**, 563–568.
33 K. S. Novoselov, D. Jiang, F. Schedin, T. J. Booth, V. V. Khotkevich, S. V. Morozov, A. K. Geim, *Proc. Natl. Acad. Sci.* USA, 2005, **102**, 10451–10453.
34 A. Reina, X. T. Jia, J. Ho, D. Nezich, H. B. Son, V. Bulovic, M. S. Dresselhaus and J. Kong, *Nano Lett.*, 2009, **9**, 30–35.
35 C. Mattevi, H. Kima and M. Chhowalla, *J. Mater. Chem.*, 2011, **21**, 3324–3334.
36 W. A. de Heer, C. Berger, X. S. Wu, P. N. First, E. H. Conrad, X. B. Li, T. B. Li, M. Sprinkle, J. Hass, M. L. Sadowski, M. Potemski and G. Martinez, *Solid State Commun.*, 2007, **143**, 92–100.
37 P. W. Sutter, J. I. Flege and E. A. Sutter, *Nat. Mater.*, 2008, **7**, 406–411.
38 S. Shivaraman, R. A. Barton, X. Yu, J. Alden, L. Herman, M. V. S. Chandrashekhar, J. Park, P. L. McEuen, J. M. Parpia, H. G. Craighead and M. G. Spencer, *Nano Lett.*, 2009, **9**, 3100–3105.
39 D. V. Kosynkin, A. L. Higginbotham, A. Sinitskii, J. R. Lomeda, A. Dimiev, B. K. Price and J. M. Tour, *Nature*, 2009, **458**, 872–876.
40 L. Y. Jiao, L. Zhang, X. R. Wang, G. Diankov and H. J. Dai, *Nature*, 2009, **458**, 877–880.
41 L. Y. Jiao, X. R. Wang, G. Diankov, H. L. Wang and H. J. Dai, *Nat. Nanotechnol.*, 2010, **5**, 321–325.
42 X. Yan, X. Cui and L. S. Li, *J. Am. Chem. Soc.*, 2010, **132**, 5944–5945.
43 X. Yan and L. S. Li, *J. Mater. Chem.*, 2011, **21**, 3295–3300.
44 S. Stankovich, R. D. Piner, X. Q. Chen, N. Q. Wu, S. T. Nguyen and R. S. Ruoff, *J. Mater. Chem.*, 2006, **16**, 155–158.
45 K. A. Worsley, P. Ramesh, S. K. Mandal, S. Niyogi, M. E. Itkis and R. C. Haddon, *Chem. Phys. Lett.*, 2007, **445**, 51–56.
46 S. Park, J. H. An, R. D. Piner, I. Jung, D. X. Yang, A. Velamakanni, S. T. Nguyen and R. S. Ruoff, *Chem. Mater.*, 2008, **20**, 6592–6594.
47 M. J. Allen, V. C. Tung and R. B. Kaner, *Chem. Rev.*, 2010, **110**, 132–145.
48 D. C. Wei and Y. Q. Liu, *Adv. Mater.*, 2010, **22**, 3225–3241.
49 S. Park and R. S. Ruoff, *Nat. Nanotechnol.*, 2009, **4**, 217–224.
50 Y. Si and E. T. Samulski, *Nano Lett.*, 2008, **8**, 1679–1682.
51 B. C. Brodie, *Philos. Trans. R. Soc.* London, 1859, **149**, 249–259.
52 L. Staudenmaier, *Ber. Dtsch. Chem. Ges.*, 1898, **31**, 1481–1487.
53 W. S. Hummers and R. E. Offeman, *J. Am. Chem. Soc.*, 1958, **80**, 1339–1339.
54 M. Hirata, T. Gotou, S. Horiuchi, M. Fujiwara and M. Ohba, *Carbon*, 2004, **42**, 2929–2937.
55 D. C. Marcano, D. V. Kosynkin, J. M. Berlin, A. Sinitskii, Z. Z. Sun, A. Slesarev, L. B. Alemany, W. Lu and J. M. Tour, *ACS Nano*, 2010, **4**, 4806–4814.
56 O. C. Compton and S. T. Nguyen, *Small*, 2010, **6**, 711–723.
57 M. J. McAllister, J. L. Li, D. H. Adamson, H. C. Schniepp, A. A. Abdala, J. Liu, M. Herrera-Alonso, D. L. Milius, R. Car, R. K. Prud''homme and I. A. Aksay, *Chem. Mater.*, 2007, **19**, 4396–4404.
58 A. Buchsteiner, A. Lerf and J. Pieper, *J. Phys. Chem. B*, 2006, **110**, 22328–22338.
59 S. Stankovich, R. D. Piner, S. T. Nguyen and R. S. Ruoff, *Carbon*, 2006, **44**, 3342–3347.
60 J. I. Paredes, S. Villar-Rodil, A. Martinez-Alonso and J. M. D. Tascon, *Langmuir*, 2008, **24**, 10560–10564.
61 D. R. Dreyer, S. Park, C. W. Bielawski and R. S. Ruoff, *Chem. Soc. Rev.*, 2010, **39**, 228–240.
62 V. C. Tung, M. J. Allen, Y. Yang and R. B. Kaner, *Nat. Nanotechnol.*, 2009, **4**, 25–29.
63 O. C. Compton, D. A. Dikin, K. W. Putz, L. C. Brinson and S. T. Nguyen, *Adv. Mater.*, 2010, **22**, 892–896.
64 D. Li, M. B. Mueller, S. Gilje, R. B. Kaner, G. G. Wallace and G. Gordon, *Nat. Nanotechnol.*, 2008, **3**, 101–105.
65 J. F. Shen, Y. Z. Hu, M. Shi, X. Lu, C. Qin, C. Li and M. X. Ye, *Chem. Mater.*, 2009, **21**, 3514–3520.
66 H. J. Shin, K. K. Kim, A. Benayad, S. M. Yoon, H. K. Park, I. S. Jung, M. H. Jin, H. K. Jeong, J. M. Kim, J. Y. Choi and Y. H. Lee, *Adv. Funct. Mater.*, 2009, **19**, 1987–1992.
67 G. X. Wang, J. Yang, J. Park, X. L. Gou, B. Wang, H. Liu and J. Yao, *J. Phys. Chem. C*, 2008, **112**, 8192–8195.
68 G. X. Wang, X. P. Shen, B. Wang, J. Yao and J. Park, *Carbon*, 2009, **47**, 1359–1364.
69 X. B. Fan, W. C. Peng, Y. Li, X. Y. Li, S. L. Wang, G. L. Zhang and F. B. Zhang, *Adv. Mater.*, 2008, **20**, 4490–4493.
70 W. F. Chen, L. F. Yan and P. R. Bangal, *J. Phys. Chem. C*, 2010, **114**, 19885–19890.
71 T. N. Zhou, F. Chen, K. Liu, H. Deng, Q. Zhang, J. W. Feng and Q. A. Fu, *Nanotechnology*, 2011, **22**, 045704.
72 X. P. Shen, L. Jiang, Z. Y. Ji, J. L. Wu, H. Zhou and G. X. Zhu, *J. Colloid Interface Sci.*, 2010, **354**, 493–497.
73 J. F. Che, L. Y. Shen and Y. H. Xiao, *J. Mater. Chem.*, 2010, **20**, 1722–1727.
74 M. J. Fernandez-Merino, L. Guardia, J. I. Paredes, S. Villar-Rodil, P. Solis-Fernandez, A. Martinez-Alonso and J. M. D. Tascon, *J. Phys. Chem. C*, 2010, **114**, 6426–6432.
75 J. Gao, F. Liu, Y. L. Liu, N. Ma, Z. Q. Wang and X. Zhang, *Chem. Mater.*, 2010, **22**, 2213–2218.
76 C. Z. Zhu, S. J. Guo, Y. X. Fang and S. J. Dong, *ACS Nano*, 2010, **4**, 2429–2437.
77 D. R. Dreyer, S. Murali, Y. Zhu, R. S. Ruoff and C. W. Bielawski, *J. Mater. Chem.*, 2011, **21**, 3443–3447.
78 S. F. Pei, J. P. Zhao, J. H. Du, W. C. Ren and H. M. Cheng, *Carbon*, 2010, **48**, 4466–4474.
79 Z. J. Fan, K. Wang, T. Wei, J. Yan, L. P. Song and B. Shao, *Carbon*, 2010, **48**, 1686–1689.
80 Z. J. Fan, K. Wang, J. Yan, T. Wei, L. J. Zhi, J. Feng, Y. M. Ren, L. P. Song and F. Wei, *ACS Nano*, 2011, **5**, 191–198.
81 Z. Zhang, H. H. Cheng, C. Y. Xing, M. Y. Guo, F. G. Xu, X. D. Wang, H. Gruber, B. L. Zhang and J. L. Tang, *Nano Res.*, 2011, **4**, 599–611.
82 Y. Wang, Z. X. Shi and J. Yin, *ACS Appl. Mater. Interfaces*, 2011, **3**, 1127–1133.
83 F. Yang, Y. Q. Liu, L. A. Gao and J. Sun, *J. Phys. Chem. C*, 2010, **114**, 22085–22091.
84 Y. W. Zhu, M. D. Stoller, W. W. Cai, A. Velamakanni, R. D. Piner, D. Chen and R. S. Ruoff, *ACS Nano*, 2010, **4**, 1227–1233.
85 W. F. Chen and L. F. Yan, *Nanoscale*, 2010, **2**, 559–563.
86 Y. Zhou, Q. L. Bao, L. A. L. Tang, Y. L. Zhong and K. P. Loh, *Chem. Mater.*, 2009, **21**, 2950–2956.
87 A. V. Murugan, T. Muraliganth and A. Manthiram, *Chem. Mater.*, 2009, **21**, 5004–5006.
88 W. F. Chen, L. F. Yan and P. R. Bangal, *Carbon*, 2010, **48**, 1146–1152.
89 M. Zhou, Y. L. Wang, Y. M. Zhai, J. F. Zhai, W. Ren, F. A. Wang and S. J. Dong, *Chem.–Eur. J.*, 2009, **15**, 6116–6120.
90 S. J. An, Y. W. Zhu, S. H. Lee, M. D. Stoller, T. Emilsson, S. Park, A. Velamakanni, J. H. An and R. S. Ruoff, *J. Phys. Chem. Lett.*, 2010, **1**, 1259–1263.
91 Y. Y. Shao, J. Wang, M. Engelhard, C. M. Wang and Y. H. Lin, *J. Mater. Chem.*, 2010, **20**, 743–748.
92 Y. H. Ding, P. Zhang, Q. Zhuo, H. M. Ren, Z. M. Yang and Y. Jiang, *Nanotechnology*, 2011, **22**, 215601.
93 E. C. Salas, Z. Z. Sun, A. Luttge and J. M. Tour, *ACS Nano*, 2010, **4**, 4852–4856.
94 L. Huang, Y. Liu, L. C. Ji, Y. Q. Xie, T. Wang and W. Z. Shi, *Carbon*, 2011, **49**, 2431–2436.
95 M. Baraket, S. G. Walton, Z. Wei, E. H. Lock, J. T. Robinson and P. Sheehan, *Carbon*, 2010, **48**, 3382–3390.
96 D. C. Guo, G. X. Zhang, J. F. Liu and X. M. Sun, *J. Phys. Chem. C*, 2011, **115**, 11327–11335.
97 J. I. Paredes, S. Villar-Rodil, M. J. Fernandez-Merino, L. Guardia, A. Martinez-Alonso and J. M. D. Tascon, *J. Mater. Chem.*, 2011, **21**, 298–306.
98 S. Niyogi, E. Bekyarova, M. E. Itkis, J. L. McWilliams, M. A. Hamon and R. C. Haddon, *J. Am. Chem. Soc.*, 2006, **128**, 7720–7721.
99 Y. X. Xu, H. Bai, G. W. Lu, C. Li and G. Q. Shi, *J. Am. Chem. Soc.*, 2008, **130**, 5856–5857.
100 M. Quintana, K. Spyrou, M. Grzelczak, W. R. Browne, P. Rudolf and M. Prato, *ACS Nano*, 2010, **4**, 3527–3533.
101 T. Ramanathan, A. A. Abdala, S. Stankovich, D. A. Dikin, M. Herrera-Alonso, R. D. Piner, D. H. Adamson, H. C. Schniepp, X. Chen, R. S. Ruoff, S. T. Nguyen, I. A. Aksay, R. K.

Prud'homme and L. C. Brinson, *Nat. Nanotechnol.*, 2008, **3**, 327–331.
102 Z. F. Liu, Q. Liu, Y. Huang, Y. F. Ma, S. G. Yin, X. Y. Zhang, W. Sun and Y. S. Chen, *Adv. Mater.*, 2008, **20**, 3924–3930.
103 X. L. Li, X. R. Wang, L. Zhang, S. W. Lee and H. J. Dai, *Science*, 2008, **319**, 1229–1232.
104 H. F. Yang, C. S. Shan, F. H. Li, D. X. Han, Q. X. Zhang and L. Niu, *Chem. Commun.*, 2009, 3880–3882.
105 M. C. Hsiao, S. H. Liao, M. Y. Yen, P. I. Liu, N. W. Pu, C. A. Wang and C. C. M. Ma, *ACS Appl. Mater. Interfaces*, 2010, **2**, 3092–3099.
106 Z. Liu, J. T. Robinson, X. M. Sun and H. J. Dai, *J. Am. Chem. Soc.*, 2008, **130**, 10876–10877.
107 Y. F. Xu, Z. B. Liu, X. L. Zhang, Y. Wang, J. G. Tian, Y. Huang, Y. F. Ma, X. Y. Zhang and Y. S. Chen, *Adv. Mater.*, 2009, **21**, 1275–1279.
108 A. J. Patil, J. L. Vickery, T. B. Scott and S. Mann, *Adv. Mater.*, 2009, **21**, 3159–3164.
109 X. Y. Yang, X. Y. Zhang, Z. F. Liu, Y. F. Ma, Y. Huang and Y. S. Chen, *J. Phys. Chem. C*, 2008, **112**, 17554–17558.
110 W. Lv, M. Guo, M. H. Liang, F. M. Jin, L. Cui, L. J. Zhi and Q. H. Yang, *J. Mater. Chem.*, 2010, **20**, 6668–6673.
111 J. Geng and H. T. Jung, *J. Phys. Chem. C*, 2010, **114**, 8227–8234.
112 Y. Y. Liang, D. Q. Wu, X. L. Feng and K. Mullen, *Adv. Mater.*, 2009, **21**, 1679–1683.
113 S. Z. Zu and B. H. Han, *J. Phys. Chem. C*, 2009, **113**, 13651–13657.
114 S. Stankovich, D. A. Dikin, G. H. B. Dommett, K. M. Kohlhaas, E. J. Zimney, E. A. Stach, R. D. Piner, S. T. Nguyen and R. S. Ruoff, *Nature*, 2006, **442**, 282–286.
115 J. J. Liang, Y. Huang, L. Zhang, Y. Wang, Y. F. Ma, T. Y. Guo and Y. S. Chen, *Adv. Funct. Mater.*, 2009, **19**, 2297–2302.
116 M. A. Rafiee, J. Rafiee, Z. Wang, H. H. Song, Z. Z. Yu and N. Koratkar, *ACS Nano*, 2009, **3**, 3884–3890.
117 T. Kuilla, S. Bhadra, D. H. Yao, N. H. Kim, S. Bose and J. H. Lee, *Prog. Polym. Sci.*, 2010, **35**, 1350–1375.
118 H. Kim, A. A. Abdala and C. W. Macosko, *Macromolecules*, 2010, **43**, 6515–6530.
119 J. R. Potts, D. R. Dreyer, C. W. Bielawski and R. S. Ruoff, *Polymer*, 2011, **52**, 5–25.
120 R. Verdejo, M. M. Bernal, L. J. Romasanta and M. A. Lopez-Manchado, *J. Mater. Chem.*, 2011, **21**, 3301–3310.
121 R. Muszynski, B. Seger and P. V. Kamat, *J. Phys. Chem. C*, 2008, **112**, 5263–5266.
122 G. Goncalves, P. A. A. P. Marques, C. M. Granadeiro, H. I. S. Nogueira, M. K. Singh and J. Gracio, *Chem. Mater.*, 2009, **21**, 4796–4802.
123 X. Huang, Z. S. Li, Y. Z. Huang, S. X. Wu, X. Z. Zhou, S. Z. Li, C. L. Gan, F. Boey, C. A. Mirkin and H. Zhang, *Nat. Commun.*, 2011, **2**, 292.
124 B. S. Kong, J. X. Geng and H. T. Jung, *Chem. Commun.*, 2009, 2174–2176.
125 R. Pasricha, S. Gupta and A. K. Srivastava, *Small*, 2009, **5**, 2253–2259.
126 S. Bai, X. P. Shen, G. X. Zhu, Z. Xu and Y. J. Liu, *Carbon*, 2011, **49**, 4563–4570.
127 J. Li and C. Y. Liu, *Eur. J. Inorg. Chem.*, 2010, 1244–1248.
128 S. Zhang, Y. Y. Shao, H. G. Liao, M. H. Engelhard, G. P. Yin and Y. H. Lin, *ACS Nano*, 2011, **5**, 1785–1791.
129 B. Seger and P. V. Kamat, *J. Phys. Chem. C*, 2009, **113**, 7990–7995.
130 E. Yoo, T. Okata, T. Akita, M. Kohyama, J. Nakamura and I. Honma, *Nano Lett.*, 2009, **9**, 2255–2259.
131 G. M. Scheuermann, L. Rumi, P. Steurer, W. Bannwarth and R. Muelhaupt, *J. Am. Chem. Soc.*, 2009, **131**, 8262–8270.
132 N. Li, Z. Y. Wang, K. K. Zhao, Z. J. Shi, S. K. Xu and Z. N. Gu, *J. Nanosci. Nanotechnol.*, 2010, **10**, 6748–6751.
133 K. S. Subrahmanyam, A. K. Manna, S. K. Pati and C. N. R. Rao, *Chem. Phys. Lett.*, 2010, **497**, 70–75.
134 N. A. Luechinger, E. K. Athanassiou and W. J. Stark, *Nanotechnology*, 2008, **19**, 445201.
135 X. B. Bin, J. Z. Chen, H. Cao, L. T. Chen and J. Z. Yuan, *J. Phys. Chem. Solids*, 2009, **70**, 1–7.
136 G. X. Wang, B. Wang, X. L. Wang, J. Park, S. X. Dou, H. Ahn and K. Kim, *J. Mater. Chem.*, 2009, **19**, 8378–8384.
137 J. H. Warner, M. H. Ruemmeli, A. Bachmatiuk, M. Wilson and B. Buechner, *ACS Nano*, 2010, **4**, 470–476.
138 J. Bian, X. W. Wei, L. Wang and Z. P. Guan, *Chinese Phys. Lett.*, 2011, **22**, 57–60.
139 J. K. Wassei, K. C. Cha, V. C. Tung, Y. Yang and R. B. Kaner, *J. Mater. Chem.*, 2011, **21**, 3391–3396.
140 S. Das, R. Seelaboyina, V. Verma, I. Lahiri, J. Y. Hwang, R. Banerjee and W. B. Choi, *J. Mater. Chem.*, 2011, **21**, 7289–7295.
141 X. C. Dong, B. Li, A. Wei, X. H. Cao, M. B. Chan-Park, H. Zhang, L. J. Li, W. Huang and P. Chen, *Carbon*, 2011, **49**, 2944–2949.
142 D. S. Yu, K. Park, M. Durstock and L. M. Dai, *J. Phys. Chem. Lett.*, 2011, **2**, 1113–1118.
143 J. Yan, T. Wei, B. Shao, F. Q. Ma, Z. J. Fan, M. L. Zhang, C. Zheng, Y. C. Shang, W. Z. Qian and F. Wei, *Carbon*, 2010, **48**, 1731–1737.
144 Z. B. Lei, N. Christov and X. S. Zhao, *Energy Environ. Sci.*, 2011, **4**, 1866–1873.
145 Z. J. Fan, J. Yan, T. Wei, G. Q. Ning, L. J. Zhi, J. C. Liu, D. X. Cao, G. L. Wang and F. Wei, *ACS Nano*, 2011, **5**, 2787–2794.
146 T. T. Baby and R. Sundara, *J. Phys. Chem. C*, 2011, **115**, 8527–8533.
147 P. Wang, Y. M. Zhai, D. J. Wang and S. J. Dong, *Nanoscale*, 2011, **3**, 1640–1645.
148 H. Y. Koo, H. J. Lee, H. A.Go, Y. B. Lee, T. S. Bae, J. K. Kim and W. S. Choi, *Chem.–Eur. J.*, 2011, **17**, 1214–1219.
149 C. Xu, X. Wang, L. C. Yang and Y. P. Wu, *J. Solid State Chem.*, 2009, **182**, 2486–2490.
150 C. Chen, W. M. Cai, M. C. Long, B. X. Zhou, Y. H. Wu, D. Y. Wu and Y. J. Feng, *ACS Nano*, 2010, **4**, 6425–6432.
151 H. K. He and C. Gao, *ACS Appl. Mater. Interfaces*, 2010, **2**, 3201–3210.
152 S. Chen, J. W. Zhu and X. Wang, *J. Phys. Chem. C*, 2010, **114**, 11829–11834.
153 Z. Gao, J. Wang, Z. S. Li, W. L. Yang, B. Wang, M. J. Hou, Y. He, Q. Liu, T. Mann, P. P. Yang, M. L. Zhang and L. H. Liu, *Chem. Mater.*, 2011, **23**, 3509–3516.
154 J. L. Wu, S. Bai, X. P. Shen and L. Jiang, *Appl. Surf. Sci.*, 2010, **257**, 747–751.
155 C. Z. Yuan, L. R. Hou, L. Yang, C. G. Fan, D. K. Li, J. M. Li, L. F. Shen, F. Zhang and X. G. Zhang, *Mater. Lett.*, 2011, **65**, 374–377.
156 Y. Wang, H. B. Yao, X. H. Wang and S. H. Yu, *J. Mater. Chem.*, 2011, **21**, 562–566.
157 Y. Lin, K. Zhang, W. F. Chen, Y. D. Liu, Z. G. Geng, J. Zeng, N. Pan, L. F. Yan, X. P. Wang and J. G. Hou, *ACS Nano*, 2010, **4**, 3033–3038.
158 Y. C. Qiu, K. Y. Yan, S. H. Yang, L. M. Jin, H. Deng and W. S. Li, *ACS Nano*, 2010, **4**, 6515–6526.
159 S. J. Kim, S. H. Ku, S. Y. Lim, J. H. Kim and C. B. Park, *Adv. Mater.*, 2011, **23**, 2009–2014.
160 C. Nethravathi, B. Viswanath, C. Shivakumara, N. Mahadevaiah and M. Rajamathi, *Carbon*, 2008, **46**, 1773–1781.
161 B. Das, B. Choudhury, A. Gomathi, A. K. Manna, S. K. Pati and C. N. R. Rao, *ChemPhysChem*, 2011, **12**, 937–943.
162 Y. L. Cao, X. L. Li, I. A. Aksay, J. Lemmon, Z. M. Nie, Z. G. Yang and J. Liu, *Phys. Chem. Chem. Phys.*, 2011, **13**, 7660–7665.
163 H. L. Wang, Y. Yang, Y. Y. Liang, J. T. Robinson, Y. G. Li, A. Jackson, Y. Cui and H. J. Dai, *Nano Lett.*, 2011, **11**, 2644–2647.
164 S. L. Chou, J. Z. Wang, M. Choucair, H. K. Liu, J. A. Stride and S. X. Dou, *Electrochem. Commun.*, 2010, **12**, 303–306.
165 J. Z. Wang, C. Zhong, S. L. Chou and H. K. Liu, *Electrochem. Commun.*, 2010, **12**, 1467–1470.
166 L. Kou and C. Gao, *Nanoscale*, 2011, **3**, 519–528.
167 L. S. Walker, V. R. Marotto, M. A. Rafiee, N. Koratkar and E. L. Corral, *ACS Nano*, 2011, **5**, 3182–3190.
168 F. Ji, Y. L. Li, J. M. Feng, D. Su, Y. Y. Wen, Y. Feng and F. Hou, *J. Mater. Chem.*, 2009, **19**, 9063–9067.
169 S. B. Yang, X. L. Feng, X. C. Wang and K. Mullen, *Angew. Chem., Int. Ed.*, 2011, **50**, 5339–5343.
170 Y. Q. Sun, C. Li, Y. X. Li, H. Bai, Z. Y. Yao and G. Q. Shi, *Chem. Commun.*, 2010, **46**, 4740–4742.
171 X. H. Li, J. S. Chen, X. C. Wang, J. H. Sun and M. Antonietti, *J. Am. Chem. Soc.*, 2011, **133**, 8074–8077.
172 Q. J. Xiang, J. G. Yu and M. Jaroniec, *J. Phys. Chem. C*, 2011, **115**, 7355–7363.
173 R. Kumar, D. Varandani, B. R. Mehta, V. N. Singh, Z. H. Wen, X. L. Feng and K. Mullen, *Nanotechnology*, 2011, **22**, 275719.

174 N. Zhang, H. X. Qiu, Y. Liu, W. Wang, Y. Li, X. D. Wang and J. P. Gao, *J. Mater. Chem.*, 2011, **21**, 11080–11083.
175 H. L. Wang, Y. Yang, Y. Y. Liang, L. F. Cui, H. S. Casalongue, Y. G. Li, G. S. Hong, Y. Cui and H. J. Dai, *Angew. Chem., Int. Ed.*, 2011, **50**, 7364–7368.
176 H. X. Chang, Z. H. Sun, K. Y. F. Ho and X. M. Tao, *Nanoscale*, 2011, **3**, 258–264.
177 H. J. Li, G. Zhu, Z. H. Liu, Z. P. Yang and Z. L. Wang, *Carbon*, 2010, **48**, 4391–4396.
178 Y. Q. Zhou and Y. Wang, *Nanoscale*, 2011, **3**, 2615–2620.
179 H. L. Wang, H. S. Casalongue, Y. Y. Liang and H. J. Dai, *J. Am. Chem. Soc.*, 2010, **132**, 7472–7477.
180 J. Choi, J. Jin, I. G. Jung, J. M. Kim, H. J. Kim and S. U. Son, *Chem. Commun.*, 2011, **47**, 5241–5243.
181 S. Kim, H. Choi, M. Jung, S. Y. Choi and S. Ju, *Nanotechnology*, 2010, **21**, 425203.
182 B. Kumar, K. Y. Lee, H. K. Park, S. J. Chae, Y. H. Lee and S. W. Kee, *ACS Nano*, 2011, **5**, 4197–4204.
183 J. X. Zhu, Y. K. Sharma, Z. Y. Zeng, X. J. Zhang, M. Srinivasan, S. Mhaisalkar, H. Zhang, H. H. Hng and Q. Y. Yan, *J. Phys. Chem. C*, 2011, **115**, 8400–8406.
184 C. Z. Zhu, S. J. Guo, Y. X. Fang, L. Han, E. K. Wang and S. J. Dong, *Nano Res.*, 2011, **4**, 648–657.
185 V. Jousseaume, J. Cuzzocrea, N. Bernier and V. T. Renard, *Appl. Phys. Lett.*, 2011, **98**, 123103.
186 R. Lv, T. Cui, M. Jun, Q. Zhang, A. Cao, D. S. Su, Z. Zhang, S. Yoon, J. Miyawaki, I. Mochida and F. Kang, *Adv. Funct. Mater.*, 2011, **21**, 999–1006.
187 Y. J. Kim, J. H. Lee and G. C. Yi, *Appl. Phys. Lett.*, 2009, **95**, 213101.
188 C. Y. Li, Z. Li, H. W. Zhu, K. L. Wang, J. Q. Wei, X. A. Li, P. Z. Sun, H. Zhang and D. H. Wu, *J. Phys. Chem. C*, 2010, **114**, 14008–14012.
189 J. J. Xu, K. Wang, S. Z. Zu, B. H. Han and Z. X. Wei, *ACS Nano*, 2010, **4**, 5019–5026.
190 H. T. Hu, X. B. Wang, J. C. Wang, L. Wan, F. M. Liu, H. Zheng, R. Chen and H. C. Xu, *Chem. Phys. Lett.*, 2010, **484**, 247–253.
191 S. Myung, A. Solanki, C. Kim, J. Park, K. S. Kim and K. B. Lee, *Adv. Mater.*, 2011, **23**, 2221–2225.
192 J. S. Chen, Z. Y. Wang, X. C. Dong, P. Chen and X. W. Lou, *Nanoscale*, 2011, **3**, 2158–2161.
193 X. Liu, Y. S. Hu, J. O. Müller, R. Schlogl, J. Maier and D. S. Su, *ChemSusChem*, 2010, **3**, 261–265.
194 L. Jiang, X. P. Shen, J. L. Wu and K. C. Shen, *J. Appl. Polym. Sci.*, 2010, **118**, 275–279.
195 Y. B. Tang, C. S. Lee, J. Xu, Z. T. Liu, Z. H. Chen, Z. B. He, Y. L. Cao, G. D. Yuan, H. S. Song, L. M. Chen, L. B. Luo, H. M. Cheng, W. J. Zhang, I. Bello and S. T. Lee, *ACS Nano*, 2010, **4**, 3482–3488.
196 S. Watcharotone, D. A. Dikin, S. Stankovich, R. Piner, I. Jung, G. H. B. Dommett, G. Evmenenko, S. E. Wu, S. F. Chen, C. P. Liu, S. T. Nguyen and R. S. Ruoff, *Nano Lett.*, 2007, **7**, 1888–1892.
197 Z. J. Fan, K. Wang, J. Yan and T. Wei, *Mater. Res. Bull.*, 2011, **46**, 315–318.
198 Y. C. Fan, L. J. Wang, J. L. Li, J. Q. Li, S. K. Sun, F. Chen, L. D. Chen and W. Jiang, *Carbon*, 2010, **48**, 1743–1749.
199 W. Lv, F. Sun, D. M. Tang, H. T. Fang, C. Liu, Q. H. Yang and H. M. Cheng, *J. Mater. Chem.*, 2011, **21**, 9014–9019.
200 L. Wang, D. Wang, X. Y. Dong, Z. J. Zhang, X. F. Pei, X. J. Chen, B. Chen and J. Jin, *Chem. Commun.*, 2011, **47**, 3556–3558.
201 X. Z. Tang, Z. W. Cao, H. B. Zhang, J. Liu and Z. Z. Yu, *Chem. Commun.*, 2011, **47**, 3084–3086.
202 M. R. Das, R. K. Sarma, R. Saikia, V. S. Kale, M. V. Shelke and P. Sengupta, *Colloids Surf., B*, 2011, **83**, 16–22.
203 H. W. Tien, Y. L. Huang, S. Y. Yang, J. Y. Wang and C. C. M. Ma, *Carbon*, 2011, **49**, 1550–1560.
204 Y. M. Li, L. H. Tang and J. H. Li, *Electrochem. Commun.*, 2009, **11**, 846–849.
205 O. L. Yue, K. Zhang, X. M. Chen, L. Wang, J. S. Zhao, J. F. Liu and J. B. Jia, *Chem. Commun.*, 2010, **46**, 3369–3371.
206 S. Q. Chen, P. Chen, M. H. Wu, D. Y. Pan and Y. Wang, *Electrochem. Commun.*, 2010, **12**, 1302–1306.
207 K. Zhang, Q. L. Yue, G. F. Chen, Y. L. Zhai, L. Wang, H. S. Wang, J. S. Zhao, J. F. Liu, J. B. Jia and H. B. Li, *J. Phys. Chem. C*, 2011, **115**, 379–389.
208 C. Xu, X. Wang and J. W. Zhu, *J. Phys. Chem. C*, 2008, **112**, 19841–19845.
209 Y. J. Li, W. Gao, L. J. Ci, C. M. Wang and P. M. Ajayan, *Carbon*, 2010, **48**, 1124–1130.
210 L. F. Dong, R. R. S. Gari, Z. Li, M. M. Craig and S. F. Hou, *Carbon*, 2010, **48**, 781–787.
211 C. V. Rao, A. L. M. Reddy, Y. Ishikawa and P. M. Ajayan, *Carbon*, 2011, **49**, 931–936.
212 Y. Chen, Y. Li, D. Sun, D. B. Tian, J. R. Zhang and J. J. Zhu, *J. Mater. Chem.*, 2011, **21**, 7604–7611.
213 X. Yang, M. S. Xu, W. M. Qiu, X. Q. Chen, M. Deng, J. L. Zhang, H. Iwai, E. Watanabe and H. Z. Chen, *J. Mater. Chem.*, 2011, **21**, 8096–8103.
214 C. Xu, X. Wang, J. W. Zhu, X. J. Yang and L. Lu, *J. Mater. Chem.*, 2008, **18**, 5625–5629.
215 J. W. Zhu, G. Y. Zeng, F. D. Nie, X. M. Xu, S. Chen, Q. F. Han and X. Wang, *Nanoscale*, 2010, **2**, 988–994.
216 X. Y. Yang, X. Y. Zhang, Y. F. Ma, Y. Huang, Y. S. Wang and Y. S. Chen, *J. Mater. Chem.*, 2009, **19**, 2710–2714.
217 X. Y. Zhang, X. Y. Yang, Y. F. Ma, Y. Huang and Y. S. Chen, *J. Nanosci. Nanotechnol.*, 2010, **10**, 2984–2987.
218 V. Chandra, J. Park, Y. Chun, J. W. Lee, I. C. Hwang and K. S. Kim, *ACS Nano*, 2010, **4**, 3979–3986.
219 T. N. Lambert, C. A. Chavez, B. Hernandez-Sanchez, P. Lu, N. S. Bell, A. Ambrosini, T. Friedman, T. J. Boyle, D. R. Wheeler and D. L. Huber, *J. Phys. Chem. C*, 2009, **113**, 19812–19823.
220 L. S. Zhang, L. Y. Jiang, H. J. Yan, W. D. Wang, W. Wang, W. G. Song, Y. G. Guo and L. J. Wan, *J. Mater. Chem.*, 2010, **20**, 5462–5467.
221 C. Z. Zhu, S. J. Guo, P. Wang, L. Xing, Y. X. Fang, Y. M. Zhai and S. J. Dong, *Chem. Commun.*, 2010, **46**, 7148–7150.
222 J. T. Zhang, Z. G. Xiong and X. S. Zhao, *J. Mater. Chem.*, 2011, **21**, 3634–3640.
223 F. H. Li, J. F. Song, H. F. Yang, S. Y. Gan, Q. X. Zhang, D. X. Han, A. Ivaska and L. Niu, *Nanotechnology*, 2009, **20**, 455602.
224 X. Y. Wang, X. F. Zhou, K. Yao, J. G. Zhang and Z. P. Liu, *Carbon*, 2011, **49**, 133–139.
225 D. H. Wang, R. Kou, D. Choi, Z. G. Yang, Z. M. Nie, J. Li, L. V. Saraf, D. H. Hu, J. G. Zhang, G. L. Graff, J. Liu, M. A. Pope and I. A. Aksay, *ACS Nano*, 2010, **4**, 1587–1595.
226 S. B. Yang, X. L. Feng, L. Wang, K. Tang, J. Maier and K. Mullen, *Angew. Chem. Int. Ed.*, 2010, **49**, 4795–4799.
227 C. Nethravathi, T. Nisha, N. Ravishankar, C. Shivakumara and M. Rajamathi, *Carbon*, 2009, **47**, 2054–2059.
228 C. X. Guo, H. B. Yang, Z. M. Sheng, Z. S. Lu, Q. L. Song and C. M. Li, *Angew. Chem., Int. Ed.*, 2010, **49**, 3014–3017.
229 M. Du, T. Yang and K. Jiao, *J. Mater. Chem.*, 2010, **20**, 9253–9260.
230 C. P. Fu, Y. F. Kuang, Z. Y. Huang, X. A. Wang, N. N. Du, J. H. Chen and H. H. Zhou, *Chem. Phys. Lett.*, 2010, **499**, 250–253.
231 Y. J. Hu, J. Jin, P. Wu, H. Zhang and C. X. Cai, *Electrochim. Acta*, 2010, **56**, 491–500.
232 C. B. Liu, K. Wang, S. L. Luo, Y. H. Tang and L. Y. Chen, *Small*, 2011, **7**, 1203–1206.
233 S. Liu, J. Q. Wang, J. Zeng, J. F. Ou, Z. P. Li, X. H. Liu and S. R. Yang, *J. Power Sources*, 2010, **195**, 4628–4633.
234 Y. G. Zhou, J. J. Chen, F. B. Wang, Z. H. Sheng and X. H. Xia, *Chem. Commun.*, 2010, **46**, 5951–5953.
235 Y. J. Hu, H. Zhang, P. Wu, H. Zhang, B. Zhou and C. X. Cai, *Phys. Chem. Chem. Phys.*, 2011, **13**, 4083–4094.
236 S. X. Wu, Z. Y. Yin, Q. Y. He, X. A. Huang, X. Z. Zhou and H. Zhang, *J. Phys. Chem. C*, 2010, **114**, 11816–11821.
237 S. X. Wu, Z. Y. Yin, Q. Y. He, G. Lu, X. Z. Zhou and H. Zhang, *J. Mater. Chem.*, 2011, **21**, 3467–3470.
238 Q. Cheng, J. Tang, J. Ma, H. Zhang, N. Shinya and L. C. Qin, *Carbon*, 2011, **49**, 2917–2925.
239 X. Z. Zhou, X. Huang, X. Y. Qi, S. X. Wu, C. Xue, F. Y. C. Boey, Q. Y. Yan, P. Chen and H. Zhang, *J. Phys. Chem. C*, 2009, **113**, 10842–10846.
240 Y. K. Kim, H. K. Na, Y. W. Lee, H. Jang, S. W. Han and D. H. Min, *Chem. Commun.*, 2010, **46**, 3185–3187.
241 X. M. Chen, G. H. Wu, J. M. Chen, X. Chen, Z. X. Xie and X. R. Wang, *J. Am. Chem. Soc.*, 2011, **133**, 3693–3695.
242 X. W. Liu, J. J. Mao, P. d. Liu and X. W. Wei, *Carbon*, 2011, **49**, 477–483.
243 P. V. Kamat, *J. Phys. Chem. Lett.*, 2010, **1**, 520–527.

244 G. Williams, B. Seger and P. V. Kamat, *ACS Nano*, 2008, **2**, 1487–1491.
245 B. Li, X. T. Zhang, X. H. Li, L. Wang, R. Y. Han, B. B. Liu, W. T. Zheng, X. L. Li and Y. C. Liu, *Chem. Commun.*, 2010, **46**, 3499–3501.
246 T. N. Lambert, C. A. Chavez, N. S. Bell, C. M. Washburn, D. R. Wheeler and M. T. Brumbache, *Nanoscale*, 2011, **3**, 188–191.
247 G. Williams and P. V. Kamat, *Langmuir*, 2009, **25**, 13869–13873.
248 O. Akhavan, *Carbon*, 2011, **49**, 11–18.
249 Y. H. Ng, A. Iwase, N. J. Bell, A. Kudo and R. Amal, *Catal. Today*, 2011, **164**, 353–357.
250 X. Huang, X. Z. Zhou, S. X. Wu, Y. Y. Wei, X. Y. Qi, J. Zhang, F. Boey and H. Zhang, *Small*, 2010, **6**, 513–516.
251 I. V. Lightcap, T. H. Kosel and P. V. Kamat, *Nano Lett.*, 2010, **10**, 577–583.
252 G. H. Moon, Y. Park, W. Kim and W. Choi, *Carbon*, 2011, **49**, 3454–3462.
253 H. M. A. Hassan, V. Abdelsayed, A. E. R. S. Khder, K. M. AbouZeid, J. Terner, M. S. El-Shall, S. I. Al-Resayes and A. A. El-Azhary, *J. Mater. Chem.*, 2009, **19**, 3832–3837.
254 S. Sharma, A. Ganguly, P. Papakonstantinou, X. P. Miao, M. X. Li, J. L. Hutchison, M. Delichatsios and S. Ukleja, *J. Phys. Chem. C*, 2010, **114**, 19459–19466.
255 P. Kundu, C. Nethravathi, P. A. Deshpande, M. Rajamathi, G. Madras and N. Ravishankar, *Chem. Mater.*, 2011, **23**, 2772–2780.
256 K. Jasuja, J. Linn, S. Melton and V. Berry, *J. Phys. Chem. Lett.*, 2010, **1**, 1853–1860.
257 A. F. Zedan, S. Sappal, S. Moussa and M. S. El-Shall, *J. Phys. Chem. C*, 2010, **114**, 19920–19927.
258 H. T. Hua, X. B. Wang, F. M. Liu, J. C. Wang and C. H. Xu, *Synth. Met.*, 2011, **161**, 404–410.
259 M. Zhang, D. N. Lei, X. M. Yin, L. B. Chen, Q. H. Li, Y. G. Wang and T. H. Wang, *J. Mater. Chem.*, 2010, **20**, 5538–5543.
260 J. Yan, T. Wei, W. M. Qiao, B. Shao, Q. K. Zhao, L. J. Zhang and Z. J. Fan, *Electrochim. Acta*, 2010, **55**, 6973–6978.
261 M. Zhang, D. Lei, Z. F. Du, X. M. Yin, L. B. Chen, Q. H. Li, Y. G. Wang and T. H. Wang, *J. Mater. Chem.*, 2011, **21**, 1673–1676.
262 X. J. Liu, L. K. Pan, T. Lv, T. Lu, G. Zhu, Z. Sun and C. Q. Sun, *Catal. Sci. Technol.*, 2011, **1**, 1189–1193.
263 Y. Lin, D. W. Baggett, J. W. Kim, E. J. Siochi and J. W. Connell, *ACS Appl. Mater. Interfaces*, 2011, **3**, 1652–1664.
264 Z. S. Wu, W. C. Ren, L. B. Gao, B. L. Liu, J. P. Zhao and H. M. Cheng, *Nano Res.*, 2010, **3**, 16–22.
265 K. Vinodgopal, B. Neppolian, I. V. Lightcap, F. Grieser, M. Ashokkumar and P. V. Kamat, *J. Phys. Chem. Lett.*, 2010, **1**, 1987–1993.
266 S. Chandra, S. Bag, R. Bhar and P. Pramanik, *J. Nanopart. Res.*, 2011, **13**, 2769–2777.
267 J. J. Guo, S. M. Zhu, Z. X. Chen, Y. Li, Z. Y. Yong, Q. L. Liu, J. B. Li, C. L. Feng and D. Zhang, *Ultrason. Sonochem.*, 2011, **18**, 1082–1090.
268 J. J. Shi and J. J. Zhu, *Electrochim. Acta*, 2011, **56**, 6008–6013.
269 J. J. Shi, G. H. Yang and J. J. Zhu, *J. Mater. Chem.*, 2011, **21**, 7343–7349.
270 S. Q. Chen and Y. Wang, *J. Mater. Chem.*, 2010, **20**, 9735–9739.
271 Z. S. Wu, W. C. Ren, L. Wen, L. B. Gao, J. P. Zhao, Z. P. Chen, G. M. Zhou, F. Li and H. M. Cheng, *ACS Nano*, 2010, **4**, 3187–3194.
272 Z. S. Wu, D. W. Wang, W. Ren, J. Zhao, G. Zhou, F. Li and H. M. Cheng, *Adv. Funct. Mater.*, 2010, **20**, 3595–3602.
273 G. M. Zhou, D. W. Wang, F. Li, L. L. Zhang, N. Li, Z. S. Wu, L. Wen, G. Q. Lu and H. M. Cheng, *Chem. Mater.*, 2010, **22**, 5306–5313.
274 Z. Y. Ji, J. L. Wu, X. P. Shen, H. Zhou and H. T. Xi, *J. Mater. Sci.*, 2011, **46**, 1190–1195.
275 K. H. Chang, Y. F. Lee, C. C. Hu, C. I. Chang, C. L. Liu and Y. L. Yang, *Chem. Commun.*, 2010, **46**, 7957–7959.
276 H. W. Wang, Z. A. Hu, Y. Q. Chang, Y. L. Chen, H. Y. Wu, Z. Y. Zhang and Y. Y. Yang, *J. Mater. Chem.*, 2011, **21**, 10504–10511.
277 V. K. Singh, M. K. Patra, M. Manoth, G. S. Gowd, S. R. Vadera and N. Kumar, *New Carbon Mater.*, 2009, **24**, 147–152.
278 J. F. Shen, Y. Z. Hu, M. Shi, N. Li, H. W. Ma and M. X. Ye, *J. Phys. Chem. C*, 2010, **114**, 1498–1503.
279 H. P. Cong, J. J. He, Y. Lu and S. H. Yu, *Small*, 2010, **6**, 169–173.
280 D. Marquardt, C. Vollmer, R. Thomann, P. Steurer, R. Mülhaupt, E. Redel and C. Janiak, *Carbon*, 2011, **49**, 1326–1332.
281 Q. Su, Y. Y. Liang, X. L. Feng and K. Mullen, *Chem. Commun.*, 2010, **46**, 8279–8281.
282 S. B. Yang, G. L. Cui, S. P. Pang, Q. Cao, U. Kolb, X. L. Feng, J. Maier and K. Mullen, *ChemSusChem*, 2010, **3**, 236–239.
283 K. Gotoh, K. Kawabata, E. Fujii, K. Morishige, T. Kinumoto, Y. Miyazaki and H. Ishida, *Carbon*, 2009, **47**, 2120–2124.
284 K. Gotoh, T. Kinumoto, E. Fujii, A. Yamamoto, H. Hashimoto, T. Ohkubo, A. Itadani, Y. Kuroda and H. Ishida, *Carbon*, 2011, **49**, 1118–1125.
285 J. F. Shen, M. Shi, B. Yan, H. W. Ma, N. Li and M. X. Ye, *J. Mater. Chem.*, 2011, **21**, 7795–7801.
286 W. B. Zou, J. W. Zhu, Y. X. Sun and X. Wang, *Mater. Chem. Phys.*, 2011, **125**, 617–620.
287 J. L. Wu, X. P. Shen, L. Jiang, K. Wang and K. M. Chen, *Appl. Surf. Sci.*, 2010, **256**, 2826–2830.
288 K. F. Zhou, Y. H. Zhu, X. L. Yang, X. Jiang and C. Z. Li, *New J. Chem.*, 2011, **35**, 353–359.
289 Y. Fan, H. T. Lu, J. H. Liu, C. P. Yang, Q. S. Jing, Y. X. Zhang, X. K. Yang and K. J. Huang, *Colloids Surf., B*, 2011, **83**, 78–82.
290 J. F. Shen, M. Shi, B. Yan, H. W. Ma, N. Li and M. X. Ye, *Nano Res.*, 2011, **4**, 795–806.
291 J. F. Shen, B. Yan, M. Shi, H. W. Ma, N. Li and M. X. Ye, *J. Mater. Chem.*, 2011, **21**, 3415–3421.
292 K. F. Zhou, Y. H. Zhu, X. L. Yang and C. Z. Li, *Electroanalysis*, 2011, **23**, 862–869.
293 J. Z. Wang, C. Zhong, D. Wexler, N. H. Idris, Z. X. Wang, L. Q. Chen and H. K. Liu, *Chem.–Eur. J.*, 2011, **17**, 661–667.
294 X. P. Shen, J. L. Wu, S. Bai and H. Zhou, *J. Alloys Compd.*, 2010, **506**, 136–140.
295 W. H. Shi, J. X. Zhu, D. H. Sim, Y. Y. Tay, Z. Y. Lu, X. J. Zhang, Y. Sharma, M. Srinivasan, H. Zhang, H. H. Hng and Q. Y. Yan, *J. Mater. Chem.*, 2011, **21**, 3422–3427.
296 X. D. Huang, X. F. Zhou, L. Zhou, K. Qian, Y. H. Wang, Z. P. Liu and C. Z. Yu, *ChemPhysChem*, 2011, **12**, 278–281.
297 G. B. Jung, Y. Myung, Y. J. Cho, Y. J. Sohn, D. M. Jang, H. S. Kim, C. W. Lee, J. Park, I. Maeng, J. H. Son and C. Kang, *J. Phys. Chem. C*, 2010, **114**, 11258–11265.
298 B. J. Li, H. Q. Cao, J. Shao, G. Q. Li, M. Z. Qu and G. Yin, *Inorg. Chem.*, 2011, **50**, 1628–1632.
299 H. W. Wang, Z. A. Hu, Y. Q. Chang, Y. L. Chen, Z. Q. Lei, Z. Y. Zhang and Y. Y. Yang, *Electrochim. Acta*, 2010, **55**, 8974–8980.
300 J. X. Zhu, T. Zhu, X. Z. Zhou, Y. Y. Zhang, X. W. Lou, X. D. Chen, H. Zhang, H. H. Hng and Q. Y. Yan, *Nanoscale*, 2011, **3**, 1084–1089.
301 S. Chen, J. W. Zhu, H. A. Huang, G. Y. Zeng, F. D. Nie and X. Wang, *J. Solid State Chem.*, 2010, **183**, 2552–2557.
302 Y. S. He, D. W. Bai, X. W. Yang, J. Chen, X. Z. Liao and Z. F. Ma, *Electrochem. Commun.*, 2010, **12**, 570–573.
303 J. O. Hwang, D. H. Lee, J. Y. Kim, T. H. Han, B. H. Kim, M. Park, K. No and S. O. Kim, *J. Mater. Chem.*, 2011, **21**, 3432–3437.
304 D. Choi, M. Y. Choi, W. M. Choi, H. J. Shin, H. K. Park, J. S. Seo, J. Park, S. M. Yoon, S. J. Chae, Y. H. Lee, S. W. Kim, J. Y. Choi, S. Y. Lee and J. M. Kim, *Adv. Mater.*, 2010, **22**, 2187–2192.
305 T. V. Cuong, V. H. Pham, J. S. Chung, E. W. Shin, D. H. Yoo, S. H. Hahn, J. S. Huh, G. H. Rue, E. J. Kim, S. H. Hur and P. A. Kohl, *Mater. Lett.*, 2010, **64**, 2479–2482.
306 H. L. Wang, J. T. Robinson, G. Diankov and H. J. Dai, *J. Am. Chem. Soc.*, 2010, **132**, 3270–3271.
307 H. L. Wang, L. F. Cui, Y. A. Yang, H. S. Casalongue, J. T. Robinson, Y. Y. Liang, Y. Cui and H. J. Dai, *J. Am. Chem. Soc.*, 2010, **132**, 13978–13980.
308 Y. Y. Liang, H. L. Wang, H. S. Casalongue, Z. Chen and H. J. Dai, *Nano Res.*, 2010, **3**, 701–705.
309 Y. J. Mai, X. L. Wang, J. Y. Xiang, Y. Q. Qiao, D. Zhang, C. D. Gu and J. P. Tu, *Electrochim. Acta*, 2011, **56**, 2306–2311.
310 A. N. Cao, Z. Liu, S. S. Chu, M. H. Wu, Z. M. Ye, Z. W. Cai, Y. L. Chang, S. F. Wang, Q. H. Gong and Y. F. Liu, *Adv. Mater.*, 2010, **22**, 103–106.
311 P. Wang, T. F. Jiang, C. Z. Zhu, Y. M. Zhai, D. J. Wang and S. J. Dong, *Nano Res.*, 2010, **3**, 794–799.
312 Q. Li, B. D. Guo, J. G. Yu, J. R. Ran, B. H. Zhang, H. J. Yan and J. R. Gong, *J. Am. Chem. Soc.*, 2011, **133**, 10878–10884.

313 L. P. Xue, C. F. Shen, M. B. Zheng, H. L. Lu, N. W. Li, G. B. Ji, L. J. Pan and J. M. Cao, *Mater. Lett.*, 2011, **65**, 198–200.
314 K. Chang and W. X. Chen, *Chem. Commun.*, 2011, **47**, 4252–4254.
315 Z. S. Lu, C. X. Guo, H. B. Yang, Y. Qiao, J. Guo and C. M. Li, *J. Colloid Interface Sci.*, 2011, **353**, 588–592.
316 H. Q. Zhou, C. Y. Qiu, Z. Liu, H. C. Yang, L. J. Hu, J. Liu, H. F. Yang, C. Z. Gu and L. F. Sun, *J. Am. Chem. Soc.*, 2010, **132**, 944–946.
317 H. Q. Zhou, C. Y. Qiu, F. Yu, H. C. Yang, M. J. Chen, L. J. Hu and L. F. Sun, *J. Phys. Chem. C*, 2011, **115**, 11348–11354.
318 Z. T. Luo, L. A. Somers, Y. P. Dan, T. Ly, N. J. Kybert, E. J. Mele and A. T. C. Johnson, *NanoLett.*, 2010, **10**, 777–781.
319 A. T. N''Diaye, S. Bleikamp, P. J. Feibelman and T. Michely, *Phys. Rev. Lett.*, 2006, **97**, 215501.
320 A. T. N''Diaye, T. Gerber, C. Busse, J. Myslivecek, J. Coraux and T. Michely, *New J. Phys.*, 2009, **11**, 103045.
321 Y. Pan, M. Gao, L. Huang, F. Liu and H. J. Gao, *Appl. Phys. Lett.*, 2009, **95**, 093106.
322 Z. H. Zhou, F. Gao and D. W. Goodman, *Surf. Sci.*, 2010, **604**, L31–L38.
323 N. G. Shang, P. Papakonstantinou, P. Wang, S. Ravi and P. Silva, *J. Phys. Chem. C*, 2010, **114**, 15837–15841.
324 M. H. Maneshian, F. L. Kuo, K. Mahdak, J. Hwang, R. Banerjee and N. D. Shepherd, *Nanotechnology*, 2011, **22**, 205703.
325 K. H. Yu, G. H. Lu, S. Mao, K. H. Chen, H. Kim, Z. H. Wen and J. H. Chen, *ACS Appl. Mater. Interfaces*, 2011, **3**, 2703–2709.
326 J. A. Lin, M. Penchev, G. P. Wang, R. K. Paul, J. B. Zhong, X. Y. Jing, M. Ozkan and C. S. Ozkan, *Small*, 2010, **6**, 2448–2452.
327 D. Kondo, S. Sato and Y. Awano, *Appl. Phys. Express*, 2008, **1**, 074003.
328 L. L. Zhang, Z. G. Xiong and X. S. Zhao, *ACS Nano*, 2010, **4**, 7030–7036.
329 Z. J. Fan, J. Yan, L. J. Zhi, Q. Zhang, T. Wei, J. Feng, M. L. Zhang, W. Z. Qian and F. Wei, *Adv. Mater.*, 2010, **22**, 3723–3728.
330 X. R. Wang, S. M. Tabakman and H. J. Dai, *J. Am. Chem. Soc.*, 2008, **130**, 8152–8153.
331 H. Alles, J. Aarik, A. Aidla, A. Fay, J. Kozlova, A. Niilisk, M. Paers, M. Raehn, M. Wiesner, P. Hakonen and V. Sammelselg, *Cent. Eur. J. Phys.*, 2011, **9**, 319–324.
332 K. Zou, X. Hong, D. Keefer and J. Zhu, *Phys. Rev. Lett.*, 2010, **105**, 126601.
333 X. B. Meng, D. S. Geng, J. A. Liu, M. N. Banis, Y. Zhang, R. Y. Li and X. L. Sun, *J. Phys. Chem. C*, 2010, **114**, 18330–18337.
334 X. B. Meng, D. S. Geng, J. A. Liu, R. Y. Li and X. L. Sun, *Nanotechnology*, 2011, **22**, 165602.
335 X. Y. Zhang, H. P. Li, X. L. Cui and Y. H. Lin, *J. Mater. Chem.*, 2010, **20**, 2801–2806.
336 H. D. Liu, P. Gao, J. H. Fang and G. Yang, *Chem. Commun.*, 2011, **47**, 9110–9112.
337 H. F. Xiang, B. B. Tian, P. C. Lian, Z. Li and H. H. Wang, *J. Alloys Compd.*, 2011, **509**, 7205–7209.
338 H. Zhao, J. Yang, L. Wang, C. G. Tian, B. J. Jiang and H. G. Fu, *Chem. Commun.*, 2011, **47**, 2014–2016.
339 Z. M. Wang, W. D. Wang, N. Coombs, N. Soheilnia and G. A. Ozin, *ACS Nano*, 2010, **4**, 7437–7450.
340 D. H. Lee, J. E. Kim, T. H. Han, J. W. Hwang, S. Jeon, S. Y. Choi, S. H. Hong, W. J. Lee, R. S. Ruoff and S. O. Kim, *Adv. Mater.*, 2010, **22**, 1247–1252.
341 Y. T. Kim, J. H. Han, B. H. Hong and Y. U. Kwon, *Adv. Mater.*, 2010, **22**, 515–518.
342 J. M. Lee, Y. B. Pyun, J. Yi, J. W. Choung and W. I. Park, *J. Phys. Chem. C*, 2009, **113**, 19134–19138.
343 J. Y. Son, Y. H. Shin, H. Kim and H. M. Jang, *ACS Nano*, 2010, **4**, 2655–2658.
344 F. A. He, J. T. Fan, F. Song, L. M. Zhang and H. L. W. Chan, *Nanoscale*, 2011, **3**, 1182–1188.
345 J. B. Liu, S. H. Fu, B. Yuan, Y. L. Li and Z. X. Deng, *J. Am. Chem. Soc.*, 2010, **132**, 7279–7281.
346 F. A. He, J. T. Fan, D. Ma, L. M. Zhang, C. Leung and H. L. Chan, *Carbon*, 2010, **48**, 3139–3144.
347 Y. Zhang, B. A. Chen, L. M. Zhang, J. Huang, F. H. Chen, Z. P. Yang, J. L. Yao and Z. J. Zhang, *Nanoscale*, 2011, **3**, 1446–1450.
348 T. A. Pham, B. C. Choi and Y. T. Jeong, *Nanotechnology*, 2010, **21**, 465603.
349 A. P. Tuan, B. C. Choi, K. T. Lim and Y. T. Jeong, *Appl. Surf. Sci.*, 2011, **257**, 3350–3357.
350 T. A. Pham, N. A. Kumar and Y. T. Jeong, *Synth. Met.*, 2010, **160**, 2028–2036.
351 Y. K. Kim and D. H. Min, *Carbon*, 2010, **48**, 4283–4288.
352 X. Y. Zhang, Z. B. Liu, Y. Huang, X. J. Wan, J. G. Tian, Y. F. Ma and Y. S. Chen, *J. Nanosci. Nanotechnol.*, 2009, **9**, 5752–5756.
353 X. Y. Zhang, Y. Huang, Y. Wang, Y. F. Ma, Z. F. Liu and Y. S. Chen, *Carbon*, 2009, **47**, 334–337.
354 Z. B. Liu, Y. F. Xu, X. Y. Zhang, X. L. Zhang, Y. S. Chen and J. G. Tian, *J. Phys. Chem. B*, 2009, **113**, 9681–9686.
355 Y. Zhang, L. Q. Ren, S. R. Wang, A. Marathe, J. Chaudhuri and G. G. Li, *J. Mater. Chem.*, 2011, **21**, 5386–5391.
356 J. Huang, L. M. Zhang, B. A. Chen, N. Ji, F. H. Chen, Y. Zhang and Z. J. Zhang, *Nanoscale*, 2010, **2**, 2733–2738.
357 X. M. Geng, L. Niu, Z. Y. Xing, R. S. Song, G. T. Liu, M. T. Sun, G. S. Cheng, H. J. Zhong, Z. H. Liu, Z. J. Zhang, L. F. Sun, H. X. Xu, L. Lu and L. W. Liu, *Adv. Mater.*, 2010, **22**, 638–642.
358 J. B. Liu, Y. L. Li, Y. M. Li, J. H. Li and Z. X. Deng, *J. Mater. Chem.*, 2010, **20**, 900–906.
359 F. Liu, J. Y. Choi and T. S. Seo, *Chem. Commun.*, 2010, **46**, 2844–2846.
360 Y. Wang, S. J. Zhen, Y. Zhang, Y. F. Li and C. Z. Huang, *J. Phys. Chem. C*, 2011, **115**, 12815–12821.
361 M. Feng, R. Q. Sun, H. B. Zhan and Y. Chen, *Nanotechnology*, 2010, **21**, 075601.
362 L. Qiu, X. W. Yang, X. L. Gou, W. R. Yang, Z. F. Ma, G. G. Wallace and D. Li, *Chem.–Eur. J.*, 2010, **16**, 10653–10658.
363 C. Zhang, L. L. Ren, X. Y. Wang and T. X. Liu, *J. Phys. Chem. C*, 2010, **114**, 11435–11440.
364 G. X. Zhu, Y. J. Liu, Z. Xu, T. A. Jiang, C. Zhang, X. Li and G. Qi, *ChemPhysChem*, 2010, **11**, 2432–2437.
365 G. H. Lu, S. Mao, S. Park, R. S. Ruoff and J. H. Chen, *Nano Res.*, 2009, **2**, 192–200.
366 S. B. Yang, X. L. Feng, S. Ivanovici and K. Mullen, *Angew. Chem., Int. Ed.*, 2010, **49**, 8408–8411.
367 W. J. Hong, H. Bai, Y. X. Xu, Z. Y. Yao, Z. Z. Gu and G. Q. Shi, *J. Phys. Chem. C*, 2010, **114**, 1822–1826.
368 S. Liu, J. Q. Tian, L. Wang, H. L. Li, Y. W. Zhang and X. P. Sun, *Macromolecules*, 2010, **43**, 10078–10083.
369 Y. X. Fang, S. J. Guo, C. Z. Zhu, Y. M. Zhai and E. K. Wang, *Langmuir*, 2010, **26**, 11277–11282.
370 L. L. Li, K. P. Liu, G. H. Yang, C. M. Wang, J. R. Zhang and J. J. Zhu, *Adv. Funct. Mater.*, 2011, **21**, 869–878.
371 S. Y. Wang, X. Wang and S. P. Jiang, *Phys. Chem. Chem. Phys.*, 2011, **13**, 6883–6891.
372 J. T. Zhang, J. W. Jiang and X. S. Zhao, *J. Phys. Chem. C*, 2011, **115**, 6448–6454.
373 D. S. Yu and L. M. Dai, *J. Phys. Chem. Lett.*, 2010, **1**, 467–470.
374 Y. K. Kim and D. H. Min, *Langmuir*, 2009, **25**, 11302–11306.
375 J. L. Xiang and L. T. Drazl, *ACS Appl. Mater. Interfaces*, 2011, **3**, 1325–1332.
376 C. Z. Zhu, S. J. Guo, Y. M. Zhai and S. J. Dong, *Langmuir*, 2010, **26**, 7614–7618.
377 K. K. Manga, Y. Zhou, Y. L. Yan and K. P. Loh, *Adv. Funtc. Mater.*, 2009, 19–3643.
378 X. R. Zhang, S. G. Li, X. Jin and S. S. Zhang, *Chem. Commun.*, 2011, **47**, 4929–4931.
379 M. Alazemi, I. Dutta, F. Wang, R. H. Blunk and A. P. Angelopoulos, *Carbon*, 2010, **48**, 4063–4073.
380 Z. P. Li, J. Q. Wang, X. H. Liu, S. Liu, J. F. Ou and S. R. Yang, *J. Mater. Chem.*, 2011, **21**, 3397–3403.
381 H. B. Yao, L. H. Wu, C. H. Cui, H. Y. Fang and S. H. Yu, *J. Mater. Chem.*, 2010, **20**, 5190–5195.
382 D. Chen, X. Y. Wang, T. X. Liu, X. D. Wang and J. Li, *ACS Appl. Mater. Interfaces*, 2010, **2**, 2005–2011.
383 Y. Li, X. B. Fan, J. J. Qi, J. Y. Ji, S. L. Wang, G. L. Zhang and F. B. Zhang, *Nano Res.*, 2010, **3**, 429–437.
384 A. R. Siamaki, A. E. R. S. Khder, V. Abdelsayed, M. S. El-Shall and B. F. Gupton, *J. Catal.*, 2011, **279**, 1–11.
385 Z. H. Tang, S. L. Shen, J. Zhuang and X. Wang, *Angew. Chem., Int. Ed.*, 2010, **49**, 4603–4607.
386 Y. Li, X. B. Fan, J. J. Qi, J. Y. Ji, S. L. Wang, G. L. Zhang and F. B. Zhang, *Mater. Res. Bull.*, 2010, **45**, 1413–1418.

387 L. H. Tang, Y. Wang, Y. M. Li, H. B. Feng, J. Lu and J. H. Li, *Adv. Funct. Mater.*, 2009, **19**, 2782–2789.
388 R. Kou, Y. Y. Shao, D. H. Wang, M. H. Engelhard, J. H. Kwak, J. Wang, V. V. Viswanathan, C. M. Wang, Y. H. Lin, Y. Wang, I. A. Aksay and J. Liu, *Electrochem. Commun.*, 2009, **11**, 954–957.
389 S. M. Choi, M. H. Seo, H. J. Kim and W. B. Kim, *Carbon*, 2011, **49**, 904–909.
390 Y. C. Xin, J. G. Liu, W. M. Liu, J. Gao, Y. Xie, Y. Yin and Z. G. Zou, *J. Power Sources*, 2011, **196**, 1012–1018.
391 E. Yoo, T. Okada, T. Akita, M. Kohyama, I. Honma and J. Nakamura, *J. Power Sources*, 2011, **196**, 110–115.
392 Y. Y. Shao, S. Zhang, C. M. Wang, Z. M. Nie, J. Liu, Y. Wang and Y. H. Lin, *J. Power Sources*, 2010, **195**, 4600–4605.
393 H. Y. Li, X. H. Zhang, H. L. Pang, C. T. Huang and J. H. Chen, *J. Solid State Electrochem.*, 2010, **14**, 2267–2274.
394 C. Nethravathi, E. A. Anumol, M. Rajamathi and N. Ravishankar, *Nanoscale*, 2011, **3**, 569–571.
395 S. Bong, Y. R. Kim, I. Kim, S. Woo, S. Uhm, J. Lee and H. Kim, *Electrochem. Commun.*, 2010, **12**, 129–131.
396 S. Y. Wang, S. P. Jiang and X. Wang, *Electrochim. Acta*, 2011, **56**, 3338–3344.
397 C. V. Rao, A. L. M. Reddy, Y. Ishikawa and P. M. Ajayan, *Carbon*, 2011, **49**, 931–936.
398 S. Zhang, Y. Y. Shao, H. G. Liao, J. Liu, I. A. Aksay, G. P. Yin and Y. H. Lin, *Chem. Mater.*, 2011, **23**, 1079–1081.
399 S. J. Guo, S. J. Dong and E. K. Wang, *ACS Nano*, 2010, **4**, 547–555.
400 R. Y. Y. Shao, D. H. Mei, Z. M. Nie, D. H. Wang, C. M. Wang, V. V. Viswanathan, S. Park, I. A. Aksay, Y. H. Lin, Y. Wang and J. Liu, *J. Am. Chem. Soc.*, 2011, **133**, 2541–2547.
401 Y. C. Zhao, L. Zhan, J. N. Tian, S. L. Nie and Z. Ning, *Electrochim. Acta*, 2011, **56**, 1967–1972.
402 M. H. Seo, S. M. Choi, H. J. Kim and W. B. Kim, *Electrochem. Commun.*, 2011, **13**, 182–185.
403 R. N. Singh and R. Awasthi, *Catal. Sci. Technol.*, 2011, **1**, 778–783.
404 J. Yang, C. G. Tian, L. Wang and H. G. Fu, *J. Mater. Chem.*, 2011, **21**, 3384–3390.
405 F. H. Li, H. F. Yang, C. S. Shan, Q. X. Zhang, D. X. Han, A. Ivaska and L. Niu, *J. Mater. Chem.*, 2009, **19**, 4022–4025.
406 Y. Y. Liang, Y. G. Li, H. L. Wang, J. G. Zhou, J. Wang, T. Regier and H. J. Dai, *Nat. Mater.*, 2011, **10**, 780–786.
407 Y. G. Li, H. L. Wang, L. M. Xie, Y. Y. Liang, G. S. Hong and H. J. Dai, *J. Am. Chem. Soc.*, 2011, **133**, 7296–7299.
408 Y. Qian, S. B. Lu and F. L. Gao, *Mater. Lett.*, 2011, **65**, 56–58.
409 H. Zhang, X. J. Lv, Y. M. Li, Y. Wang and J. H. Li, *ACS Nano*, 2010, **4**, 380–386.
410 J. C. Liu, H. W. Bai, Y. J. Wang, Z. Y. Liu, X. W. Zhang and D. D. Sun, *Adv. Funct. Mater.*, 2010, **20**, 4175–4181.
411 Y. H. Zhang, Z. R. Tang, X. Z. Fu and Y. J. Xu, *ACS Nano*, 2010, **4**, 7303–7314.
412 H. J. Zhang, P. P. Xu, G. D. Du, Z. W. Chen, K. Oh, D. Y. Pan and Z. Jiao, *Nano Res.*, 2011, **4**, 274–283.
413 J. Du, X. Y. Lai, N. L. Yang, J. Zhai, D. Kisailus, F. B. Su, D. Wang and L. Jiang, *ACS Nano*, 2011, **5**, 590–596.
414 G. D. Jiang, Z. F. Lin, C. Chen, L. H. Zhu, Q. Chang, N. Wang, W. Wei and H. Q. Tang, *Carbon*, 2011, **49**, 2693–2701.
415 N. Li, G. Liu, C. Zhen, F. Li, L. L. Zhang and H. M. Cheng, *Adv. Funct. Mater.*, 2011, **21**, 1717–1722.
416 W. Q. Fan, Q. H. Lai, Q. H. Zhang and Y. Wang, *J. Phys. Chem. C*, 2011, **115**, 10694–10701.
417 Z. G. Xiong, L. L. Zhang, J. Z. Ma and X. S. Zhao, *Chem. Commun.*, 2010, **46**, 6099–6101.
418 E. P. Gao, W. Z. Wang, M. Shang and J. H. Xu, *Phys. Chem. Chem. Phys.*, 2011, **13**, 2887–2893.
419 N. H. Ng, A. Iwase, A. Kudo and R. Amal, *J. Phys. Chem. Lett.*, 2010, **1**, 2607–2612.
420 L. Jia, D. H. Wang, Y. X. Huang, A. W. Xu and H. Q. Yu, *J. Phys. Chem. C*, 2011, **115**, 11466–11473.
421 B. J. Li and H. Q. Cao, *J. Mater. Chem.*, 2011, **21**, 3346–3349.
422 T. G. Xu, L. W. Zhang, H. Y. Cheng and Y. F. Zhu, *Appl. Catal., B*, 2011, **101**, 382–387.
423 F. Zhou, R. Shi and Y. F. Zhu, *J. Mol. Catal. A: Chem.*, 2011, **340**, 77–82.
424 X. F. Zhang, X. Quan, S. Chen and H. T. Yu, *Appl. Catal., B*, 2011, **105**, 237–242.
425 Y. S. Fu and X. Wang, *Ind. Eng. Chem. Res.*, 2011, **50**, 7210–7218.
426 M. S. Zhu, P. L. Chen and M. H. Liu, *ACS Nano*, 2011, **5**, 4529–4536.
427 M. Pumera, *Energy Environ. Sci.*, 2011, **4**, 668–674.
428 S. J. Guo and S. J. Dong, *Chem. Soc. Rev.*, 2011, **40**, 2644–2672.
429 L. L. Zhang, R. Zhou and X. S. Zhao, *J. Mater. Chem.*, 2010, **20**, 5983–5992.
430 J. Yan, Z. J. Fan, T. Wei, W. Z. Qian, M. L. Zhang and F. Wei, *Carbon*, 2010, **48**, 3825–3833.
431 S. Chen, J. W. Zhu, X. D. Wu, Q. F. Han and X. Wang, *ACS Nano*, 2010, **4**, 2822–2830.
432 Z. S. Wu, W. C. Ren, D. W. Wang, F. Li, B. L. Liu and H. M. Cheng, *ACS Nano*, 2010, **4**, 5835–5842.
433 Z. J. Fan, J. Yan, T. Wei, L. J. Zhi, G. Q. Ning, T. Y. Li and F. Wei, *Adv. Funct. Mater.*, 2011, **21**, 2366–2375.
434 G. Yu, L. Hu, M. Vosgueritchian, H. Wang, X. Xie, J. R. McDonough, X. Cui, Y. Cui and Z. Bao, *Nano Lett.*, 2011, **11**, 2905–2911.
435 B. Wang, J. Park, C. Y. Wang, H. Ahn and G. X. Wang, *Electrochim. Acta*, 2010, **55**, 6812–6817.
436 J. Yan, T. Wei, W. M. Qiao, B. Shao, Q. K. Zhao, L. J. Zhang and Z. J. Fan, *Electrochim. Acta*, 2010, **55**, 6973–6978.
437 W. W. Zhou, J. P. Liu, T. Chen, K. S. Tan, X. T. Jia, Z. Q. Luo, C. X. Cong, H. P. Yang, C. M. Li and T. Yu, *Phys. Chem. Chem. Phys.*, 2011, **13**, 14462–14465.
438 T. Lu, Y. P. Zhang, H. B. Li, L. K. Pan, Y. L. Li and Z. Sun, *Electrochim. Acta*, 2010, **55**, 4170–4173.
439 Y. P. Zhang, H. B. Li, L. K. Pan, T. Lu and Z. Sun, *J. Electroanal. Chem.*, 2009, **634**, 68–71.
440 Y. L. Chen, Z. A. Hu, Y. Q. Chang, H. W. Wang, Z. Y. Zhang and Y. Y. Yang, *J. Phys. Chem. C*, 2011, **115**, 2563–2571.
441 B. J. Li, H. Q. Cao, J. Shao, M. Z. Qu and J. H. Warner, *J. Mater. Chem.*, 2011, **21**, 5069–5075.
442 X. H. Xia, J. P. Tu, Y. J. Mai, R. Chen, X. L. Wang, C. D. Gu and X. B. Zhao, *Chem.–Eur. J.*, 2011, **17**, 10898–10905.
443 Y. Wang, C. X. Guo, J. H. Luo, T. Chen, H. B. Yang and C. M. Li, *Dalton Trans.*, 2011, **40**, 6388–6391.
444 B. J. Li, H. Q. Cao, G. Yin, Y. X. Lu and J. F. Yin, *J. Mater. Chem.*, 2011, **21**, 10645–10648.
445 J. W. Lee, T. Ahn, D. Soundararajan, J. M. Ko and J. D. Kim, *Chem. Commun.*, 2011, **47**, 6305–6307.
446 S. Y. Yang, K. H. Chang, H. W. Tien, Y. F. Lee, S. M. Li, Y. S. Wang, J. Y. Wang, C. C. M. Ma and C. C. Hu, *J. Mater. Chem.*, 2011, **21**, 2374–2380.
447 Q. Cheng, J. Tang, J. Ma, H. Zhang, N. Shinya and L. C. Qin, *Phys. Chem. Chem. Phys.*, 2011, **13**, 17615–17624.
448 G. X. Wang, X. P. Shen, J. Yao and J. Park, *Carbon*, 2009, **47**, 2049–2053.
449 M. H. Liang and L. J. Zhi, *J. Mater. Chem.*, 2009, **19**, 5871–5878.
450 S. M. Paek, E. Yoo and I. Honma, *Nano Lett.*, 2009, **9**, 72–75.
451 J. Yao, X. P. Shen, B. Wang, H. K. Liu and G. X. Wang, *Electrochem. Commun.*, 2009, **11**, 1849–1852.
452 Y. M. Li, X. J. Lv, J. Lu and J. H. Li, *J. Phys. Chem. C*, 2010, **114**, 21770–21774.
453 Z. Y. Wang, H. Zhang, N. Li, Z. J. Shi, Z. N. Gu and G. P. Cao, *Nano Res.*, 2010, **3**, 748–756.
454 H. Kim, S. W. Kim, Y. U. Park, H. Gwon, D. H. Seo, Y. Kim and K. Kang, *Nano Res.*, 2010, **3**, 748–756.
455 S. J. Ding, D. Luan, F. Y. C. Beoy, J. S. Chen and X. W. Lou, *Chem. Commun.*, 2011, **47**, 7155–7157.
456 P. C. Lian, X. F. Zhu, H. F. Xiang, Z. Li, E. S. Yang and H. H. Wang, *Electrochim. Acta*, 2010, **56**, 834–840.
457 L. W. Ji, Z. K. Tan, T. R. Kuykendall, S. Aloni, S. D. Sun, E. Lin, V. Battaglia and Y. G. Zhang, *Phys. Chem. Chem. Phys.*, 2011, **13**, 7170–7177.
458 H. Kim, D. H. Seo, S. W. Kim, J. Kim and K. Kang, *Carbon*, 2011, **49**, 326–332.
459 B. Wang, X. L. Wu, C. Y. Shu, Y. G. Guo and C. R. Wang, *J. Mater. Chem.*, 2010, **20**, 10661–10664.
460 D. H. Wang, D. W. Choi, J. Li, Z. G. Yang, Z. M. Nie, R. Kou, D. H. Hu, C. M. Wang, L. V. Saraf, J. G. Zhang, I. A. Aksay and J. Liu, *ACS Nano*, 2009, **3**, 907–914.
461 S. J. Ding, J. S. Cheng, D. Y. Luan, F. Y. C. Boey, S. Madhavi and X. W. Lou, *Chem. Commun.*, 2011, **47**, 5780–5782.
462 X. J. Zhu, Y. W. Zhu, S. Murali, M. D. Stollers and R. S. Ruoff, *ACS Nano*, 2011, **5**, 3333–3338.

463 G. Wang, T. Liu, Y. J. Luo, X. Tong, L. J. Wan, Y. Zhao, H. Wang, Z. Y. Ren and J. B. Bai, *J. Alloys Compd.*, 2011, **509**, L216–L220.
464 G. Wang, J. T. Bai, Y. H. Wang, Z. Y. Ren and J. B. Bai, *Scr. Mater.*, 2011, **65**, 339–342.
465 L. F. Shen, C. Z. Yuan, H. J. Luo, X. G. Zhang, S. D. Yang and X. J. Lu, *Nanoscale*, 2011, **3**, 572–574.
466 B. J. Li, H. Q. Cao, J. Shao, H. Zheng, Y. X. Lu, J. F. Yin and M. Z. Qu, *Chem. Commun.*, 2011, **47**, 3159–3161.
467 K. Chang and W. X. Cheng, *ACS Nano*, 2011, **5**, 4720–4728.
468 J. K. Lee, K. B. Smith, C. M. Hayner and H. H. Kung, *Chem. Commun.*, 2010, **46**, 2025–2027.
469 L. W. Ji, Z. K. Tan, T. Kuykendall, E. J. An, Y. B. Fu, V. Battaglia and Y. G. Zhang, *Energy Environ. Sci.*, 2011, **4**, 3611–3616.
470 E. Yoo, J. Kim, E. Hosono, H. Zhou, T. Kudo and I. Honma, *Nano Lett.*, 2008, **8**, 2277–2282.
471 Y. Ding, Y. Jiang, F. Xu, J. Yin, H. Ren, Q. Zhuo, Z. Long and P. Zhang, *Electrochem. Commun.*, 2010, **12**, 10–13.
472 D. W. Choi, D. H. Wang, V. V. Viswanathan, I. T. Bae, W. Wang, Z. M. Nie, J. G. Zhang, G. L. Graff, J. Liu, Z. G. Yang and T. Duong, *Electrochem. Commun.*, 2010, **12**, 378–381.
473 X. F. Zhou, F. Wang, Y. M. Zhu and Z. P. Liu, *J. Mater. Chem.*, 2011, **21**, 3353–3358.
474 C. V. Rao, A. L. M. Reddy, Y. Ishikawa and P. M. Ajayan, *ACS Appl. Mater. Interfaces*, 2011, **3**, 2966–2972.
475 G. D. Du, K. H. Seng, Z. P. Guo, J. Liu, W. X. Li, D. Z. Jia, C. Cook, Z. W. Liu and H. K. Liu, *RSC Adv.*, 2011, **1**, 690–697.
476 Y. H. Hu, H. Wang and B. Hu, *ChemSusChem*, 2010, **3**, 782–796.
477 N. L. Yang, J. Zhai, D. Wang, Y. S. Chen and L. Jiang, *ACS Nano*, 2010, **4**, 887–894.
478 S. R. Sun, L. Gao and Y. Q. Liu, *Appl. Phys. Lett.*, 2010, **96**, 083113.
479 M. Y. Yen, M. C. Hsiao, S. H. Liao, P. I. Liu, H. M. Tsai, C. C. M. Ma, N. W. Pu and M. D. Ger, *Carbon*, 2011, **49**, 3597–3606.
480 S. R. Kim, M. K. Parvez and M. Chhowalla, *Chem. Phys. Lett.*, 2009, **483**, 124–127.
481 H. B. Yang, G. H. Guai, C. X. Guo, Q. L. Song, S. P. Jiang, Y. L. Wang, W. Zhang and C. M. Li, *J. Phys. Chem. C*, 2011, **115**, 12209–12215.
482 S. S. Li, Y. H. Luo, W. Lv, W. J. Yu, S. D. Wu, P. X. Hou, Q. H. Yang, Q. B. Meng, C. Liu and H. M. Cheng, *Adv. Energy Mater.*, 2011, **1**, 486–490.
483 H. Choi, H. Kim, S. Hwang, M. Kang, D. W. Jung and M. Jeon, *Scr. Mater.*, 2011, **64**, 601–604.
484 H. Choi, H. Kim, S. Hwang, W. Choi and M. Jeon, *Sol. Energy Mater. Sol. Cells*, 2011, **95**, 323–325.
485 J. Chen, C. Li, G. Eda, Y. Zhang, W. Lei, M. Chhowalla, W. I. Milne and W. Q. Deng, *Chem. Commun.*, 2011, **47**, 6084–6086.
486 G. Zhu, T. Xu, T. A. Lv, L. K. Pan, Q. F. Zhao and Z. Sun, *J. Electroanal. Chem.*, 2011, **650**, 248–251.
487 S. R. Sun, L. Gao, Y. Q. Liu and J. Sun, *Appl. Phys. Lett.*, 2011, **98**, 093112.
488 Y. Y. Shao, J. Wang, H. Wu, J. Liu, I. A. Aksay and Y. H. Lin, *Electroanal.*, 2010, **22**, 1027–1036.
489 M. Pumera, A. Ambrosi, A. Bonanni, E. L. K. Chng and H. L. Poh, *TrAC, Trends Anal. Chem.*, 2010, **29**, 954–965.
490 D. Chen, L. H. Tang and J. H. Li, *Chem. Soc. Rev.*, 2010, **39**, 3157–3180.
491 F. Schedin, A. K. Geim, S. V. Morozov, E. W. Hill, P. Blake, M. I. Katsnelson and K. S. Novoselov, *Nat. Mater.*, 2007, **6**, 652–655.
492 J. L. Johnson, A. Behnam, S. J. Pearton and A. Ural, *Adv. Mater.*, 2010, **22**, 4877–4880.
493 U. Lange, T. Hirsch, V. M. Mirsky and O. S. Wolfbeis, *Electrochim. Acta*, 2011, **56**, 3707–3712.
494 M. Shafiei, P. G. Spizzirri, R. Arsat, J. Yu, J. du Plessis, S. Dubin, R. B. Kaner, K. Kalantar-Zadeh and W. Wlodarski, *J. Phys. Chem. C*, 2010, **114**, 13796–13801.
495 A. Kaniyoor, R. I. Jafri, T. Arockiadoss and S. Ramaprabhu, *Nanoscale*, 2009, **1**, 382–386.
496 Z. X. Jiang, J. J. Wang, L. H. Meng, Y. D. Huang and L. Liu, *Chem. Commun.*, 2011, **47**, 6350–6352.
497 H. J. Song, L. C. Zhang, C. L. He, Y. Qu, Y. F. Tian and Y. Lv, *J. Mater. Chem.*, 2011, **21**, 5972–5977.
498 H. Y. Jeong, D. S. Lee, H. K. Choi, D. H. Lee, J. E. Kim, J. Y. Lee, W. J. Lee, S. O. Kim and S. Y. Choi, *Appl. Phys. Lett.*, 2010, **96**, 213105.
499 S. J. Guo, D. Wen, Y. M. Zhai, S. J. Dong and E. K. Wang, *ACS Nano*, 2010, **4**, 3959–3968.
500 K. F. Zhou, Y. H. Zhu, X. L. Yang, J. Luo, C. Z. Li and S. R. Luan, *Electrochim. Acta*, 2010, **55**, 3055–3060.
501 K. J. Huang, D. J. Niu, X. Liu, Z. W. Wu, Y. Fan, Y. F. Chang and Y. Y. Wu, *Electrochim. Acta*, 2011, **56**, 2947–2953.
502 L. M. Lu, H. B. Li, F. L. Qu, X. B. Zhang, G. L. Shen and R. Q. Yu, *Biosens. Bioelectron.*, 2011, **26**, 3500–3504.
503 Q. Zeng, J. S. Cheng, X. F. Liu, H. T. Bai and J. H. Jiang, *Biosens. Bioelectron.*, 2011, **26**, 3456–3463.
504 T. T. Baby, S. S. J. Aravind, T. Arockiadoss, R. B. Rakhi and S. Ramaprabhu, *Sens. Actuators, B*, 2010, **145**, 71–77.
505 C. S. Shan, H. F. Yang, D. X. Han, Q. X. Zhang, A. Ivaska and L. Niu, *Biosens. Bioelectron.*, 2010, **25**, 1070–1074.
506 C. L. Sun, H. H. Lee, J. M. Yang and C. C. Wu, *Biosens. Bioelectron.*, 2011, **26**, 3450–3455.
507 F. H. Li, J. Chai, H. F. Yang, D. X. Han and L. Niu, *Talanta*, 2010, **81**, 1063–1068.
508 R. S. Dey and C. R. Raj, *J. Phys. Chem. C*, 2010, **114**, 21427–21433.
509 S. Mao, G. H. Lu, K. H. Y. Z. Bo and J. H. Chen, *Adv. Mater.*, 2010, **22**, 3521–3526.
510 X. C. Dong, W. Huang and P. Chen, *Nanoscale Res. Lett.*, 2011, **6**, 60.
511 Y. Wang, S. Zhang, D. Du, Y. Y. Shao, Z. H. Li, J. Wang, M. H. Engelhard, J. H. Li and Y. H. Lin, *J. Mater. Chem.*, 2011, **21**, 5319–5325.
512 J. F. Liang, Z. B. Chen, L. Guo and L. D. Li, *Chem. Commun.*, 2011, **47**, 5476–5478.
513 H. C. Chang, X. J. Wu, C. Y. Wu, Y. Chen, H. Jiang and X. M. Wang, *Analyst*, 2011, **136**, 2735–2740.
514 Y. P. He, Q. L. Shen, J. B. Zheng, M. Z. Wang and B. Liu, *Electrochim. Acta*, 2011, **56**, 2471–2476.
515 L. M. Li, Z. F. Du, S. A. Liu, Q. Y. Liu, Q. Y. Hao, Y. G. Wang, Q. H. Li and T. H. Wang, *Talanta*, 2010, **82**, 1637–1641.
516 D. Du, J. Liu, X. Y. Zhang, X. L. Cui and Y. H. Li, *J. Mater. Chem.*, 2011, **21**, 8032–8037.
517 K. Wang, Q. Liu, X. Y. Wu, Q. M. Guan and H. N. Li, *Talanta*, 2010, **82**, 372–376.
518 K. Wang, Q. Liu, Q. M. Guan, J. Wu, H. N. Li and J. J. Yan, *Biosens. Bioelectron.*, 2011, **26**, 2252–2257.
519 G. F. Wang, H. Huang, G. Zhang, X. J. Zhang, B. Fang and L. Wang, *Anal. Methods*, 2010, **2**, 1692–1697.
520 M. H. Yang, A. Javadi and S. Q. Gong, *Sens. Actuators, B*, 2011, **155**, 357–360.
521 B. L. Su, D. P. Tang, Q. F. Li, J. Tang and G. N. Chen, *Anal. Chim. Acta*, 2011, **692**, 116–124.
522 J. M. Gong, T. Zhou, D. D. Song and L. Z. Zhang, *Sens. Actuators, B*, 2010, **150**, 491–497.
523 C. Xu and X. Wang, *Small*, 2009, **5**, 2212–2217.
524 J. Lee, S. Shim, B. Kim and H. S. Shin, *Chem. –Eur. J.*, 2011, **17**, 2381–2387.
525 X. Q. Fu, F. L. Bei, X. Wang, S. O''Brien and J. R. Lombardi, *Nanoscale*, 2010, **2**, 1461–1466.
526 K. Jasuja and V. Berry, *ACS Nano*, 2009, **3**, 2358–2366.
527 Y. Y. Wang, Z. H. Ni, H. L. Hu, Y. F. Hao, C. P. Wong, T. Yu, J. T. L. Thong and Z. X. Shen, *Appl. Phys. Lett.*, 2010, **97**, 163111.
528 Z. Zhang, F. G. Xu, W. S. Yang, M. Y. Guo, X. D. Wang, B. L. Zhang and J. L. Tang, *Chem. Commun.*, 2011, **47**, 6440–6442.
529 G. Lu, H. Li, C. Liusman, Z. Y. Yin, S. X. Wu and H. Zhang, *Chem. Sci.*, 2011, **2**, 1817–1821.
530 R. Wen, Y. X. Fang and E. K. Wang, *ACS Nano*, 2011, **5**, 6425–6433.
531 H. M. Sun, L. Y. Cao and L. H. Lu, *Nano Res.*, 2011, **4**, 550–562.
532 N. W. Li, M. B. Zheng, X. F. Chang, G. B. Ji, H. L. Lu, L. P. Xue, L. J. Pan and J. M. Cao, *J. Solid State Chem.*, 2011, **184**, 953–958.
533 H. Jabeen, V. Chandra, S. Jung, J. W. Lee, K. S. Kim and S. B. Kim, *Nanoscale*, 2011, **3**, 3583–3585.
534 K. Zhang, V. Dwivedi, C. Y. Chi and J. S. Wu, *J. Hazard. Mater.*, 2010, **182**, 162–168.
535 T. S. Sreeprasad, S. M. Maliyekkal, K. P. Lisha and T. Pradeep, *J. Hazard. Mater.*, 2011, **186**, 921–931.
536 W. P. Xu, L. C. Zhang, J. P. Li, Y. Lu, H. H. Li, Y. N. Ma, W. D. Wang and S. H. Yu, *J. Mater. Chem.*, 2011, **21**, 4593–4597.
537 J. Z. Ma, J. T. Zhang, Z. G. Xiong, Y. Yong and X. S. Zhao, *J. Mater. Chem.*, 2011, **21**, 3350–3352.
538 L. Liu, J. C. Liu, Y. J. Wang, X. L. Yan and D. D. Sun, *New J. Chem.*, 2011, **35**, 1418–1423.

539 J. F. Shen, M. Shi, N. Li, B. Yan, H. W. Ma, Y. Z. Hu and M. X. Ye, *Nano Res.*, 2010, **3**, 339–349.
540 H. Bai, C. Li and G. Q. Shi, *Adv. Mater.*, 2011, **23**, 1088–1114.
541 D. Zhou and B. H. Han, *Adv. Funct. Mater.*, 2010, **20**, 2717–2722.
542 H. L. Li, S. P. Pang, S. Wu, X. L. Feng, K. Mullen and C. Bubeck, *J. Am. Chem. Soc.*, 2011, **133**, 9423–9429.
543 H. Li, S. Pang, X. Feng, K. Mullen and C. Bubeck, *Chem. Commun.*, 2010, **46**, 6243–6245.
544 L. Y. Cao, H. M. Sun, J. Li and L. H. Lu, *Anal. Methods*, 2011, **3**, 1587–1594.
545 L. Y. Cao, Y. L. Liu, B. H. Zhang and L. H. Lu, *ACS Appl. Mater. Interfaces*, 2010, **2**, 2339–2346.
546 E. Jin, X. F. Lu, L. L. Cui, D. M. Chao and C. Wang, *Electrochim. Acta*, 2010, **55**, 7230–7234.
547 Y. Zhang, X. M. Sun, L. Z. Zhu, H. B. Shen and N. Q. Jia, *Electrochim. Acta*, 2011, **56**, 1239–1245.